Traffic emitted semi-volatile organic compounds (SVOCs) and

intermediate volatility organic compounds (IVOCs) analysed by

GC×GC-ToF-MS

by

Ruixin Xu

A thesis submitted to the University of Birmingham for the degree of

DOCTOR OF PHILOSOPHY

Division of Environmental Health and Risk Management
School of Geography, Earth and Environmental Sciences
College of Life and Environmental Sciences
University of Birmingham

January 2020

Abstract

Many uncertainties exist regarding the chemical composition of semi-volatile and intermediate volatility organic compounds (S/IVOCs), as traditional gas chromatographic methods are unable to separate them adequately. Air samples were collected at four sites in central London and were analysed using thermal desorption coupled to comprehensive gas chromatography time-of-flight mass spectrometry (GC×GC-ToF-MS).

Main S/IVOC groups identified and quantified include C_{13}-C_{36} alkanes (linear and branched alkanes), C_{12}-C_{25} monocyclic alkanes, C_{13}-C_{27} bicyclic alkanes and C_{10}-C_{24} monocyclic aromatics in the gas phase and particle phase. Diagnostic ratios of n-alkanes as well as correlation analysis of S/IVOCs and traffic tracers suggest traffic is a major contributor with a minor contribution from other sources. The distribution of hydrocarbons is similar in background and roadside air, indicating the importance of road traffic as a source of hydrocarbons in the urban atmosphere of London. Emission factors estimated in this study are broadly similar to those measured elsewhere in the world, despite differences in traffic fleet composition. Gas-particle partitioning of n-alkanes is discussed and compared between sites. The S/IVOC concentrations identified contribute to a small fraction of the total OH reactivity and SOA formation in background London.

Acknowledgements

I would like to acknowledge the FASTER team workers. I thank Mr Christopher Stark for all his effortds and help in the lab; thank Dr David Beddows, Dr Ajit Singh and Mr James Brean for their help during the sampling campaigns in London; thank Dr Jian Zhong, Prof Rob MacKenzie , Dr Xiaoming Cai, Dr Irina Nikolova and Dr Soheil Zeraati Rezaei for their advice and discussion in the weekly FASTER meeting.

I am lucky to be able to work with great people in the lab and office at the University of Birmingham. I would like to thank Juan, Peter, Eva, Arie, Kamolrat, Jiali, Sophy, Dewi, Dimitris, Clarissa for many interesting conversation and lovely activities to release me from the pressure.

Finally, I thank my father Mr Chuanbao Xu and my mother Mrs Qin Wang for their love and support. Thanks for their understanding and encouragement, making me brave to move forward.

Contents

List of Figures

List of Tables

Chapter 1 Research background

This chapter describes the research background of this study, giving a brief introduction of the traffic-emitted particles, semi-volatile organic compounds (SVOCs) and intermediate volatility organic compounds (IVOCs) within traffic emitted particles, the composition of traffic emitted S/IVOCs as well as the contribution of S/IVOCs to the potential formation of secondary organic aerosol (SOA). Then, a description of the reason why we choose the GC×GC-ToF-MS as an analysis method by reviewing the advantages of GC×GC technology and previous S/IVOC studies analysed by GC/ GC×GC methods. This chapter shows the research questions and the aim of this study.

1.1 Traffic emitted particles

With the increasing population living in cities, urban air quality has become an important factor in global health. Recent epidemiological studies have consistently demonstrated the link between particulate matter exposure and cardiovascular health outcomes (Rissler et al., 2012; Fan et al., 2006; Masiol et al., 2012). Roadside particle is a complex mixture that consists of pollutants from multiple emission sources include anthropogenic sources and biogenic sources. Anthropogenic primary particles are typically from vehicle exhaust and lubricating oil residues, tyre and brake lining wear, and weathered street surface while natural biogenic particles are mainly from the leaves and other parts of plant pulverised by the passing traffic (Omar et al., 2007). The particles emitted from traffic consist of exhaust type and non-exhaust types. Exhaust type is the fuel-related emission while non-exhaust type comes from abrasion of vehicles parts such as brakes, clutch, and tyres (Alam et al., 2016b; Pant and Harrison, 2013). As a major emission source within the urban environment, particulate matter originated from traffic has gained many interests over the last few decades. However, a number of research questions

remain knowledge gaps, concerning the properties of road traffic-emitted particulate matter, especially the composition of primary vehicle exhaust particles and its contribution to the formation of the secondary organic aerosol (SOA).

Around 72% of particles by number arose from traffic on the adjacent roadway at a London roadside, which 38% of those in the nucleation mode (Dp <30 nm) and 53% in the exhaust solid mode (Aitken, 30< Dp< 100nm) (Harrison et al., 2016; Harrison et al., 2011).The majority of ultrafine particles (UFP, diameter Dp <100 nm) within the urban environment arise from road traffic emissions, especially the diesel associated emissions. Road traffic is identified as the largest emission source of UPF in the UK national emission inventory (AQEG, 2005). The settlement of fine particles is prolonged, and their suspension in the air can remain for a considerable time. The sinking process is driven by the emission of new particles (i.e., vehicle exhaust), dry deposition, resuspension, street sweeping and precipitation, contributing to a considerable amount of the particles and toxic substance to the atmosphere (Rogge et al., 1993b; Rogge et al., 1993c). The majority of the fine roadside particles is carbonaceous and can be emitted directly as primary organic aerosol and/or formed as secondary organic aerosol (Alam et al., 2016b). Medical studies have proved that the fine fraction of aerosol particles can be embedded deeply in human lung tissue, causing respiratory diseases and exacerbating cardiovascular diseases (Miller et al., 1979; Utell and Samet, 1996; Omar et al., 2007). In addition to the harmful health outcomes, particulate matter also speeds the building deterioration and decreases visibility (Rajkumar and Chang, 2000). Organic compounds occupy 10–40% of the $PM_{2.5}$ and PM_{10} in mass in the polluted urban environment while they represent around 30–50% of the PM_{10} in mass in the rural area (Chow et al., 1994).

There are more than 37 million vehicles in the UK (Alam et al., 2016b). In 1994, 7.4% of the total vehicles were using the diesel engine, and this number increased to 34.5% by 2013. In 2014, 50% of the vehicles were diesel-powered cars while 48% were petrol-powered vehicles and 2% were vehicles using alternative fuel in the UK (Alam et al., 2016b; SMMT, 2015; ExxonMobil, 2014). The significant increase in the use of diesel indicates the great contribution from diesel vehicles to the emission of roadside particles. The organic composition of the diesel exhaust has been characterised in several past studies (Schauer et al., 1999; Isaacman et al., 2012; Alam et al., 2018). The contribution of diesel-related primary emissions to the fine particle emission in the atmosphere has also been discussed in the literature via organic chemical tracer techniques and transport modelling studies (Schauer et al., 1999).

1.2 Combustion in the engine and emissions from the tailpipe

The organic compounds can emit from the engine to the atmosphere via different pathways, such as exhaust of gasoline and diesel engines and also via non-tailpipe emissions (i.e., evaporation from gasoline vehicles) (Gentner et al., 2013; Gentner et al., 2009; Gentner et al., 2012). Emitted organics are of liquid fuel origin, including uncombusted hydrocarbons (C_xH_y), incomplete combusted products (e.g., paraffinic, olefinic or aromatic) and probably oxygenated compounds (Gentner et al., 2013). Hydrocarbons are not the substances that expected to be found in high-temperature combustion gases unlike nitric oxide (NO) and carbon monoxide (CO). Chemical equilibrium calculations suggest that the quantities of hydrocarbon in homogeneous high-temperature combustion and the oxidation reactions for hydrocarbons under such conditions are immeasurable. Therefore, the presence of unburned hydrocarbons in the engine exhaust must be related to the temperature or heterogeneity combustion but not the homogeneous part of the combustion system (Springer, 2012). The reaction produces hydrogen

peroxide (H_2O_2) and releases heat at relatively low temperatures (around 700K). Ignition in engine occurs when the temperature reaches where H_2O_2 thermally decomposes (Westbrook, 2000). The effect of heterogeneity on unburned hydrocarbons can be explained as ignition inhibition. Ignition of reactants occurs when the internal heat generation caused by pre-combustion within the parcel of reactants exceeds the heat loss from the fuel-air mixture. Thus, a layer of unburned fuel-air mixture next to the cool combustion chamber walls cannot be ignited successfully due to the walls can cause large heat losses from the mixture. Under typical engine operation conditions, a significant portion of reactant mixtures quenched by the cold combustion chamber walls are burned during the expansion process or in the post exhaust system (Springer, 2012), while the comparison between fuel composition and engine-out hydrocarbons indicates that a fraction of the initial fuel survives the combustion and subsequent combustion oxidative processes during the expansion and exhaust system (Kirchstetter et al., 1999; Leppard et al., 1992). Temperature and fuel-air ratios are important factors that determine the final concentrations emitted from exhaust system (Springer, 2012). The unburned compounds in gasoline and diesel dominate the gas-phase reactive carbon in vehicle emission that can be potential sources of SOA (Kirchstetter et al., 1996; Schauer et al., 1999). Gentner et al. (2012) reported that emission factors of unburned gas-phase organic carbons detected in diesel exhaust are more than twice those in gasoline exhaust. A previous study showed that non-tailpipe emission accounts for around 30% of the emissions from gasoline vehicles in the urban environment (Gentner et al., 2009).

A number of previous studies have reported that the organic composition detected in the engine exhaust strongly correlated with the liquid fuels as the products from the incomplete combustion are expected to present in the exhaust (Gentner et al., 2012; Kirchstetter et al., 1999;

Leppard et al., 1992; Alam et al., 2018). Kirchstetter et al. (1999) reported a linear relationship between some of the individual organics in gasoline and a tunnel in San Francisco, indicating a substantial fraction of the nonmethane organic carbon (NMOC) detected in the tunnel were of unburned gasoline origin. Combustion produced species (i.e., ethene, propene, isobutene, and formaldehyde) did not present in gasoline, but presented in the tunnel and contributed to the overall reactivity of organic tunnel emissions. Organics presented in gasoline and detected in the tunnel were higher than expected as running loss evaporation emissions were suggested to contribute the emissions of unburned gasoline. VOCs were abundant in the gasoline emission and C_1-C_3 organics accounted for around 20% of the NMOC mass in the tunnel (Kirchstetter et al., 1999; Leppard et al., 1992).

Alam et al. (2018) compared the chemical composition of diesel fuel and the emission from a diesel-powered engine, suggesting the similarities in the chemical composition and differences in the relative amounts of the compound classes. The major components of the gas-phase exhaust originated from diesel fuel and all of the compounds found in diesel fuel were shown to present in the gas-phase emissions. There was a decrease in the high molecular weight branched alkanes ($>C_{20}$), probably due to the efficient combustion of these homologues or partitioning into the particle phase. Alkanes (n+i) in the gas-phase exhaust were lower than those in diesel fuel, which might attribute to the preferred combustion of these species (Burcat et al., 2012). In contrast, cyclic alkanes (monocyclic and bicyclic) and aromatics (monocyclic and bicyclic) were observed to have increased relative amounts in the gas-phase emission compared with those in the diesel fuel, probably as a result of them being formed by the combustion of larger molecules. Several oxygenates (i.e. ketones and carboxylic acids) were

also identified in gas-phase emission as combustion products of diesel fuel but only accounted little fraction of the total gas-phase exhaust (Alam et al., 2018).

Oxides of nitrogen (NO_x) from vehicle emission have gained considerable attentions in decades as the fate of NO_x can play an important role in different environmental aspects, such as regional ozone formation, secondary particle formation and eutrophication (Carslaw et al., 2011). Oxides of nitrogen (i.e. NO, NO_2 and N_2O_2) are products of the combustion processes within the engine and appear in engine exhaust at high temperatures (Newhall, 1969), while are not thermodynamically stable at room temperature and destroyed slowly during the exhaust transport at atmospheric conditions (Springer, 2012). Nitrogen oxides may also settle in the lungs to form dilute nitric acid. The harmful health effect of nitrogen oxides is relatively small as the amount of formed nitric acid is minute and dilute, while long-time accumulation can cause problems (Springer, 2012). The primary nitrogen oxide formed in the engine is nitric oxide (NO), but it can be oxidised subsequently to form nitrogen dioxide in the atmosphere (McConnell, 1963). Nitric oxide is formed from the N_2 and O_2 with the existence of high temperatures. In general, NO can be formed during the combustion process in three ways, including (a) forms from the oxidation of chemically bound nitrogen in the fuel (b) forms from molecular nitrogen in the radical-rich flame zone (the main combustion zone for hydrocarbons) (c) forms from molecular nitrogen initiated by oxygen radicals and assisted by OH radicals at high temperature in the post-flame zone (Merker et al., 1993). Based on the chemical equilibrium calculation, NO concentrations in combustion products under high temperature could reach levels from several hundred parts per million (ppm) up to several mole percent determined by temperature and the ratio of fuel to air. The regular assumption for these calculations is that there is sufficient time for combustion products to reach the chemical

equilibrium at particular temperatures while some investigations point out that the burned products often cool down immediately before NO can achieve the peak temperature chemical equilibrium levels. Equilibrium calculation also predicts that NO could largely decompose to N_2 and O_2 at relatively low temperature after combustion while the reality shows that the decomposition is much slow and consequently the NO concentrations in engine remains at fixed level formed during the high temperature combustion processes (Springer, 2012). The formation of nitrogen oxides in an engine is not a new observation as a few old studies have reported it (Eyzat and Guibet, 1968; Spindt et al., 1956; Lavoie et al., 1970; McConnell, 1963).

The proportion of diesel-powered light-duty vehicles (LDVs) has grown in the UK in the last decade. The numbers of gasoline-powered LDVs and diesel-powered LDVs are similar in the UK currently while most of the heavy-duty vehicles (HDVs) in Europe are diesel-powered (Carslaw et al., 2011; Hassler et al., 2016). Diesel contributes to the majority of burned fuel for transportation in the UK (Dunmore et al., 2015). Since only the gasoline-powered vehicles have shown a remarkable reduction in NO_x emissions in the past two decades, and the NO_x emission from diesel vehicles have not declined much during the same period (Carslaw and Rhys-Tyler, 2013), the roadside NO_x emission have remained stable in the UK (Carslaw et al., 2011; Hassler et al., 2016).

1.3 Traffic emitted SVOCs and IVOCs

Semi-volatile particles make an important contribution to the total particle number emitted from the traffic source (Harrison et al., 2016; Harrison et al., 2011). Semi-volatile organic compounds (SVOCs) and intermediate volatility organic compounds (IVOCs) can partition between the gas

and particle phase under ambient conditions. SVOCs refer to organic species with an effective saturation concentration C^* between 1 and 10^3 μgm^{-3} while IVOCs refer to species with C^* between 10^4 and 10^7 μgm^{-3} (Robinson et al., 2007). Once particles are emitted, they can be modified by a number of physical and chemical processes. As the particles disperse away from the emission source, the semi-volatile organic component of the particles may partially evaporate with atmospheric dilution caused by the lack of equilibrium between the gas and the particle phase, creating substantial amounts of low-volatility gas-phase compounds (Robinson et al., 2007). S/IVOCs subsequently oxidise to form lesser volatile compounds which recondense onto solid particles, giving an increased particle mass.

S/IVOC emissions from traffic mainly comprise of aliphatic and aromatic hydrocarbons ranging between C_{12} and C_{35}, and are typically dominated by alkanes, cyclic alkanes and monocyclic aromatics (Worton et al., 2014; Gentner et al., 2012; Weitkamp et al., 2007; Alam et al., 2018). The organic carbon emission from gasoline- and diesel-powered vehicles can be classified into volatile organic compounds (VOCs), intermediate volatility organic compounds (IVOCs) and semi-volatile organic compounds (SVOCs) based on their vapour pressure. Gentner et al. (2012) reported the organic carbon emissions from diesel and gasoline present the different distribution based on carbon number. Most of the gasoline emitted hydrocarbons are VOCs while some aromatics can extend to the intermediate volatile range. The exhaust of unleaded gasoline contains a considerable amount of aromatic hydrocarbons, and monitoring this hydrocarbon group has become more important (Kerbachi et al., 2006). Only 30% of diesel emitted hydrocarbons are VOCs while most of them are less volatile (S/IVOCs). Gasoline emissions are mainly in the carbon number range below C_{12} while diesel fuel emissions are mainly in the range from C_8 to C_{25} (Gentner et al., 2012). There are very few

studies on the abundance of gaseous longer chain hydrocarbons ($\geq C_{12}$) (Dunmore et al., 2015) although the traffic emitted S/IVOCs consists of mostly higher molecular species containing 12-35 carbon atoms (Alam et al., 2018). The role of the hydrocarbons above C_{12} in the atmosphere has not been fully addressed due to the lack of detailed emission information for these species.

1.4 Chemical composition of traffic emitted S/IVOCs

Despite huge research interest and many contributions from the last decades, many uncertainties exist regarding the identities and chemical composition of the traffic emitted S/IVOCs. A key reason is that the vast majority of S/IVOC mass cannot be separated and characterised by traditional one-dimensional gas-chromatography (1D-GC) based analytical techniques (Schauer et al., 1999; 2002; Jathar et al., 2012). Instead, 90% of the hydrocarbon content of the atmospheric sample are largely uncharacterised, as presenting an unresolved complex mixture (UCM) and creating a large hump within the chromatogram (Fraser et al., 1998; Schauer et al., 1999). The UCM is often observed in samples associated with the use of fossil fuel (Nelson et al., 2006; Frysinger et al., 2003; Ventura et al., 2008), and comprises more than 80% of the semi-volatile hydrocarbons emitted from diesel and gasoline derived engines (Schauer et al., 2002; 1999; Chan et al., 2013). Unresolved complex mixture (UCM) contains a large number of isomers, and is mainly dominated by co-eluting linear (straight chain), branched and cyclic alkanes (Robinson et al., 2007; Isaacman et al., 2012; Jathar et al., 2012; Mao et al., 2009) while a minor fraction is aromatic compounds (van Deursen et al., 2000).

Previous researches on atmospheric samples processed by one-dimensional gas-chromatography (1D-GC) based analytical techniques have focused on a limited range of

homologous series and tracer compounds that can be distinguished from the bulk of UCM, generally involved n-alkanes, PAHs, hopanes and steranes (Alam et al., 2016b; Schauer et al., 1999; 2002). These species only represent a small portion of the total mass or number of compounds in the exhaust. The remaining semi-volatile emissions can play an important role in photochemical smog formation and contribute to the generation of secondary organic aerosol (SOA) (Schauer et al., 1999; Alam et al., 2018). Past studies typically classified the alkane homologues by volatility based on the retention times due to the challenges in speciating alkane isomers (Grieshop et al., 2009; Presto et al., 2012; Dunmore et al., 2015). Lack of understanding on the molecular structure can cause uncertainties on the study of the SOA formation from these hydrocarbons, as SOA yields change with the alkane structure (linear, branched and cyclic) and number of rings (Pye and Pouliot, 2012; Loza et al., 2014; Lim and Ziemann, 2009b; Tkacik et al., 2012). Therefore, studies on the molecular structure are crucial to understanding the environmental fate of these semi-volatile compounds.

A number of studies have reported the chemical components of organic compounds in the ambient air or heavy traffic influenced regions by using one dimensional GC-MS or GC×GC-MS (Lewis et al., 2000; Pio et al., 2001; Xu et al., 2003b; Xu et al., 2003a; Hamilton and Lewis, 2003; Kawashima et al., 2006; Omar et al., 2007; Chan et al., 2013). Lewis et al. (2000) worked on the analysis of the volatile organic compounds in the urban air by GC×GC technology. They collected urban air samples from the centre of Melbourne (Australia) and showed the presence of over 500 chemical species ranging from C_2 to C_{14}, including more than 100 multi-substituted monoaromatics and volatile oxygenated hydrocarbons. The comparison between the composition of urban air samples with those of gasoline and diesel vapours shows high similarities, indicating the use of fuel is the most possible source of the aromatic species

identified in their study. The chemical composition and relative emission source types in Melbourne reported by Lewis et al. (2000) are broadly similar to those reported in the United Kingdom; however, the use of diesel-powered vehicles increased recently in the UK, shifting the balance of emissions in favour of those aromatic and aliphatic species with longer-chains. Pio et al. (2001) collected aerosol samples at a rural site in Portugal and identified about 400 individual organic compounds, including aliphatic compounds, PAHs, oxy-PAHs, alcohols, aldehydes, ketones, n-alkanoic acids, n-alkenoic acids, aliphatic dicarboxylic acids, terpenic constituents and some volatile organic compound (VOC) oxidation products. In 2003, an atmospheric VOC study isolated the organic compounds in air samples by TD- GC ×GC–FID and GC ×GC–TOF-MS (Xu et al., 2003a; Xu et al., 2003b). The compounds they observed include cyclic and acyclic alkanes, PAHs, oxygenated aromatics, alcohols, aldehydes, ketones, C_7-C_{11} aromatic and n-alkane.

Hamilton and Lewis (2003) analysed the monoaromatic component in gasoline, gasoline vapours and urban air by comprehensive GC×GC. The presence of 147 mono-aromatic compounds with up to 8 carbon substituents on the ring was detected in the urban samples, while 130 of such species were observed in gasoline. The similarities they found in some aromatic regions for urban air and gasoline vapours prove the impact of fuel usage to the urban air quality. Hamilton et al. (2004) analysed the $PM_{2.5}$ aerosol samples collected at a roadside location in London, UK. Over 10,000 individual organic compounds were isolated by thermal desorption coupled to comprehensive gas chromatography-time of flight mass spectrometry (GC×GC-TOF-MS). They pointed out that the current knowledge of the chemical composition of urban organic aerosol is far from clear understanding.

In a roadside measurement in Japan, Kawashima et al. (2006) examined 47 species of C_6-C_{12} hydrocarbons by GC-MS, including benzene, toluene, and others. Kallio et al. (2006) identify the organic compounds in the air samples by GC×GC–TOF–MS collected from a forest in Finland, as a part of the QUEST campaign. Around 50 compounds were identified, and some of them for the first time. The compounds they isolated and identified included acyclic alkanes, acyclic alkenes, ketones, aldehydes, oxidised monoterpenes, aldehydes, aromatic compounds and also a few alcohols and acids. Omar et al. (2007) studied the organic composition of airborne particles and roadside dust particles in Kuala Lumpur, Malaysia. They reported the concentrations of organic source tracers, such as n-alkanes, PAHs, unresolved complex mixture (UCM), petroleum molecular markers, n-alkanols, triterpenoids and n-alkanoic acids. He et al. (2008) worked on the characterisation of $PM_{2.5}$ emissions in a Tunnel in China, and the organic compounds they quantified include n-alkanes, n-alkanoic acids, PAHs and hopanes. Williams et al. (2010a) and Zhao et al. (2013) identified multiple types of primary POA and SOA from air sample in California, and apply PMF (positive matrix factorisation) analysis to investigate the emission source.

Chan et al. (2013) analysed the UCM components of semi-volatile aliphatic hydrocarbons collected in the urban atmosphere of California. They reported the masses of C_{20}-C_{25} linear, branched and cyclic alkanes, and studied the emission source of alkane isomers based on the carbon number preference (CPI) of n-alkanes. Worton et al. (2014) worked on the composition of vehicle POA and the similarity between POA and lubricating oil. The compound classes characterised by their GC method includes linear alkanes, branched alkanes, branched cycloalkanes and aromatics. More recently, Dunmore et al. (2015) collected air samples from an urban background site North Kensington in winter London and analysed samples by using

GC×GC-ToF-MS. The authors grouped and identified low molecular weight hydrocarbons ($\leq$ C_{12}) based on their functionality and carbon number, showing the concentrations of C_6-C_{13} aliphatic and C_2-C_4 substitute mono aromatics in the gas phase. The separation of linear n-alkanes, branched alkanes and cyclic alkanes is not sufficient at carbon numbers above C_6 on the GC×GC chromatogram, so they are not fully characterised and treated as a group of aliphatic compounds (Dunmore et al., 2015).

This study chooses alkane isomers (linear, branched and cyclic) and monocyclic aromatics as target compounds based on two previous studies processed in the engine laboratory from the FASTER research group (Alam et al., 2016b; Alam et al., 2018). Alam et al. (2016b) characterised and quantified the composition of S/IVOCs in the exhaust of diesel engine by GC×GC-ToF-MS, reporting the diesel engine associated S/IVOCs are predominated by linear and branched alkanes (C_{11}-C_{33}), alkyl-cyclohexane (C_{11}-C_{25}), alkyl-benzenes, PAHs and various cyclic aromatics. The typical chromatogram shows the hydrocarbons up to C_{20} present in diesel fuel while C_{18}–C_{36} compounds form UCM and dominate in lubricating oil (Figure 1.1). Compounds observed in the gas phase of diesel exhaust are similar to those identified in diesel fuels (mainly below C_{20}) while compounds in the particle phase are similar to lubricating oil (mainly C_{21}-C_{27}). To provide a more comprehensive view on the isomer sets, Alam et al. (2017) mapped and quantified isomer sets previously unresolved in UCM in diesel fuel, lubricating oil and diesel emission samples by the GC×GC coupled to variable ionisation ToF-MS. Exhaust from diesel engines have been reported to be comprised of a limited number of compound classes, but one class consists of a substantial number of individual compounds. In addition to the typical tracer compounds linear n-alkanes, Alam et al. (2017) has expanded to more polar compound classes with larger number of carbon atom (above C_{12}), mainly including

monocyclic alkanes, bicyclic alkanes, tricyclic alkanes, monocyclic aromatics, bicyclic aromatics and alkyl-biphenyls. To compare the S/IVOC groups observed in ambient air with fuel (diesel fuel as well as lubricating oil) reported by Alam et al. (2017), this study developed a chromatogram template to map and quantify the semi-volatile organic components in air sample, mainly include alkanes, monocyclic alkanes, bicyclic alkanes and monocyclic aromatics. More details have been developed in Chapter 2 Methods.
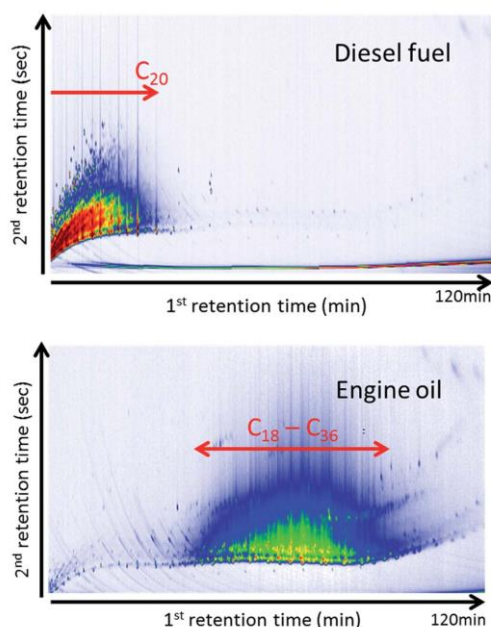
Figure 1.1: Typical GC×GC-ToF-MS chromatograms (contour plots) display diesel fuel and engine lubricant oil. x-Axis separation bases on the volatility and y-axis separation bases on the polarity. Each coloured spot represents an individual species, and the colour represents the intensity of the corresponding compound. Intensity decreases from the warmer colour (i.e., red) to colder colour (i.e., blue) (Alam et al., 2016b).

1.5 Contribution to the potential SOA formation

Recent studies reported the photo-oxidation of low-volatility gas-phase species could make a significant contribution to the formation of secondary organic aerosol (SOA) (Jathar et al., 2012; Robinson et al., 2007; Pye and Seinfeld, 2010; Weitkamp et al., 2007; Leskinen et al., 2007). Since the molecular identity of the majority of the S/IVOC mass is elusive, SOA formation attributed by these constituents of particles cannot be studied or modelled in the same manner as traditional SOA precursors, such as benzene and alpha-pinene (Jathar et al., 2012). Secondary organic aerosol (SOA) arises from chemical transformation and condensation of volatile and semi-volatile species, representing a significant portion of the submicron dry atmospheric aerosol mass (Zhang et al., 2007; Jathar et al., 2012). SOA arises from speciated VOCs has been defined as traditional SOA (T-SOA). The main fraction of SOA formation is thought to be attributed to the first-generation oxidation products of high flux volatile organic compounds (VOCs), like terpenes and single-ring aromatics (Jathar et al., 2012). However, a number of studies reported the simulations systematically underestimate the organic aerosol levels in chemical transport models (Heald et al., 2005; Vutukuru et al., 2006; Johnson et al., 2006; Morris et al., 2006). Laboratory experiments and field studies show that photo-oxidation of diesel emissions rapidly generates organic aerosols, considerably over what can be explained by known SOA precursors (i.e. T-SOA models) (Robinson et al., 2007; Jathar et al., 2012). Robinson et al. (2007) attributed the unexplained SOA formation to the oxidation of unspeciated gas-phase low-volatility organics, such as semi-volatile and intermediate volatility organic compounds (S/IVOCs). SOA produced by S/IVOCs is defined as non-traditional SOA (NT-SOA). S/IVOCs are co-emitted from combustion procedure and less volatile than VOC. Due to the low vapour pressure of S/IVOCs, their oxidation is expected to have higher SOA yields than the more volatile precursors; thus, could contribute to a substantial fraction of the

SOA within the urban area (Chan et al., 2013; Presto et al., 2010; Lim and Ziemann, 2009a). However, these species are not often accounted for in models because many of them cannot be speciated and do not contribute significantly to ozone chemistry mechanisms; furthermore, measurement of S/IVOCs requires hard-to-use sorbents (Jathar et al., 2012). SVOCs, IVOCs and VOCs form SOA in the same fundamental manner. The oxidation process in the gas phase adds functional groups precursor molecule, producing lower-volatility compounds that condense into the particle phase (Jathar et al., 2012). Pye and Seinfeld (2010) estimated the global production of organic aerosol from primary emission of S/IVOCs, predicting more abundant aerosol production is attributed to S/IVOC oxidation rather than the oxidation of traditional parent hydrocarbons (terpenes, isoprene and aromatics). In a more recent study, Zhao et al. (2014) reported a substantial fraction of predicted SOA formation comes from primary IVOC UCM (45%) while other fractions come from oxygenated IVOC UCM (19%), unspeciated primary SVOC (12%), speciated IVOCs (12%) and VOC (12%). Accounting for the partitioning and photochemical processing of S/IVOCs from the UCM will bring a better agreement between the atmospheric organic aerosol observed in the real world and that predicted based on modelling the traditional SOA precursors.

However, there are still many uncertainties on the extent of SOA formation from the photooxidation of diesel-derived atmospheric organics (Gentner et al., 2012; Bahreini et al., 2012). Robinson et al. (2007) reported a rapid and significant SOA formation from the photooxidation of diesel exhaust in a chamber, while disagreements were reported by several studies (Samy and Zielinska, 2010; Chirico et al., 2010; Bahreini et al., 2012). Samy and Zielinska (2010) and Chirico et al. (2010) observed that negligible SOA production was transformed from the diesel exhaust unless hydrocarbons or OH radicals were added to the

chamber to enhance the reactivity. Bahreini et al. (2012) did not observe significant SOA formation from diesel emission either in Los Angeles Basin (USA) and suggested the reduction on SOA formation can be achieved by reducing the gasoline-related emission on local to global scales.

The SOA formation involves the multigeneration oxidation of the parent organic. After the parent organics are consumed by the chemical reaction with the hydroxyl radicals (OH radicals), products may subsequently react with OH radicals as well, contributing to a rising level of evolving products (Yee et al., 2012). The atmospheric organics can be oxidised and transformed in various chemical conditions, such as in the gas phase, at the interface of the gas phase and particle phase, and within the bulk of organics or aqueous phase (Kroll et al., 2011). In the gas phase, two general types of reaction, functionalisation (the oxidative addition of polar functional group to the carbon skeleton) and fragmentation (the oxidative cleavage of C-C bond) occur, together with the interplay between these two fundamental classes of reactions (Yee et al., 2012; Kroll et al., 2011). The volatility of the products would have a progressive decrease when the product becomes more functionalised with oxygen-containing moieties, so that increase their propensity to partition to the particle phase (Jimenez et al., 2009; Kroll et al., 2011).

Long-chain alkanes can play an essential role in the formation of SOA as they are the main components of the unresolved complex mixture (UCM) in the fuel associated exhaust (Schauer et al., 2002; 1999; Robinson et al., 2007). Jordan et al. (2008) modelled the SOA formation from C_7-C_{12} n-alkanes based on the previous laboratory work, suggesting the majority of SOA (88-99%) formed from C_8-C_{12} n-alkanes derives from the second- and third-generation

compounds while the corresponding percentage for C_{13}-C_{17} n-alkanes is 69-78%. SOA transformed from alkanes with shorter chains is through the first and higher generation oxidation products while SOA oxidised from the alkanes with very long chains is mainly from the first-generation products (Lim and Ziemann, 2005; Pye and Pouliot, 2012; Jordan et al., 2008). Studies observed different distributions of alkane chain length and structures (i.e. straight linear chain, branched, cyclic and the combination of branched and cyclic conformations) in gasoline and diesel fuel (Isaacman et al., 2012; Gentner et al., 2012). A large number of studies pointed out that the various chemical structure leads to the difference in the chemical processes of the SOA formation based on laboratory work (Lim and Ziemann, 2005; Lim and Ziemann, 2009a; Lim and Ziemann, 2009c; Lim and Ziemann, 2009b; Lipsky and Robinson, 2006; Presto et al., 2010; Presto et al., 2009; Lambe et al., 2012; Tkacik et al., 2012) and modelling work (Pye and Pouliot, 2012; Aumont et al., 2012; Jordan et al., 2008; Zhang and Seinfeld, 2013; Cappa et al., 2013). Chan et al. (2013) modelled the transformations into SOA from branched and linear alkanes and pointed out branched alkanes may present a more critical role in the oxidation of UCM and the SOA formation based on the consideration of gas/particle partitioning, emissions and reaction rates.

Monocyclic aromatics are important species to balance OH sources within the urban air due to their rapid reaction with OH radicals. The potential ozone production from aromatic hydrocarbons is substantial, and SOA can be generated from the primary and secondary oxidation products of aromatics. Toluene is the most studies aromatic species, but all monocyclic aromatics are believed to form the potential SOA in the same manner (Hamilton and Lewis, 2003). Hamilton and Lewis (2003) discussed the potential contribution of larger monoaromatics to the formation of secondary organic aerosol (SOA) by modelling the OH

reaction with polluted urban air, showing the gas-phase oxidation generates both ring retaining and ring cleaved products. Chan et al. (2009) discussed the contribution of photooxidation of low-volatility organics to SOA formation from different anthropogenic emission sources, including diesel exhaust, wood burning and other sources (i.e. gasoline and cooking). Their target compounds are PAHs, aromatics and long-chain alkanes, showing that the oxidation from aromatics and long chain n-alkanes contribute to a smaller amount of SOA than PAHs, but still significant. Similar results from Pye and Pouliot (2012) shows that SOA from the oxidation of alkanes and PAHs have small magnitude but still occupied a substantial percentage of SOA formed by anthropogenic sources. Alkane classes can contribute to a more significant level of SOA formation when the vehicle fleet shifts to the diesel-powered vehicles and result in higher emission of long-chain alkanes ($>C_{13}$) (Pye and Pouliot, 2012).

1.6 GC×GC-ToF-MS technology

1.6.1 The advantages of comprehensive gas chromatography technique

As the most common method, the traditional gas chromatography-mass spectrometry (GC-MS) cannot entirely separate and identify the large number of compounds due to the complexity of the S/IVOC chemical composition (Schauer et al., 1999; 2002; Jathar et al., 2012; Chan et al., 2013) and the near-continuous range of physicochemical properties of hydrocarbons in the complex mixture (Alam et al., 2018). Comprehensive gas chromatography (GC×GC) enable to resolve the UCM into many thousands of individual compound peaks due to an enhanced separation capability, producing large amounts of data with rich information. The information is often more detailed and scientifically useful than the bulk of hydrocarbon to compare the main compositional attributes of samples (Alam et al., 2018). The main advantages of GC×GC include a more powerful separation ability, expanded separation space and improved sensitivity.

By reviewing a large number of publications, Arsene et al. (2011) concluded that the separation power of GC×GC had been considerably improved during last decades. GC×GC technique is an ideal application for analysing the components of volatile or semi-volatile compounds in various fields of research, such as food and beverages, environmental science, petrochemicals and fragrances (Arsene et al., 2011).

A two-dimensional separation approach is separating compounds on two columns based on different separation mechanisms. The analytes on the first column are separated mainly depending on their vapour pressure as they would be in a traditional single GC. The separation on the second column mainly depend only on the polarity of the analytes. The two columns are connected in series by a modulator which is applied to trap and release sequential portions of the 1st column effluent and injects it into the 2nd column rapidly of different selectivity for further separation (Dalluge et al., 2002).

Comprehensive GC×GC technique is able to couple with different detection techniques, such as time-of-flight mass spectrometer (TOF-MS), quadrupole mass spectrometers (qMS) and flame ionization detector (FID) (Tranchida et al., 2010; Kallio et al., 2006; Welthagen et al., 2003; Arsene et al., 2011; Dunmore et al., 2015; Laitinen et al., 2010). In this study, two-dimensional gas chromatography (GC×GC) paired with high-speed mass spectrometry (GC×GC–MS) produced a more comprehensive understanding of the composition of the traffic emitted S/IVOCs. GC×GC provides the two-dimensional chemical ordering (shown by retention times) that is for recognising the individual compounds or compound homologues, and mass spectrometry (MS) provides structure information for chemical identification (Reichenbach et al., 2005). A flame ionisation detector is used to allow the generic

quantification of any part of the chromatogram based on the retention times, but it is laborious to assign the complex comprehensive and set-up-dependent chromatogram objectively (Alam et al., 2018). More details of the two-dimensional separation settings are showed in Section 2.2 GC×GC-ToF-MS analysis.

1.6.2 General view on the previous gas chromatography studies

A number of studies have compared the application of conventional GC-MS and the advanced comprehensive GC×GC -MS on the study of chemical composition of particles in the ambient or roadside air (Arsene et al., 2011; Lewis et al., 2000; Hamilton and Lewis, 2003; Alam et al., 2018). Alam et al. (2018) reviewed the applications of the traditional single GC and comprehensive GC×GC to the studies of volatile and semi-volatile organic compounds in airborne particles and emphasised the recent advantages of GC×GC have led to its successful application in measuring an extensive range of VOCs and S/IVOCs compared to single GC. However, there are much fewer studies worked on atmospheric S/IVOCs by using GC×GC in the literature compared with the extensive application of 1D GC to ambient air samples. Arsene et al. (2011) reviewed the analysis of volatile/semi-volatile organic compounds by comprehensive GC×GC and reported only few studies worked on atmospheric measurements by GC×GC, and the studies mainly focus on the lower molecular weight species (below C_{13}), oxygenates, or forest atmospheres.

Lewis et al. (2000) ran the urban air samples and compared the generation from comprehensive chromatogram (GC×GC) and the one-dimensional separation. Clear co-eluting was found in the first retention time. In many regions of the first column separation, no single compound was observed at a sufficient concentration above the baseline what is described as a composite of

21

the elution of many chemical species with low concentrations. Compared with the single-column separation, the comprehensive separation allows to isolate a greater number of peaks and have a broader chemical classification. They believed that comprehensive gas chromatography separates and includes a significantly greater number of aromatic species compared to single column studies. Similar to the previous study of Lewis et al. (2000), Hamilton and Lewis (2003) emphasized that the co-elution always occurs in low-volatility regions of the conventional single column based technique (such as GC-FID and GC-MS), and the vast number of low concentration species can be hidden so that single column method is not able to speciate and present all analytes. Blumberg et al. (2008) compared the performance of the GC×GC and single GC under control conditions by analysing a text mixture of 131 known semi-volatiles. The authors evaluated the peak capacities of both techniques and showed the modulator is the crucial factor that limits the separation performance of existing GC×GC. To achieve the full potential of GC×GC, they suggested to reduce the injection duration from the modulator to the second column by an order of magnitude. Besides, the improvement on the resolving power of GC×GC can be achieved through more powerful techniques, such as peak deconvolution in both first and second dimensional separations. Laitinen et al. (2010) analysed organic compounds in particles with the size of 30–100 nm from wood combustion and reported the concentrations of PAHs and n-alkanes. Particles were analysed by aerosol mass spectrometry (AMS) and three chromatographic techniques, including comprehensive GC×GC-TOF-MS, GC-TOF-MS and GC-qMS. Particle analysis was performed directly from the emission sources in the case of AMS, whereas particles were collected by the filter and analysed off-line after the extraction processes in the case of chromatographic techniques. They evaluated the advantages and disadvantages of the four analytical techniques and concluded

that GC×GC-TOF-MS has the best separation efficiency and provides the most reliable identification and quantifications.

GC×GC allows a sufficient separation while the TOF-MS system offers mass spectral data for identification of all separated compounds. A number of studies have applied GC $\times$ GC–MS system rather than GC-MS to provide a more comprehensive analysis on the chemical composition of ambient air samples (Ochiai et al., 2007; Lewis et al., 2000; Xu et al., 2003b; Xu et al., 2003a; Hamilton et al., 2004; Hamilton and Lewis, 2003; Dunmore et al., 2015; Kallio et al., 2006). Ochiai et al. (2007) characterised the nanoparticles in the roadside atmosphere and worked on the quantitative analysis of selected PAHs by use of GC $\times$ GC–MS with a limited scan range. Kallio et al. (2006) analysed the air sample collected from the forest by GC×GC–TOF–MS and compared the manual and automated search in identification procedure and found that the manual search is more accurate although it is laborious and time-consuming. An automated procedure is preferable when processing a vast number of samples, but manual search allows the researcher to use common knowledges when deciding whether there is a reasonable match between the target compound and the reference in a library. Kallio et al. (2006) also applied the technique GC×GC -FID and showed n-alkanes ranging from C_{12} to C_{24} were nicely separated from those compounds with more polarity. These n-alkanes were nicely spaced on the first retention dimension although this system cannot see structure-related information. The target compounds of the samples they reported were selected PAHs and n-alkanes ranging from C_{10} to C_{30}.

Although GC $\times$ GC–MS system can provide a more sufficient separation and identification compared with the 1D GC-MS system, the data can still be enormously complex as over

thousands of peaks can be detected in a typical $PM_{2.5}$ sample within the urban environment (Welthagen et al., 2003). To provide a more overall view on the hydrocarbon homologues, GC×GC allows compounds with a similar chemical structure to be grouped based on their volatility and polarity (1st and 2nd retention time). Grouping is always seen when there is a large number of isomers in a group. Many studies worked on concentrate the chemical groups rather than structurally specific identifications (Dunmore et al., 2015). Compounds belonging to the same chemical group have similar physicochemical properties, facilitating the classification and identification when separate them into groups. Welthagen et al. (2003) applied direct thermal desorption–gas chromatography–time-of-flight-mass spectrometry (DTD–GC–TOF-MS) and comprehensive two-dimensional gas chromatography–time-of-flight mass spectrometry (GC×GC–TOF-MS) to analyse S/IVOCs detected in urban aerosol samples. They developed search criteria and rules based on the GC×GC retention time and TOF-MS fragmentation patterns to identify different chemical groups with bubble plots, facilitating the interpretation of more than 15,000 compounds. Several other studies also identified the chemical classes with similar physicochemical properties as groups to provide an overall view on the chemical composition of S/IVOCs (Dunmore et al., 2015; Alam et al., 2018).

1.7 The aim of this study

There are still many uncertainties on the composition and behaviour of S/IVOCs in the carbon number range above $C_{12,}$ although these compounds are important components of traffic emitted particles. Traditional gas chromatography-mass spectrometry (GC-MS) can limit the characterisation of chemical compounds and present them as unresolved complex mixture (UCM), which plays an important role in the formation of SOA. As a part of the FASTER study (Fundamental Studies of the Source, Properties and Environmental Behaviour of Exhaust

Nanoparticles from Road Vehicles), this research aims at the composition, emission source and behaviour of S/IVOCs emitted from road vehicles. Samples were collected at four locations in central London (UK), including the roadside of the heavily trafficked Marylebone Road (MR), two rooftop sites (WM and RU) near MR, and an urban background site Eltham (EL) during different times from January to April 2017. To achieve a better characterisation on compounds, this study collected samples by using solvent extraction (particle phase) and thermal desorption (gas phase), and applied thermal desorption coupled to comprehensive gas chromatography time-of-flight mass spectrometry (TD-GC×GC-ToF-MS) combined with the mapping and grouping methodology to classify, identify and quantify the compounds classes.

This study identifies and quantifies S/IVOCs ranging from C_{10} to C_{36} in both the gas phase and particle phase, to provide a further understanding of the composition and properties of the hydrocarbons from traffic. The main S/IVOC classes identified in this research include C_{13}-C_{36} alkanes (n+i) (defined as the sum of n-alkanes and branched alkanes), C_{12}-C_{25} monocyclic alkanes, C_{13}-C_{27} bicyclic alkanes and C_{10}-C_{24} monocyclic aromatics. Chapter 1 and Chapter 2 describes the research background and the details of methodology respectively. Chapter 3 mainly compares the composition of S/IVOCs and the average concentrations of the main chemical classes among sites. Chapter 4 investigates the emission sources and dilution of S/IVOCs in the street canyon of MR. Molecular diagnostic parameters of n-alkanes and the correlation analysis between S/IVOCs and traffic indicators are applied to distinguish the emission source of the collected S/IVOCs. The spatial distribution of S/IVOC concentrations and the effect of wind direction on the dispersion of traffic emitted pollutants in the street canyon is considered. Chapter 5 estimates the emission factors (EFs) for n-alkanes and the main S/IVOC groups at the roadside site MR, and compares the estimated EFs of n-alkanes

with those in published studies. Chapter 6 discusses the partitioning of n-alkanes between the gas phase and the particle phase. Large quantities of gas-phase S/IVOCs contribute to secondary pollutant generation following the reaction with OH radicals. The primary OH reaction and potential SOA formation from the main chemical groups are considered. Chapter 7 gives an overall conclusion of this research.

Chapter 2 Methodology

This chapter describes the methods used in the London Campaign 2017, starting with the description of the sampling and data collection, proceeding to the settings and experimental work on GC×GC-ToF-MS, identification and mapping /grouping of the S/IVOC groups, calibration and quantification of S/IVOCs.

2.1 Sampling and data collection

2.1.1   Sampling locations
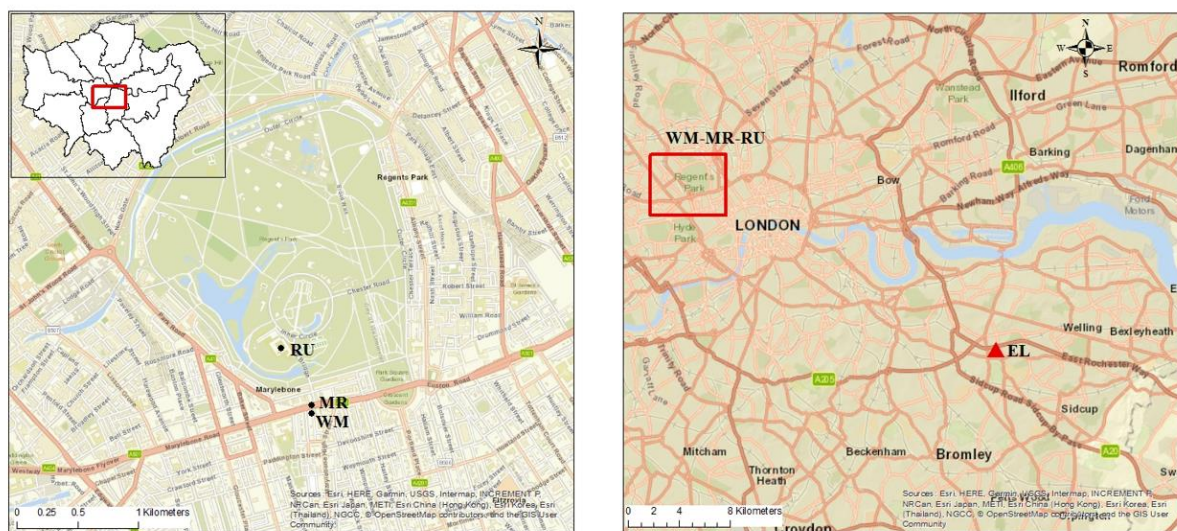
Figure 2.1: Map of the study area. The left-hand panel shows the locations of the University of Westminster (WM), Marylebone Road (MR) and Regent's University (RU) sampling sites (WM-MR-RU), while the right-hand panel shows the locations of the WM-MR-RU and Eltham (EL) sites on an expanded scale.

Multiple-site measurements were applied in central London (UK) to quantify the changes in the composition of S/IVOCs during the advection (horizontal transport) from the traffic to the cleaner atmosphere of the park. During the London field campaign 2017, ambient air samples in both the gas phase and particle phase were collected by an in-house auto-sampler at WM-

MR-RU (Figure 2.1 left panel and Figure 2.2) and EL sampling sites (Figure 2.1 right panel) from 24 Jan to 18 April 2017. A summary of sampling information is shown in Table 2.1.
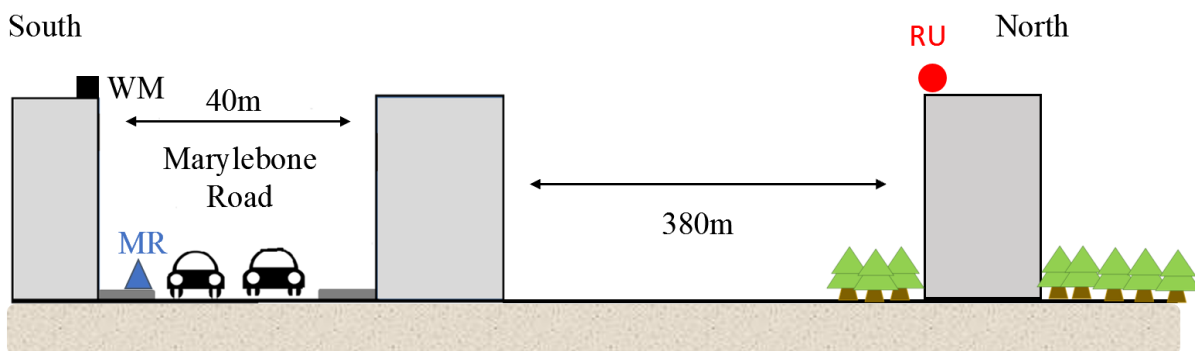
Figure 2.2: A schematic diagram shows the locations of WM, MR and RU sampling sites.

University of Westminster (WM)

Air samples were collected between 24 Jan 2017 and 19 Feb 2017 on a roof of the University of Westminster above the heavily trafficked Marylebone Road. The Marylebone Campus of the University of Westminster is located on Marylebone Road directly opposite Baker Street underground station. Sampling instruments were sited on the roof of a building (around 26 metres high) at the south side of the road overlooking the ground level Marylebone Road (MR) monitoring station.

Regent's University (RU)

Simultaneous measurements were conducted on a roof (around 16 metres high) of Regent's University (RU) from 24 January 2017 to 19 February 2017. Regent's University is located to the south of the Inner Circle of Regent's Park, where a 166-hectares (410 acres) park is lies

within north-west London. The site is located away from local roads and is about 380m north of heavily-trafficked Marylebone Road, which is the nearest major highway.

Marylebone road station (MR)

Samples were collected in a kerbside cabin on the south side of Marylebone Road directly below the WM monitoring site from 22 March to 18th April 2017. Marylebone Road is the nearest road, which is approximately 1 metre from the station. Marylebone Road has three traffic lanes for each direction, and the traffic flow is over 80,000 vehicles per day pass the site with frequent congestion. The surrounding buildings are education buildings, shops and tourist attraction, and housing, forming a street canyon. The instruments were housed in a large cabin placed on the sidewalk of Marylebone Road with an inlet around 2.5 metres above ground level.

Eltham (EL)

Samples were collected in an urban background site Eltham (EL) from 23 Feb to 21 March 2017. The monitoring site is located in the south-east of London. The nearest road A210 Bexley Road is approximately 25m to the south of the site. There is a small car park next to the monitoring station, and the surrounding area consists of lawn, trees, ponds, housing and a nearby golf club.

	WM	RU	EL	MR
Date	24/01/2017- 19/02/ 2017	23/02/2017- 21/03/2017	22/03/2017- 18/04/2017	
Number of valid samples*	27	27	19	25

*The valid samples are the samples used for data analysis. The invalid samples are samples that did not show reasonable chromatograms due to the potential contamination during the transport, storage and extraction processes.

Table 2.1: A summary of the sampling information.

2.1.2   S/IVOC sample collection
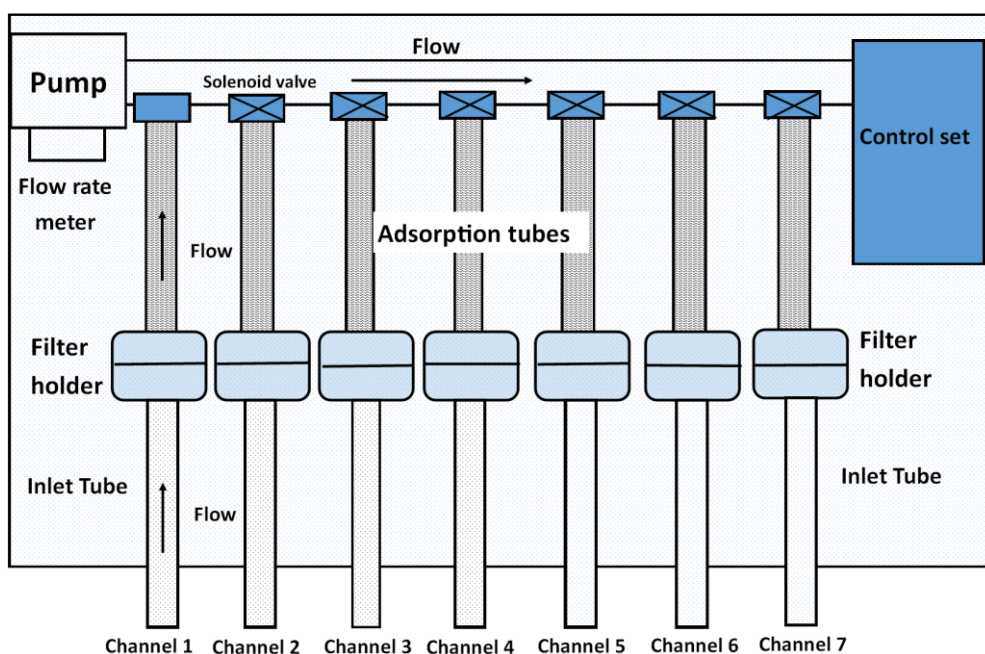
Figure 2.3: A schematic diagram of the in-house auto-sampler when the instrument is working on channel 1. Filter holder contains a PTFE filter inside to collect the particle phase, and an adsorption tube behind the filter holder is set to collect the gas phase samples.

An in-house auto-sampler was designed to collect 24h duration samples for continually seven days (Figure 2.3). The sampler has seven channels and one channel run for 24 hours. It would be turned to next channel automatically after 24h. A vacuum pump draws air through a polypropylene backed PTFE filter (47mm, 1μm pore, Whatman, Maidstone, UK) to collect the particle phase, and then through a stainless-steel thermal adsorption tube packed with 1cm quartz wool, 300mg Carbograph 2TD 40/60 (Markes International) to collect the gas phase. A flow rate meter is set to control the flow rate, which was set as 1.5 L/min during the field measurement. A calibrator (Gilian Gilibrator-2 NIOSH Primary Standard Air Flow Calibrator, SENSIDYNE, Schauenburg, German) was applied to measure the flow rate at the inlet to ensure the flow rate is consistent with the reading of the flow rate meter. After 24h duration sampling, filters were transferred to pre-cleaned filter cases which are then enclosed with aluminium foil. Adsorption tubes were capped properly. Both filter cases and tubes were stored under conditions of approximately –18℃ prior to extraction and GC×GC-ToF-MS analysis.

2.1.3 Adsorption tube breakthrough test

Adsorption tube breakthrough was evaluated with two tubes in series (Figure 2.4). The vacuum pump draws air through the particulate filter (PTFE) to stop the particle phase S/IVOCs from being collected onto the adsorption tubes, and then through the thermal adsorption tube A and B to test the breakthrough issue. The sampling pump is attached to the exhaust end of the back-up tube.
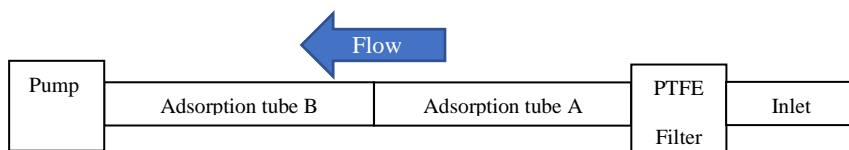
Figure 2.4: Breakthrough test settings.

The breakthrough percentage can be calculated by the equation below,

$$Breakthrough\ percentage\ (\%) = \frac{Target\ analytes\ in\ tube\ B}{Target\ anlytes\ in\ tube\ A + tube\ B} \qquad Equation\ 2.1$$

If target analytes are collected efficiently on adsorption tube A, then only a minor fraction or no breakthrough (<10%) would be observed in tube B. On the contrary, if a target analyte is presented in adsorption B at >10% of the concentration in adsorption tube A, breakthrough is significant. The compounds that experience >10% breakthrough was removed from analysis and reporting of data in this study. These compounds and corresponding breakthrough percentage include C_{11} alkanes (21%), C_{12} alkanes (>10%), C_{11} monocyclic alkanes (25%), C_{11} bicyclic alkanes (15%), C_{12} bicyclic alkanes (10%), C_9 monocyclic aromatics (30%), C_8 (65%) and C_9 aldehydes (45%), tetralin (13%) and methyl tetralin (15%).

2.1.4 Measurement of BC data

Measurements of the black carbon (BC) content of airborne particles were carried simultaneously with the collection of S/IVOC samples at the roof sites WM and RU by using aethalometers (2 Wavelength Magee Aethalometer AE22). The real-time measurement measures the mass concentration of BC by measuring the light absorbed by suspended particles at two wavelengths, including 370 nm (UV) for measuring the 'UV components' of aerosols

and 880 nm (IR) for quantitating the BC concentrations. Certain organic compound classes (such as aromatics and specific compounds in wood smoke, tobacco smoke and diesel exhaust) would present strong UV absorbance at shorter wavelengths below 400nm; therefore, the 'UV components' of aerosols can be a tracer for fuel/oil emission. A digital keypad with the interface is used for calibration and operation. The BC data were stored on a compact flash within the instrument so that they can be easily transferred to a computer for further analysis.

2.1.5   Network supporting data

Department for Environment, Food & Rural Affairs (DEFRA) (https://uk-air.defra.gov.uk/networks/) is the government department responsible for environmental protection in the UK. DEFRA monitors and reports air pollution in the UK by measuring pollutants at monitoring stations located all over the UK. The sampling sites MR and EL in this study were located in or next to the Marylebone Road and Eltham monitoring stations of DEFRA. DEFRA Automatic Hydrocarbon Network (https://uk-air.defra.gov.uk/networks/network-info?view=hc) measures hydrocarbon data by automatic instruments named as Perkin Elmer gas chromatographs. Hourly concentrations of at least 29 VOCs were measured, including n-alkanes ranging from C_2-C_8 and benzene at Marylebone Road and Eltham. DEFRA black carbon network (https://uk-air.defra.gov.uk/networks/network-info?view=ukbsn) measures black carbon by Magee Aethalometer (AE22) at Marylebone Road. DEFRA Automatic London Network (https://uk-air.defra.gov.uk/networks/network-info?view=aln) measures NO_x in 14 London sites, including Marylebone Road and Eltham. The hourly pollutant concentrations provided by DEFRA network were averaged as 24h duration to keep consistent with this study. DEFRA

North Kensington (NK) monitoring site is an urban background site in London, and the data (i.e. NO_x) from NK were used to represent the urban background level of London.

London Heathrow airport, located west of central London, is the closest station to provide comprehensive meteorological information for the sampling sites above the roof. The Heathrow site is within 25 km of the London sampling sites. Using data from UK sites, Manning et al. (2000) showed that wind data from airfield sites are representative of wind fields up to 40 km from the site. The Heathrow data represent winds above the street canyon; those within the canyon are very different. Harrison et al. (2019) showed diagrammatically the circulations within the Marylebone Road canyon (Figure 4.4). Daily mean wind direction data from London Heathrow airport monitoring station (Met Office, 2006) were used to sort the 24h duration S/IVOC samples into the north wind (N), south wind (S) and undefined wind (Duffy and Nelson, 1996) based on the predominant direction during each sampling interval. As shown in Figure 2.5, the wind angles 300-360° and 0-60° are defined as a north wind while wind angles 120-240° are defined as a south wind in this study. Marylebone Road is a relatively straight road with the direction of west-east. North wind and south wind are both cross-canyon flows, whilst an undefined wind (Duffy and Nelson, 1996) represents the along-street flows, including wind angles 60−120° (east wind) and 240-300° (west wind). The uncertainty of this method is negligible by comparing the wind directions sorted based on west-east axis and Marylebone Road which is around 15° to the west-east axis (Figure 2.1). Temperature information during the London Campaign 2017 was also taken from Heathrow airport station (Met Office, 2006) to represent the temperature at the sampling sites. The temperature in Heathrow is slighter lower than central London (average 1-2℃) due to the influence of urban heat island. The percentage

34

differences in temperature are very small and hence insignificant as the temperature is eventually expressed in Kelvin.

N (300°—60°)

UF
(240°—300°)

UF
(60° — 120°)

S (120° — 240°)
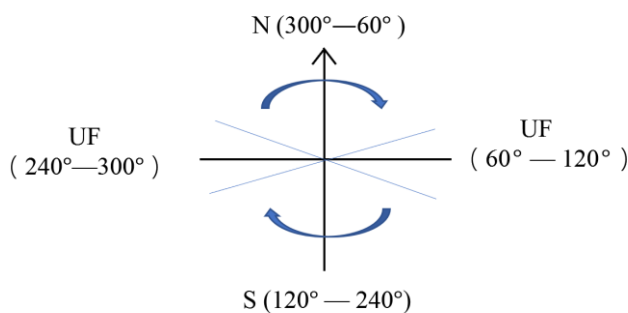
Figure 2.5: Wind direction. It shows the angles of north wind (N), south wind (S) and undefined wind (UF).

2.2 GC×GC-ToF-MS analysis

2.2.1 Comprehensive GC×GC

The most common separation and quantification method is gas chromatography equipped with mass spectrometry detection. Conventional gas chromatography is unable to separate and characterise complex chemical components adequately, presenting an unresolved complex mixture (UCM) within the chromatogram. A two-dimensional separation approach separating compounds in a mixture by volatility and polarity was adopted. Figure 2.6 shows the separation mechanisms used in single-dimensional GC and comprehensive GC×GC analysis. During the first separation of comprehensive GC×GC analysis, chemicals are separated based on their volatility in the first column and then be retained in a cryogenic modulator, which essentially works like a cold trap. The modulator is switched off after the trapping of each fraction and release the retained compounds to inject them rapidly into the second column. The second

column is much shorter and narrower than the first column, result in a much more rapid separation according to their polarity (Dalluge et al., 2002). The raw GC×GC chromatograms can be transformed to generate two-dimensional (2D) chromatograms. The axes of 2D chromatograms represent the retention time of the first-dimensional column and the second-dimensional column respectively. One convenient interpretation way is to view the contour plots where the colours and shading of the peaks represent the intensity of the signal. Peaks or plots are located and identified by their coordinate (first and second retention time) in the contour plots.
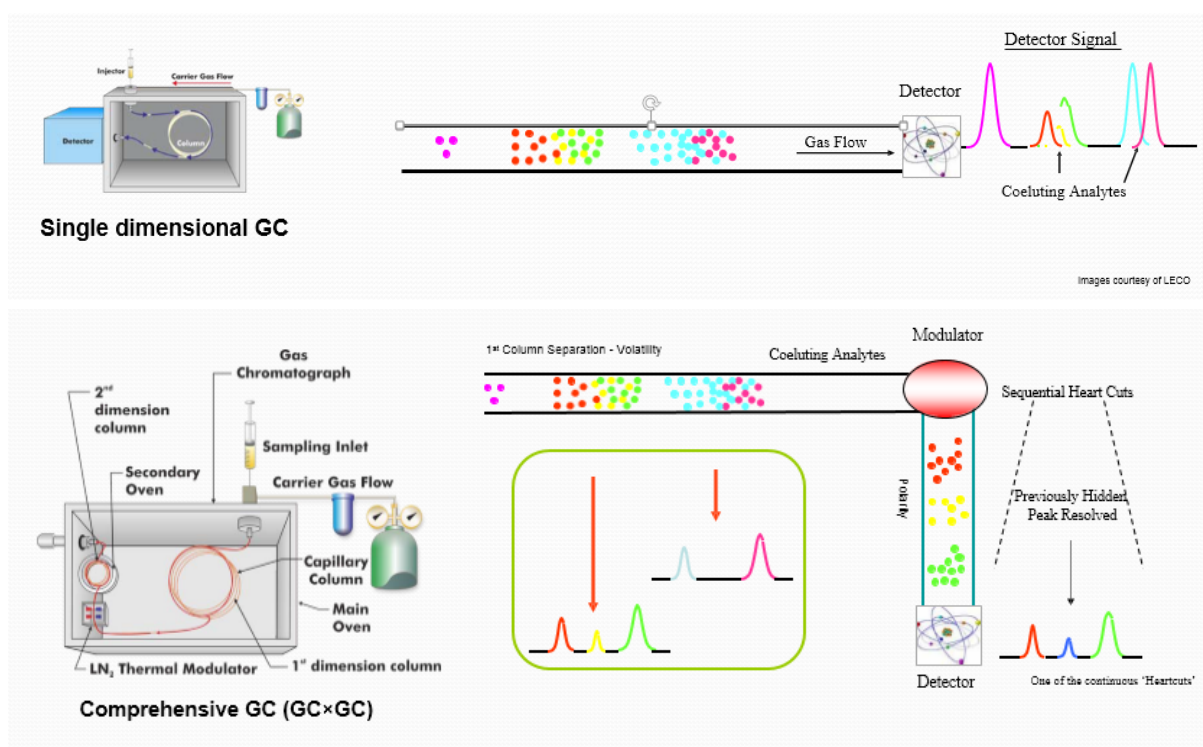
Figure 2.6: Schematic diagram shows the separation processes in single-dimensional GC and comprehensive GC (LECO, 2019).

2.2.2 GC×GC-ToF-MS setting

Analyses were conducted using thermal desorption (Unity 2, Markes International, Llantrisant, UK) coupled to an Agilent 7890B gas chromatograph (Agilent Technologies, Wilmington, DE, U.S.A.) equipped with a Zoex ZX2 cryogenic modulator (Houston, TX, U.S.A.). The first dimension was equipped with a nonpolar capillary SGE BPX5 column (30m, 0.25mm ID, 0.25 μm -5% phenyl polysilphenylene-siloxane). The second-dimension column was SGE BPX50 (4m, 0.1mm ID, 0.1 μm-50% phenyl polysilphenylene-siloxane) (Alam et al., 2016b). The comprehensive GC was coupled with a BenchToF-Select-time-of-flight mass spectrometer (Markes International, Llantrisant, UK) operated with traditional electron impact ionisation at 70 ev. The scan speed was 50 Hz with a mass resolution of >1200 full width at half maximum (fwhm). The GC sensitivity derived from the injection of 1pg octafluoronaphthalene (m/z =272), showing an S/N (signal to noise) ratio of >2000:1 rms (Alam et al., 2016a). A modulation time of 11s was applied while a total run time for each sample was 120min. Subsequent data processing was conducted using GC Image_ v2.6 (Zoex Corporation).

2.2.3 Extraction of samples

The internal standard (IS) mixture contains nine deuterated standards namely, dodecane-d26, pentadecane-d32, eicosane-d42, pentacosane-d52, triacontane-d62, biphenyl-d10, n-butylbenzene-d14, n-nonylbenzene-2, 3, 4, 5, 6-d5 (Chiron AS, Norway) and p-terphenyl-d14 (Sigma Aldrich, UK). The internal standard mixture was used in the extraction process for further identification and quantification.

Gas-phase sample analysis

Adsorption tubes were desorbed using thermal desorption. The tubes were spiked with 1ng of deuterated internal standard for qualification. Then tubes desorbed onto the cold trap at 350°C for 15 min (trap held at 20°C), and then trap released chemicals into the column with a split ratio of 100:1 (split ratio changed based on sampling sites) at 350°C for 4 min. The primary oven was held at the initial temperature 90°C for 2 min and then had an increase of 2°C/min to 240°C, followed by an increase of 3°C/min to 310 °C and held for 5 min. The secondary oven was held at the initial temperature (40°C) for 2 min and then had an increase of 3°C/min to 250°C, followed by an increase of 1.5°C/min to 315°C and held for 5 min. Helium was used as carrier gas at a constant flow rate of 1 ml/min (Alam et al., 2016b).

Particle-phase sample analysis

Whole FTFE filters were spiked with 5 μl internal standards (1ng/μL). Filters were extracted with dichloromethane (HPLC grade), using ultrasonic agitation at room temperature 20 °C for 20 mins. The filtrate was concentrated using a stream of dry nitrogen gas, to a volume of approximately 50 μl. 1μL of the extracted sample was injected with a split ratio of 100:1 (split ratio changed based on sampling sites) at 300°C. The primary oven was held at the initial temperature (120 °C) for 2 min. Temperature increased to 210°C by 2°C per min, and then increased to 325 °C by 1.5 °C per min. The initial temperature of the secondary oven was the same as the primary oven (120°C) but increased at 3°C per min to 200°C, followed by 2 °C per min to 300 °C and a final increase of 1 °C per min to 330 °C to ensure all species passed through the column. The transfer line temperature and the ion source temperature were 330 °C and 280°C respectively. Carrier gas was Helium at a constant flow rate of 1 mL per min (Alam et

al., 2016b). Blank filters were prepared, processed, and analysed in the same manner as the real particle phase samples to mitigate the analytical bias and precision.

2.2.4   Identification of the individual compounds

Comprehensive gas chromatography (GC×GC) equipped with high-speed mass spectrometry provides rich information for identifying the chemical composition of a sample. GC×GC is a powerful technology to separate the chemicals by retention times that is useful for identifying the individual compounds and grouping compounds. A 3D view of the peaks separated by GC×GC in a typical particle-phase London atmospheric sample is shown as Figure 2.7. However, GC×GC does not provide structural information on chemical identification, and one of the greatest challenges is to identify a large number of constituents. Mass spectrometry provides masses of the ionised molecule and its fragment. There are several approaches for the chemical identification with GC×GC-ToF-MS, including library search, pattern matching, and rule-based system (Reichenbach et al., 2005). In library research, sample data are compared with the reference data in NIST (National Institute of Standards and Technology) mass spectral library associated with chemical structure information. In pattern match, data are compared with the pattern of previously observed data to help build the GC×GC retention time templates. Rules-based system expresses the reasons and/or criteria for chemical identification (More details of the rules-based system are shown in Section 2.2.5).

Two match factors are typically used to estimate the similarities between the library records and measured mass spectra, including match factor (Chirico et al.) and reverse match factor (RMF). MF illustrates how well the entire mass spectrum of the selected peak in chromatogram matches the library equivalent, and MF values for positive identification are above 750. RMF

describes how well the mass measured for the selected peak matches the explicit mass present in the library equivalent, and RMF values for positive identification are above 800 (Dalluge et al., 2002; Özel et al., 2010; Alam et al., 2013).
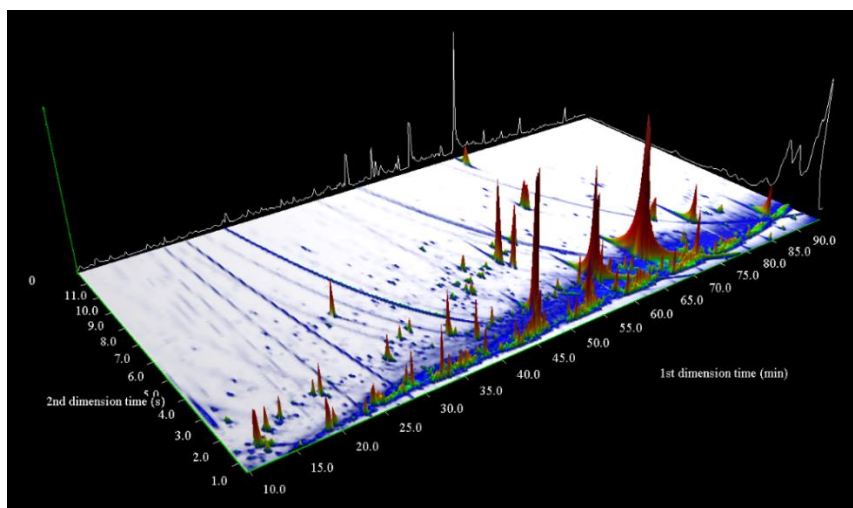
Figure 2.7: A three-dimensional image view of a typical particle-phase atmospheric sample in London produced by GC Image™ software. The white line behind the chromatogram shows the corresponding 1D chromatography.

Although an automated procedure is preferred as there were a large number of data files need to be processed but misidentification may sometimes occur (i.e. when the spectrum of the target compound was not present in the NIST library or the main fragments of two compounds are similar) (Kallio et al., 2006). Manual identification can be more accurate as it allows the researcher to elevate the intensities of the fragments in spectra and the match with the library. The individual compounds identified in this study mainly include n-alkanes, alkyl-cyclohexane and several PAHs. These individual compounds were identified in one sample and saved as a template after manually checked carefully. The automated search was applied to all samples for

saving time and template gave an overview of compounds position on the chromatogram. After that, the individual compounds were manually checked to avoid misidentification.

2.2.5 Grouping of unresolved complex mixture

Recently studies have reported the diesel derived organic compounds are predominantly found from C_{13}-C_{20}, is part of an unresolved complex mixture (UCM) (Dunmore et al., 2015; Alam et al., 2016b). The number of possible structural isomers increases with the increase of carbon atom (Goldstein and Galbally, 2007), and beyond around C_9 it is a challenge to identify the structure of all compounds present in the ambient air (Dunmore et al., 2015). A substantial number of compounds are not able to be identified due to the insufficient data available in the mass spectral library. Compounds did not match with NIST library were further investigated and isomer sets were positively identified based on their retention time. It is possible to assign individual compounds to particular chemical classes and functionalities based on their retention behaviour in comprehensive chromatography. The physicochemical similarities of isomers within the same compound class and their constant changes with the increasing carbon number and molecular sizes enable the further identification of the ordered appearance of compounds in the chromatogram. It allows the identification of species based on both of the unique mass spectral and the pattern of the database. This study grouped the chemical compounds into isomer sets based on their carbon number and functional group (Figure 2.8). Compounds within the same chemical group in a mixture have similar physicochemical properties, facilitating the identification as they were separated based on the physical and chemical properties.

Linear n-alkanes were identified as having a well-defined m/z 57 fragment ion and molecular ions. The area between two consecutive linear alkanes (usually carbon number $\pm$ 1) was

integrated to give an estimate of the total alkanes (linear and branched alkanes) within this volatility range with a specific carbon number. The graphics of monocyclic alkanes were built based on the same theory for alkanes. Alkyl-cyclohexanes were identified based on the well-defined m/z 83 peak and their molecular weight. The area between two consecutive alkyl-cyclohexanes was integrated to estimate the total monocyclic alkanes with that carbon number. The boundaries are shown on a contour plot (chromatogram) in Figure 2.8, where for example, the least polar homologues are alkanes, increasing in carbon number with the increase in the first retention time. For instance, C_{12} alkane group comprises of n-alkanes and branched alkanes with 12 carbon atoms. The retention behaviour facilitates to locate more homologous series with higher polarity on the chromatogram, such as aromatics. GC×GC has clear advantages over the tradition 1D case. The considerable peaks with a higher second dimension retention time (polarity) in Figure 2.8 that would co-elute with the aliphatic groups if the retention window is co-sampled (Dunmore et al., 2015).
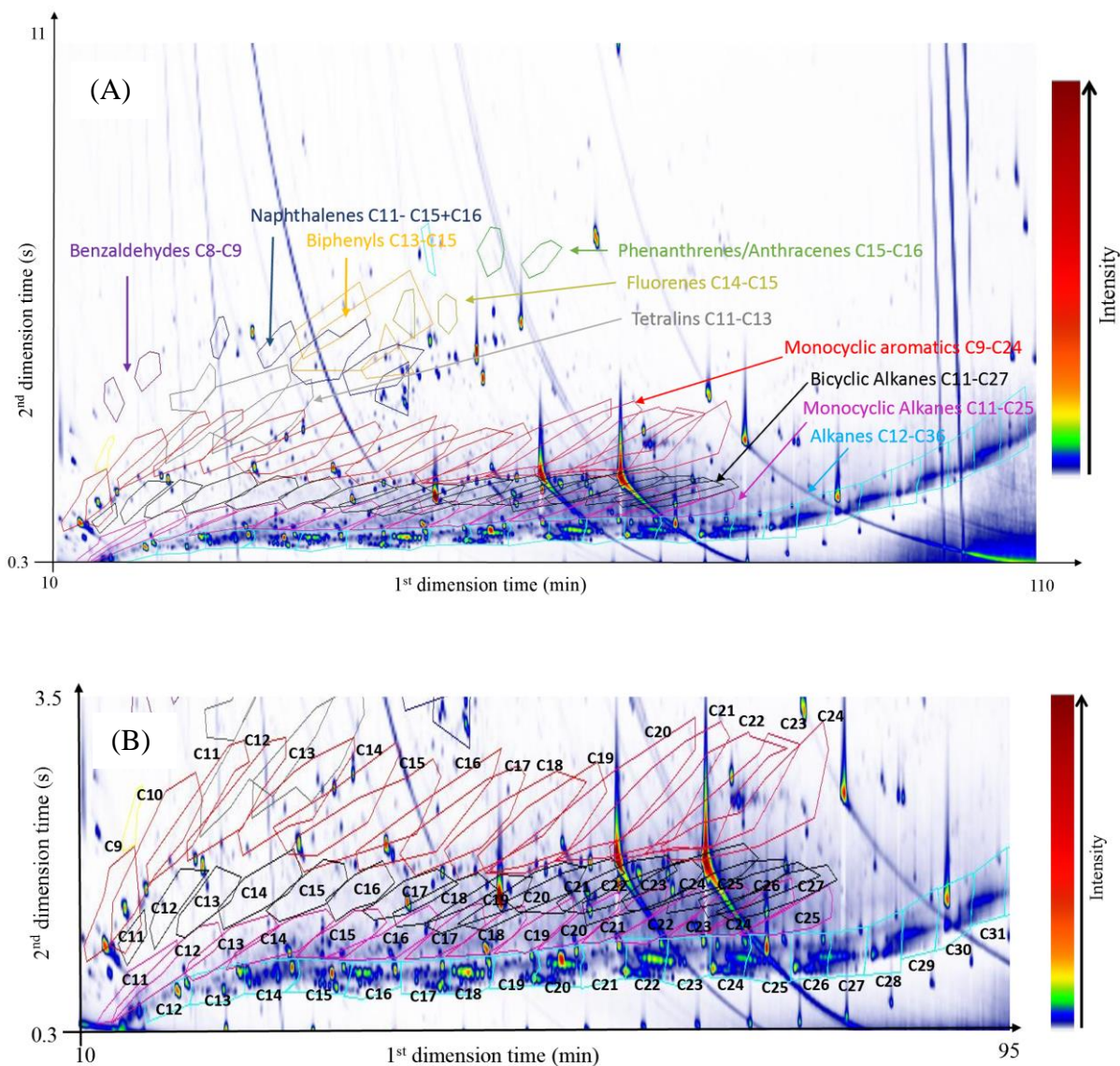
Figure 2.8: Typical GC×GC-ToF-MS chromatogram of a particle-phase air sample. It demonstrates the grouping of compounds within a sample collected on the roof of the University of Westminster (WM) in Feb 2017. X and y-axis are the retention time on the first and second column respectively, with the intensity of the compounds shown by the coloured contours. Colder colours (i.e. blue) are less intense than the warmer colours (i.e. red). Each coloured spot represents an individual compound and has the corresponding full mass spectrum. (A) A contour plot (chromatogram) displays C_{12}-C_{36} alkanes, C_{11}-C_{25} monocyclic alkanes, C_{11}-C_{27} bicyclic alkanes, C_9-C_{24} monocyclic aromatics, C_8-C_9 benzaldehydes, C_{11}-C_{16} naphthalenes, C_{13}-C_{15} biphenyls, C_{15}-C_{16} phenanthrenes/anthracenes, C_{14}-C_{15} fluorenes and C_{11}-C_{13} tetralins. Each region fenced by a coloured polygon marks out the grouped isomers of a chemical

homologue with a particular carbon number. (B) A zoomed-in contour plot displays the carbon number distribution of grouped alkanes (blue), monocyclic alkanes (pink), bicyclic alkanes (black) and monocyclic aromatics (red).

A significant problem in mapping the boundaries for each group is the overlapping of one carbon number group into the left-right adjacent group in one homologue (i.e. carbon number ±1) and the overlapping of two up-down adjacent homologues (i.e. monocyclic alkanes and bicyclic alkanes). Reichenbach et al. (2005) developed a language called the Computer Language for Identifying Chemicals (CLIC) for chemicals identification with comprehensive two-dimensional gas chromatography and mass spectrometry. CLIC allows expressions that describe rules and constraint on multiple retention times and mass fragmentation patterns (Reichenbach et al., 2005). CLIC expression was applied in this study to allow for a more stringent grouping of the isomer sets depending on their functional properties and mass spectrometric factors rather than retention behaviour only. This method identified each individual compound belonging to the appropriate compound class. The polygon selection tool within the GC Image software allows to only involve the compounds that meet the specific rules set for the polygon (Alam et al., 2018). Any peaks within the overlap area were forced to belong to the supposed compound class over another via a strict selection of mass fragmentation and molecular ion. An example of CLIC expression used for identifying C_{10}-substituted monocyclic aromatics is shown as Figure 2.9. In this study, the rules that CLIC expression set for the polygons of alkanes, monocyclic alkanes, bicyclic alkanes and monocyclic aromatics mainly depended on their retention times and molecular ions. The CLIC expression used for tetralin, biphenyls, fluorene and phenanthrene/anthracene was more complex, and examples were illustrated in the Appendix B CLIC expression.

Previous FASTER work has investigated the same isomer sets within the diesel fuel, lubricating oil and diesel emissions (gas phase and particle phase separately) by the same analysis techniques (Alam et al., 2018). The previous study employed the mass spectrometry not only with traditional ionization energy (70 ev) to compare the mass spectral patterns with libraries, but also with a lower ionization energy (10–14 eV) to explore the compounds with less fragmentation, hence retaining a larger fraction of the molecular ion and thus a better identify on the molecule (Alam et al., 2016a; Alam et al., 2018). The comparison between the mass spectra patterns resulted by 14 and 70 ev ionization benefited the identification of unknown species in diesel emissions and provided a reference of the identical retention times for a given species for this study. The polygon boundaries were established independently on the diesel fuel/emission chromatograms (Alam et al., 2018) and air chromatograms (this study) to ensure the applicability and reproducibility of mapping based on the identical retention times and interpretative mass spectrum in different samples or different runs. All the polygons can be linked to internal standards and saved as a comprehensive template in the GC Image software (Figure 2.8). Although retention times for both chromatographic dimensions might be different in separate runs due to the column changes or GC×GC maintenance, the overall template can be easily aligned in the event of slight shifts in the retention times (Alam et al., 2018).

GC×GC-ToF-MS analysis identifies 90 S/IVOC groups in atmospheric samples, including 25 alkanes, 15 monocyclic alkanes, 17 bicyclic alkanes, 16 monocyclic aromatics, 2 benzaldehydes, 5 naphthalenes, 3 biphenyls, 2 phenanthrenes/anthracenes, 2 fluorenes and 3 tetralins. Only the compounds within the coloured polygon were integrated, and these compounds accounted for approximately 78% of the total ion current of the chromatogram.
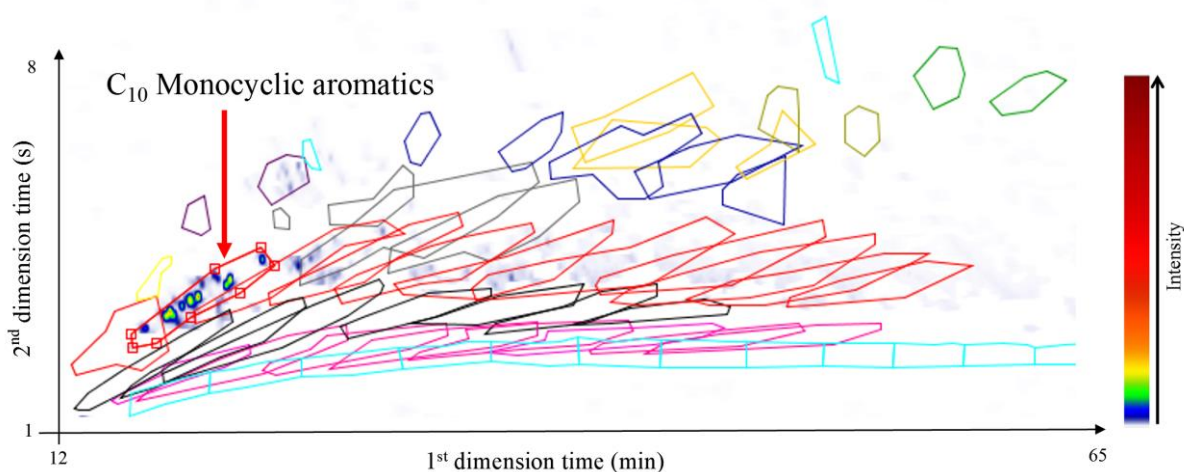
Figure 2.9: A contour plot displays C_{10}-substituted monocyclic aromatics identified by the CLIC expression. All C_{10}-substituted monocyclic aromatics are located within the marked red polygon displayed.

2.2.6 Calibrate the quantification of compounds

The relationship between the amount of target compound and the corresponding chromatographic response must be established before the quantitative analysis in GC×GC system. Natural standards were chosen for calibration and quantification, including n-alkanes (C_{11}-C_{36}), phytane and pristane (Sigma Aldrich, UK), n-alkyl-cyclohexanes (C_{11} -C_{25}), n-alkylbenzenes (C_{10}, C_{12}, C_{14}, C_{16} and C_{18}), tetralin, alkyl-tetralins (methyl-, di-, tri- and tetra-), cris- and trans-decalin, alkyl-naphthalenes (C_{11}, C_{12}, C_{13} and C_{16}) (Chrion AS, Norway) and 13 polycyclic aromatic hydrocarbons (Thames Restek UK Ltd). The term natural standard refers to the ^{1}H isotope of the target compound, in order to distinguish from the deuterated isotope (^{2}D) of the internal standard. The authentic standard mixture (72 natural standards and 9 internal standards) was expected to cover as much of the whole chromatogram as possible and can be applied to calibrate the quantification of target compounds. Briefly, a known amount of authentic standard was injected into the GC×GC -MS system to determine the corresponding

response. A full 5-point calibration was conducted to establish the calibration curve between the amount and chromatographic response of each natural standard.

The relative response factor (RRF) of the target compound can be calculated based on the following equation,

$$RRF = \frac{A_{NAT}}{A_{IS}} \times \frac{C_{IS}}{C_{NAT}}$$
<div align="right">*Equation 2.2*</div>

where A_{NAT} and A_{IS} are the peak area of natural standard and internal standard respectively while C_{NAT} and C_{IS} are the concentrations of natural standard and internal standard respectively. Ideally, the standard deviation of the RRF for a target compound in 5-point calibration should not exceed 10%. The RRF values were used for calculating the concentrations of target compounds later.

2.2.7 Quantification of individual and grouped compounds

Individual compounds were quantified based on the ratio of the chromatographic response and amount of the corresponding natural standards with the same carbon number and functionality. The concentration of target compounds can be calculated based on the equation below,

$$Concentration = \frac{A_{NAT}}{A_{IS}} \times \frac{1}{RRF} \times \frac{M_{IS}}{SS}$$
<div align="right">*Equation 2.3*</div>

where A_{NAT} and A_{IS} are the peak area of natural standard and internal standard respectively; RRF is the relative response factor of target the compound (see Equation 2.2); M_{IS} is the mass of internal standard and SS is the sample size (m^3).

Groups of isomers were quantified by applying the corresponding individual compounds with the same carbon number and functionality as surrogates. For instance, the response for C_{13} n-alkanes (n-tridecane, m/z 184) was used to quantify all isomers identified within the C_{13} alkane polygon. As discussed in section 2.2.5, C_{13} alkane polygon only counts those C_{13} isomers (m/z 184) selected by CLIC expression (based on retention times and mass spectra). The integrated ion current within a single polygon was estimated by using the response ratio of the closest internal standard on chromatogram to the corresponding natural standard with the same carbon number and functionality. The quantification of isomer sets has been discussed in Alam et al., (2018), and they reported the overall uncertainties of this method as 24% by comparing the difference between the concentrations estimated with the authentic standards and generic standards.

Chapter 3 Measured S/IVOCs in the London campaign 2017

This chapter gives a view on the grouped chemical compounds observed in the London Campaign 2017 by showing the S/IVOC chemical composition at four sampling sites. Also, it shows the carbon number distribution of alkanes (n+i), monocyclic alkanes, bicyclic alkanes, monocyclic aromatics and polycyclic aromatic hydrocarbons (PAHs) in the gas phase and particle phase.

3.1 Introduction

Aerosol particles are the unhealthiest components of air pollution and their health effects depend on their size and components (Rissler et al., 2012; Masiol et al., 2012). Vehicles are important emission sources in the urban environment, especially diesel-powered vehicles. The vehicle fleets shift to the diesel-powered vehicles in the UK in recent years, and 50% of the vehicles are diesel-powered in 2014 (Alam et al., 2016b; SMMT, 2015; ExxonMobil, 2014). The majority of traffic emitted fine particles are carbonaceous, directly emitted as primary organic aerosol (POA) or formed as secondary organic aerosol (SOA) (Jimenez et al., 2009). A substantial fraction of the POA from traffic emission is semi-volatile (May et al., 2013; Robinson et al., 2007). The traffic emitted S/IVOCs are mainly comprised of aliphatic species with a carbon number from C_{12} to C_{35} (Alam et al., 2018). The majority of the gasoline emitted hydrocarbons are VOCs (Gentner et al., 2012) while gasoline emitted S/IVOCs mainly have volatility similar to C_{12}-C_{14} n-alkanes and comprise of aliphatic species, aromatics and a large fraction of unspeciated unresolved complex mixture (UCM) (Drozd et al., 2019; Zhao et al., 2016). Only 30% of diesel emitted hydrocarbons are VOCs while most of them are S/IVOCs (Gentner et al., 2012). Jacobson et al. (2005) reported the diesel exhaust contains primarily unburned fuel (C_{15}-C_{23} organics), unburned lubricating oil (C_{15}-C_{36} organics) and sulfate. A

more recent study investigated the separation of engine oil and diesel fuel by GC×GC-ToF-MS and concluded that the diesel fuel contains hydrocarbons up to C_{20} while engine lubricating oil forms UCM at C_{18} to C_{36} (Alam et al., 2016b). It is essential to identify the constituents in diesel fuel and engine oil as both of them derive from engine exhaust emission.

Detailed knowledge of the S/IVOC chemical composition has been limited by the traditional analytical technique gas chromatographic methods, which are unable to separate and characterise complex mixture adequately. The mixture of cyclic, branched and unsaturated hydrocarbons are usually regarded as a part of the unresolved complex mixture (UCM) (Mandalakis et al., 2002). The homologous series that have been studied only represent a small fraction of the total concentrations of S/IVOCs that emit from traffic, leading to the lack of information on their chemical composition and the underestimation of the harmful effects of S/IVOCs on human health.

In this study, samples were collected at four sites in central London, and a comprehensive gas chromatography coupled with time-of-flight mass spectrometry (GC×GC-ToF-MS) provided identification and quantification for the compound classes. This study identified and quantified S/IVOCs from C_{10} to C_{36} to offer a more comprehensive understanding of the chemical composition of S/IVOCs, and particularly to investigate the impact of diesel exhaust emission on urban air. The differences of S/IVOC composition in four sampling sites were compared, and the concentrations of five main S/IVOC groups were presented and discussed in this chapter, including alkanes (n+i) (defined as a sum of linear n-alkanes and branched alkanes), monocyclic alkanes, bicyclic alkanes, monocyclic aromatics and PAHs. The S/IVOC composition identified in the London Campaign 2017 was compared with those reported for diesel fuel exhaust.

3.2 S/IVOC chemical composition

The identified and quantified chemical groups were C_{13}-C_{36} alkanes (n+i), C_{12}-C_{25} monocyclic alkanes, C_{13}-C_{27} bicyclic alkanes, C_{10}-C_{24} monocyclic aromatics, C_{11}-C_{16} naphthalenes, C_{12}-C_{13} tetralins and other species, including C_{13}-C_{15} biphenyls, C_{14}-C_{15} fluorenes, C_{15}-C_{16} phenanthrenes/anthracenes (PHE/ANT). Figure 3.1 shows bar charts and stacked area graphs comparing the organic compound composition, expressed as the relative abundance in total mass concentrations (sum of gas and particle phase) collected at the four sampling sites. Samples were collected on the roof of University of Westminster (WM) above Marylebone Road and a roof of Regent's University (RU) located in Regent's Park simultaneously from 24 Jan to 19 Feb 2017. Acyclic alkanes (n+i) were the most abundant hydrocarbons (52% at WM and 57% at RU) followed by monocyclic alkanes (19% at WM and 17% at RU) and monocyclic aromatics (16% at WM and 16% at RU). Samples were collected at the urban background site Eltham from 23 Feb to 21 March 2017, and after that MR sampling was run from 22 March to 18th April 2017. The chemical composition at EL followed a similar pattern with WM and RU as alkanes (n+i) contributed to 48% of total compounds while monocyclic alkanes occupied the second largest percentage (23%). At MR, alkanes (n+i) were still dominant but dropped to 36% as there were more significant contributions from monocyclic alkanes (24%), bicyclic alkanes (15%) and monocyclic aromatics (18%). Average concentrations of grouped compounds appear in Table S1, and of specific individual compounds in Table S2.

The concentrations of total hydrocarbons collected at four sites were higher in the gas phase (WM 463 ng/m^3, RU 294 ng/m^3, MR 1743 ng/m^3 and EL 837 ng/m^3) than in the particle phase (WM 341 ng/m^3, RU 293 ng/m^3, MR 705 ng/m^3 and EL 548 ng/m^3). Expectedly S/IVOC concentrations at MR were the highest of all sites as it is a heavily trafficked site. The

concentrations of hydrocarbons at the urban background EL were found to be higher than the two roof sites WM and RU, and concentrations at roof site WM were higher than RU. Figure 3.1 shows two major peaks at C_{11} to C_{20} and at C_{21} to C_{28} consistently presented at four sampling sites, similar to the carbon distribution of S/IVOCs observed in diesel exhaust (Alam et al., 2016b; Alam et al., 2018), implying these two peaks may derive from diesel fuel and engine oil respectively.

Few published studies have reported the S/IVOC composition of diesel fuel (mainly below C_{20}) (Isaacman et al., 2012; Welthagen et al., 2007; Gentner et al., 2012; Alam et al., 2018). Gentner et al. (2012) reported the mass distribution of hydrocarbons ranging from C_8 to C_{25} in diesel fuel, demonstrating a sharp peak at around C_{10} to C_{13} and a broader peak at around C_{16}-C_{20}. These peaks were attributed to cycloalkanes and aromatics as alkanes were distributed relatively evenly between C_{10} and C_{20}, which is in broad agreement with the carbon distribution in this study (Figure 3.1). Isaacman et al. (2012) reported that the diesel fuel composition in the carbon number range of C_{15}-C_{25} consisted of 73% aliphatic and 27% aromatics. More specifically, alkanes occupied nearly half (41%) of the observed mass fraction of diesel fuel, followed by 14% cycloalkanes, 11% bicyclic alkanes and 6% benzenes (Isaacman et al., 2012). These results are broadly consistent with the result of Alam et al. (2018), who reported that the diesel fuel which they analysed comprised 62% alkanes (n+i), 14% monocyclic alkanes, 5% bicyclic alkanes, and 5% benzenes.

SVOCs emitted from gasoline- and diesel-powered engines (above C_{20}) are mainly from engine oil (Drozd et al., 2019; Alam et al., 2016b). Studies worked on the chemical composition of engine lubricating oil reported that the most abundant groups were straight, branched and cyclic

alkanes ($\geq 80\%$) and the most substantial contribution was from cycloalkanes ($\geq 27\%$) (Worton et al., 2014; Sakurai et al., 2003). Sakurai et al. (2003) claimed the organic compounds ranging from C_{24} to C_{32} within the diesel exhaust almost entirely came from unburned oil. Worton et al. (2014) reported that the observed chemical composition of vehicle POA (C_{22}-C_{32}) collected in a tunnel was similar to fresh lubricating oil. Liang et al. (2018), also using a GC $\times$ GC-ToF-MS method analysed three motor oils, a mineral oil and a base oil. The motor engine oils (two 5W30 synthetics and one 5W30 semi-synthetic) comprised 5-8% n-alkanes, 24-35% branched alkanes and 30-41% cyclic alkanes with a carbon number distribution peaking at C_{24}-C_{26}. Use of the oils in an engine for up to six months caused a reduction in the overall hydrocarbon content, but little change in the overall distribution of compounds by carbon number (Liang et al., 2018). The chemical composition of diesel fuel and lubricating oil in the literature well explains the overwhelming presence of acyclic alkanes and cyclic alkanes in the urban air samples. The similarities found in the aliphatic and aromatic region above C_{12} in urban air and diesel exhaust demonstrate the impact of diesel-powered vehicles on urban air quality.
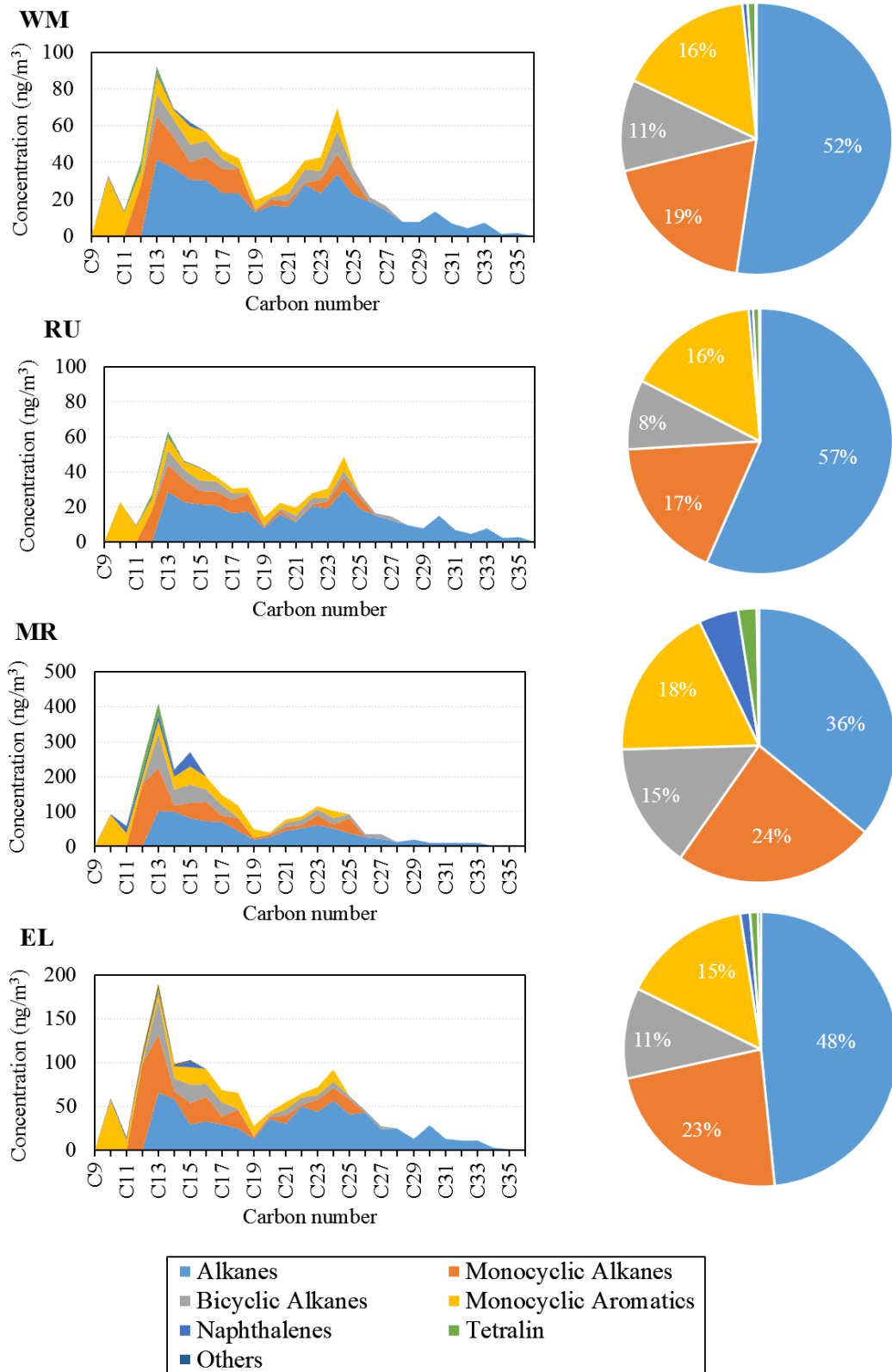
Figure 3.1: The S/IVOC composition (sum of gas and particle phase) identified at WM, RU, MR and EL, London Campaign 2017.

3.3 Alkanes (n+i)
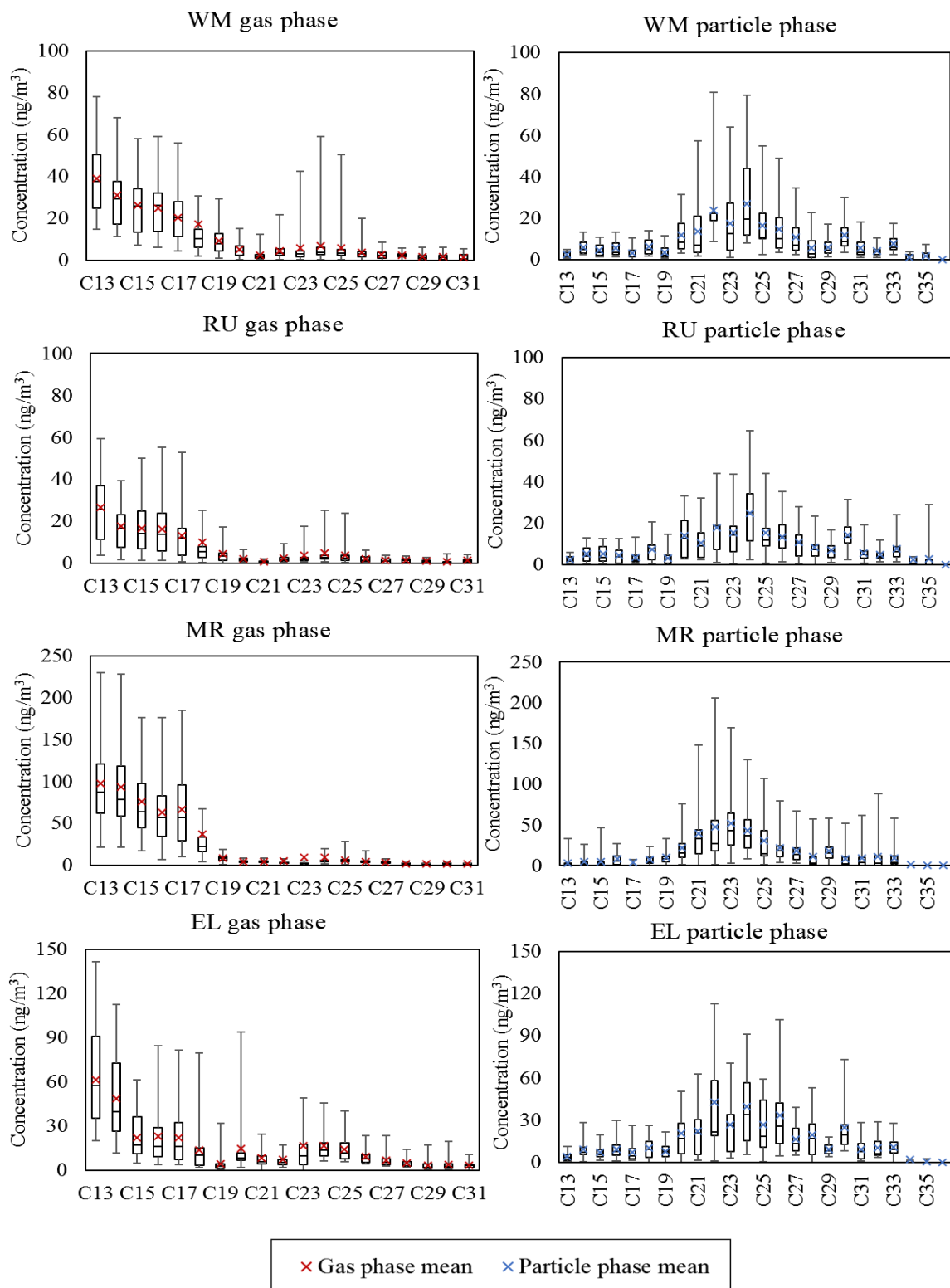
Figure 3.2: Concentrations of alkanes (n+i) in the gas phase and particle phase at WM, RU, MR and EL, London Campaign 2017.

Many studies have worked on alkanes as they are especially suited for investigating the origin and fate of atmospheric aerosols. Alkane constituents are usually the dominant organic components of the atmospheric particles (Alves, 2008). Alkanes can derive from biogenic and anthropogenic sources and can be differentiated based on their carbon preference. Biogenic sources include particles shed from the epicuticular waxes of plants, suspended pollen, microorganisms and insects. Anthropogenic sources include the combustion of fossil fuels, agricultural debris and wood (Rogge et al., 1993d). Thus, alkanes present in all aerosols, including urban, rural area and maritime samples. The abundant presence in aerosols, relatively low reactivity and low volatility make alkanes suitable as monitoring tracers for investigating the origin and transport of particles under the ambient atmospheric conditions (Omar et al., 2007). Alkane classes (acyclic and cyclic) are abundant in gasoline, diesel fuel and lubricating oil; therefore, alkane classes (acyclic and cyclic) are identified as major components of vehicle emitted exhaust (He et al., 2008; Alam et al., 2018).

Alkane (n+i) homologues including linear n-alkanes and branched alkanes were grouped depending on their carbon number. Alkanes (n+i) from C_{13} to C_{31} were detected in the gas phase and C_{13} to C_{36} were detected in the particle phase (Figure 3.2). The low molecular weight C_{13} to C_{18} alkanes were the most abundant homologues in the gas phase, while the homologues above C_{20} were the most abundant in the particle phase. Incomplete combustion of diesel fuel and engine lubricating oil emit alkanes in the range of C_5-C_{34} (Omar et al., 2007). Under the ambient atmosphere, plant wax is the other major contributor to high molecular weight alkanes ranging from C_{25} to C_{37}. In this case, odd carbon numbers are predominant and C_{max} is in the range from C_{25}-C_{33} depending on the plant species and locations (Omar et al., 2007). Carbon preference index (CPI) and C_{max} of n-alkanes are discussed in Section 4.2.

Alam et al. (2018) compared the chemical composition of S/IVOCs identified in diesel fuel, lubricating oil and diesel exhaust (both gas phase and particle phase) by using the same techniques as in this study, suggesting the majority of S/IVOCs identified in the diesel gas-phase exhaust were consistent with the diesel fuel but showed significantly difference in their relative concentrations. Alkanes (n+i) were the most abundant class in the diesel gas-phase exhaust (around 40%) but lower than that for diesel fuel probably due to their preferred combustion. Bearing in mind the substantial vapour contribution to compounds of $\leq C_{19}$, the distribution of the acyclic and cyclic alkane classes (Figure 3.2, Figure 3.3 and Figure 3.5) is very similar to that reported for gas-phase diesel exhaust measured by Alam et al. (2018). The most abundant concentrations of particle-phase alkane classes (acyclic and cyclic) were observed at around C_{21}-C_{27}, consistent with lubricating oil and the particle-phase diesel exhaust. Chan et al. (2013) analysed the particle-phase C_{20}-C_{25} acyclic (linear and branched) alkanes in the urban atmosphere of California and reported a peak at $C_{23,}$ which is similar to the distribution of the particle-phase alkanes in this study.

In the ambient atmosphere, diesel-related hydrocarbon emissions are overwhelming in the gas phase (Dunmore et al., 2015), consistent with the laboratory and tailpipe studies (Gordon et al., 2013). For the roof sites WM and RU, lighter alkanes ($Cn \leq C_{20}$) that may derive from diesel fuel combustion made the greatest contribution to the concentrations of the gas-phase alkanes (around 82%). For the roadside site MR, shorter-chain alkanes ($Cn \leq C_{20}$) occupied a larger fraction of gas-phase alkanes (90%). In contrast to the great contribution to the roadside emission, only 69% of the total gas-phase alkanes at the urban background site EL have carbon atoms of $\leq C_{20}$, indicating the responsibility of other emission sources to the heavier alkanes and/or the possibility that chemical reactions have comsumed the reactive gas-phase alkanes in

the urban background. In the particle phase, the contribution from alkanes ($Cn \leq C_{20}$) that may derive from diesel fuel combustion was significantly lesser (20% for WM, 22% for RU, 17% for MR and 20% for EL) whilst a greater percentage of alkanes were high molecular weight homologues that may derive from engine oil or plant wax.

3.4 Monocyclic alkanes and bicyclic alkanes
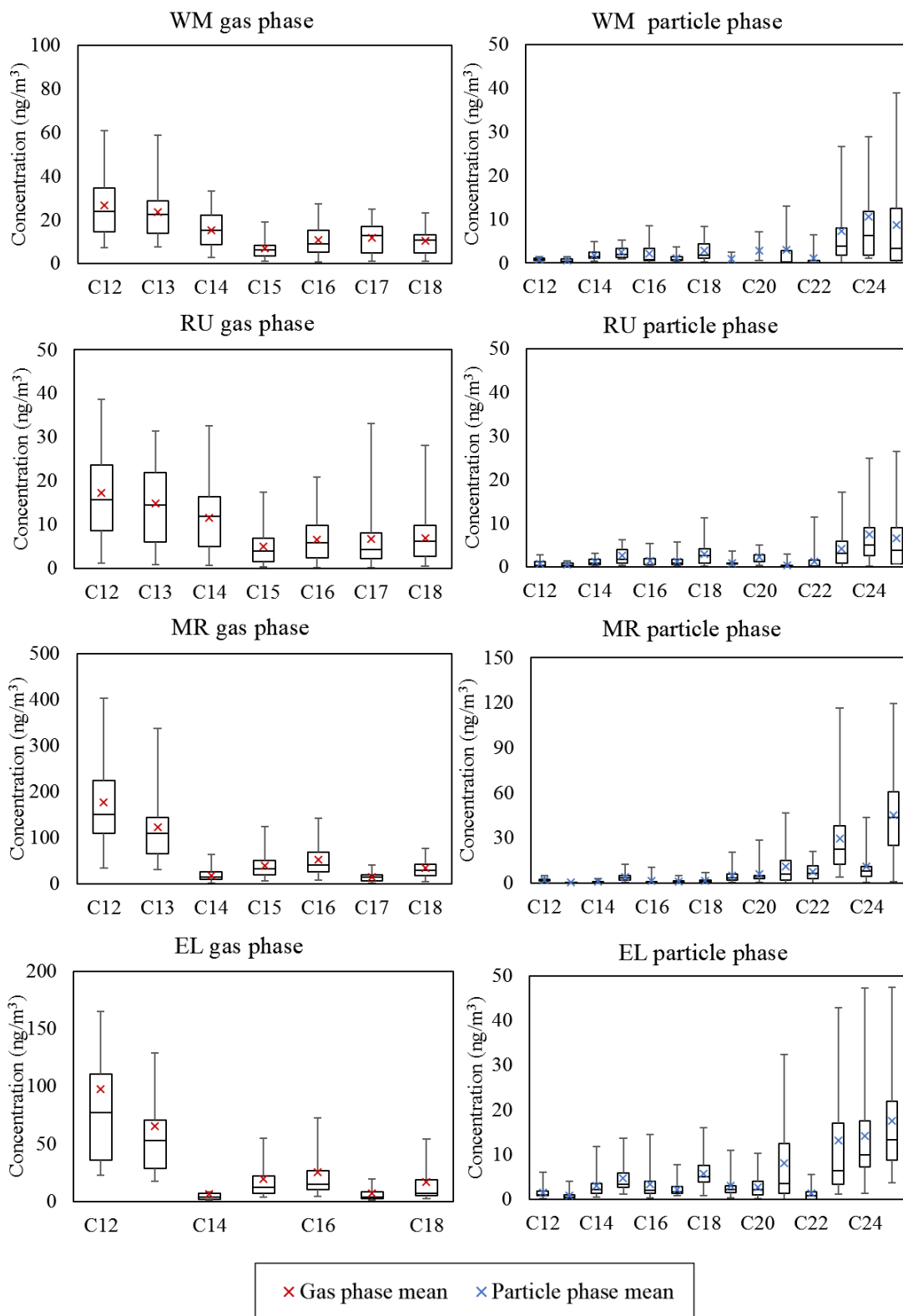
Figure 3.3: Concentrations of monocyclic alkanes in the gas phase and particle phase at WM, RU, MR and EL, London Campaign 2017.

C_n
(n=7,8,9...20)

C_n
(n=6,7,8 ...19)

C_n
(n=5,6,7...18)
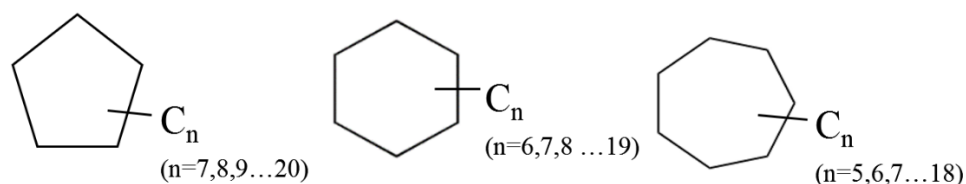
Figure 3.4: Chemical structure of typical monocyclic alkanes observed in this study. From left to right, the monocyclic alkanes are alkyl-cyclopentane, alkyl-cyclohexane and alkyl-cycloheptane (include isomers).

In organic chemistry, hydrocarbons not only exist in the linear chain form but also as rings. The monocyclic alkanes are the saturated hydrocarbons, consisting of only hydrogen and carbon atoms arranged in the structure containing a single ring with single carbon-carbon bonds and alkyl side chain/chains. The chemical structure of bicyclic alkanes contains two rings with single carbon-carbon bonds. In past studies, the mixture of cyclic alkanes and branched alkanes were typically regarded as part of the unresolved complex mixture (UCM) (Mandalakis et al., 2002) or were classified as groups of compounds (Dunmore et al., 2015). This study elucidated the composition of the "traditionally unresolved complex mixture" (UCM) by separating the monocyclic alkanes and bicyclic alkanes components from UCM based on the $GC \times GC$ retention behaviour.

Monocyclic alkanes ranging from C_{12} to C_{18} were detected in the gas phase while C_{12} to C_{25} were detected in the particle phase (Figure 3.3). Alkyl-cyclopentane, alkyl-cyclohexane and alkyl-cycloheptane and their derivatives were dominant in the monocyclic alkane groups (Figure 3.4). Alkenes were observed but not well separated from the monocyclic alkane polygons. The observed alkenes had very low concentration so that the influence of alkenes on

the group concentration was estimated as negligible. Based on the chemical composition analysis of gasoline and diesel fuel, it is unlikely to observe significant alkene quantities in traffic emitted organics (Gentner et al., 2012). Bicyclic alkanes ranging from C_{13} to C_{17} were detected in the gas phase while C_{13} to C_{27} were detected in the particle phase (Figure 3.5). Figure 3.6 shows the chemical structure of the typical bicyclic alkanes detected in this study. Monocyclic alkanes were the second dominant compound class of the S/IVOCs detected in this study and responsible for 17-24% of the total S/IVOC composition (sum of the gas and particle phases) while bicyclic alkanes contributed less to the total S/IVOCs (8% -15%) (Figure 3.1). The majority of the traffic-derived monocyclic alkanes and bicyclic alkanes detected in the gas phase may come from diesel fuel combustion as they are all low molecular weight compounds ($<C_{20}$). Isaacman et al. (2012) reported the semi-volatile organic compound composition of diesel fuel, and cycloalkanes accounted for a more significant fraction of diesel fuel (14%) than bicyclic alkanes (11%), consistent with the urban air samples. Within the monocyclic alkane groups, individual alkyl-cyclohexanes from C_{12} to C_{25} were separated and quantified in this study. Concentrations of alkyl-cyclohexanes presented a similar carbon distribution to grouped monocyclic alkanes and on average accounted for 34% of the monocyclic alkane groups. The detailed concentrations of alkyl-cyclohexanes are shown in Table S2.
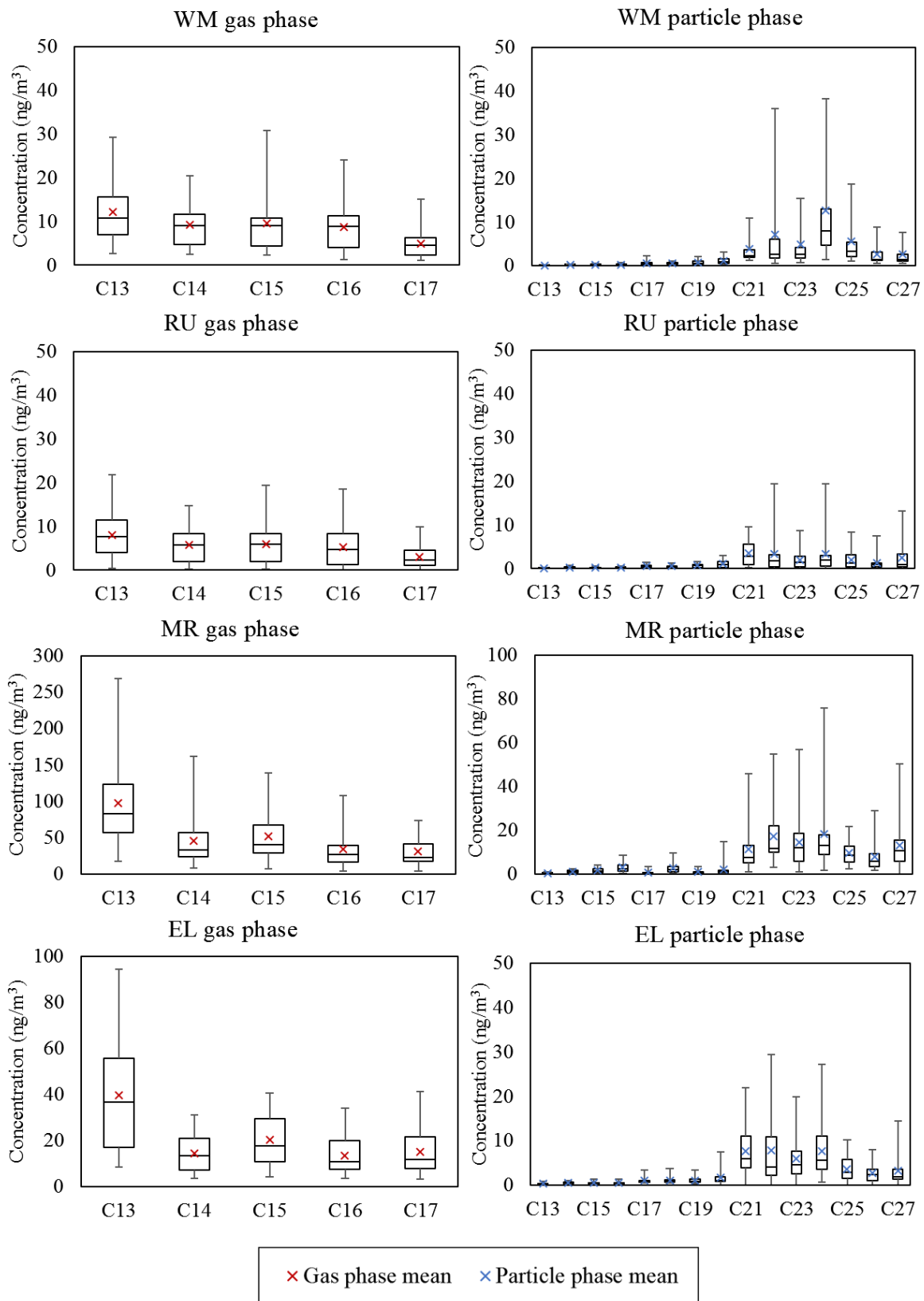
Figure 3.5: Concentrations of bicyclic alkanes in the gas phase and particle phase at WM, RU, MR and EL, London Campaign 2017.
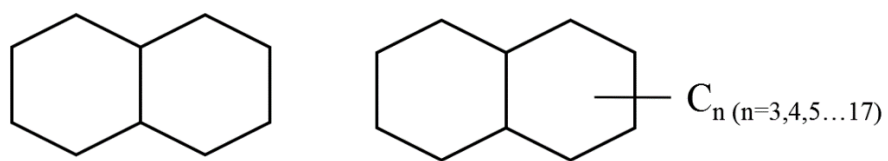
Figure 3.6: Chemical structure of typical bicyclic alkanes observed in this study. From left to right, the bicyclic alkanes are decalin and alkyl-decalin (include methyl-, ethyl-, propyl- etc. and methyl-, dimethyl-, trimethyl- etc.).

3.5 Monocyclic aromatics
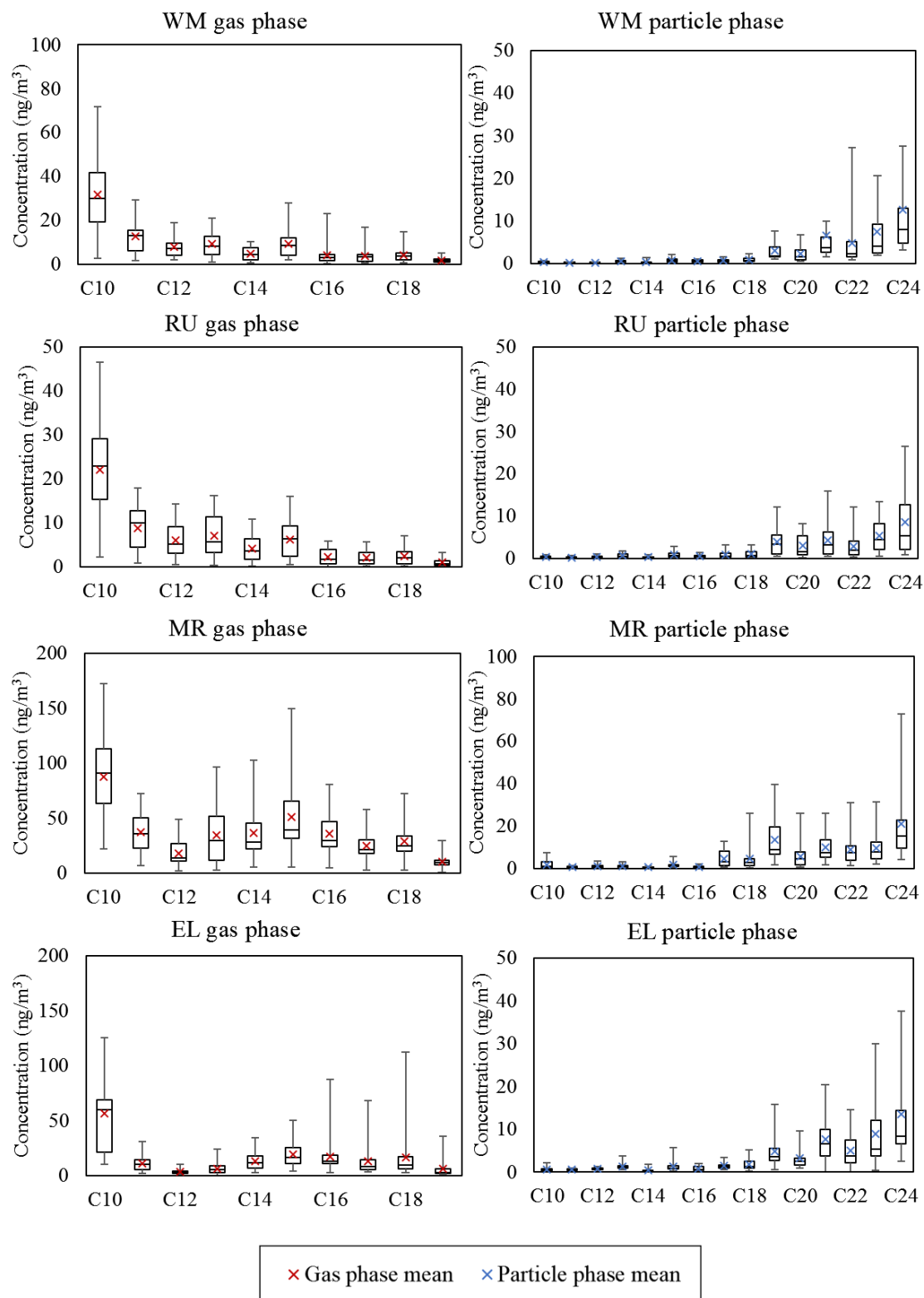
Figure 3.7: Concentrations of monocyclic aromatics in the gas phase and particle phase at WM, RU, MR and EL, London Campaign 2017.

Aromatic hydrocarbons account for a significant fraction of the S/IVOC emitted by traffic in the urban atmosphere (Bailey and Eggleston, 1993; Carr et al., 2002; Hwa et al., 2002). Approximately 30% of the gasoline mass and 20% of the diesel fuel mass are aromatics while the remaining components are mainly comprised by alkane classes (acyclic and cyclic) (Gentner et al., 2013). Monocyclic aromatic hydrocarbons are toxic and some of them are considered as carcinogens, such as benzene (Fernandes et al., 2002). Besides, monocyclic aromatics participate in the photochemical reactions, contributing to the formation of SOA. Monocyclic aromatics, especially benzene, toluene, ethylbenzene, (*m,p*)-and o-xylene (BTEX), have become important targets for assessment. Many recent studies only quantitated BTEX due to the lack of appropriate standards (Kerbachi et al., 2006; Zhao et al., 2004).

The present study has classified the monocyclic aromatics as groups based on their retention behaviour and mass spectrum patterns. Monocyclic aromatics ranging from C_{10} to C_{19} were detected in the gas phase while C_{10} to C_{24} were detected in the particle phase. Monocyclic aromatic homologues occupied the third largest percentage of the total chemicals (16% at WM and RU, 18% at MR, 15% at EL) (Figure 3.1). Concentrations of C_{10} to C_{11} were the highest homologues in the gas phase with a peak at C_{15} while concentrations in the particle phase were steady throughout the carbon range C_{10} to C_{19} and had a slight increase above C_{19} (Figure 3.7). Alam et al. (2018) reported 23.5% and 6% of monocyclic aromatics (C_{11}-C_{33}) in the gas-phase and particle-phase diesel emissions respectively. Monocyclic aromatics ranging from C_{10} to C_{11} represent a large fraction of the IVOC emission of gasoline exhaust (Drozd et al., 2019), suggesting the light monocyclic aromatics in the gas phase may derive from both gasoline- and diesel-powered vehicles. The similarities between particle-phase monocyclic aromatics in

urban air and diesel emissions reported by Alam et al. (2018) imply the contribution of lubricating oil to the emissions of particle-phase monocyclic aromatics.

3.6 Polycyclic aromatic hydrocarbons

Polycyclic aromatic hydrocarbons (PAHs) are more investigated than the other organic classes as some congeners are carcinogenic and/or mutagenic. PAHs are produced in a number of processes in which the incomplete combustion of carbon-containing materials occurs. The major anthropogenic source responsible for the emission of PAHs in the urban environment is fossil-fuel combustion, such as the operation of diesel engines and gasoline engines, incineration, domestic heating and various industrial processes. The natural sources of PAHs include forest fire, microbiological processing of detritus and biosynthesis processes carried by algae, plants and bacteria (Alves et al., 2016; Cincinelli et al., 2007). Atmospheric PAHs in the ambient air can partition between the gas phase and the particle phase, being incorporated onto aerosols via adsorption and condensation processes (Alves, 2008; Leal-Granadillo et al., 2000). Collins et al. (1998) concluded the carcinogenicity of PAHs based on the data from International Agency for Research on Cancer (IARC) and Environmental Protection Agency (DePaul and Sheih), reporting that naphthalene, acenaphthylene, fluorene, phenanthrene, anthracene, fluoranthene, perylene are unclassifiable as to carcinogenicity, whilst chrysene, benz[a]anthracene, benzo[k]fluoranthene, benzo[b]fluoranthene, benzo[a]pyrene are considered to be carcinogenic.

Table 3.1 shows the average concentrations of PAHs in the gas and particle phases observed in the London Campaign 2017. The concentrations of gas-phase PAHs occupied on average 76% to 97% of the total concentrations of PAHs (sum of the gas and particle phases). The main

identified PAHs include naphthalene, acenaphthylene, acenaphthene, fluorene, phenanthrene, anthracene, pyrene, and fluoranthene. The predominant PAHs detected in the gas phase were naphthalene (2 rings), anthracene and phenanthrene (3 rings). Intermediate 4-ring PAHs were distributed between both the gas phase and the particle phase. Fluoranthene and pyrene (4 rings) were relatively abundant PAHs in the particle phase. Fluoranthene and pyrene are reported as dominant PAH compounds in diesel exhaust particles (Mirante et al., 2013). High concentrations of 4-ring PAHs are attributed to enhanced adsorption/condensation of these semi-volatile compounds onto pre-existing particles (Wang et al., 2009; Mirante et al., 2013). Some PAHs with 5 rings were observed only in the air particle phase, such as chrysene, benzo[a]anthracene, perylene, benzo[k]fluoranthene, benzo[b]fluoranthene, benzo[a]pyrene. However, these 5-ring PAHs have not been collected efficiently for data analysis. They had very low concentrations and presented no significant differences among sites; therefore, they are not discussed here.

Table 3.1: Concentrations of individual PAHs (ng/m^3) at the four sites during the London campaign 2017. G indicates the gas phase and P for the particle phase.

		WM		RU		MR		EL	
PAHs	Carbon No	G	P	G	P	G	P	G	P
Naphthalene	C_{10}	0.72	0.05	0.50	0.05	5.26	0.08	3.17	0.00
Acenaphthylene	C_{12}	0.03	0.01	0.02	0.01	4.15	0.01	2.21	0.00
Acenaphthene	C_{12}	0.11	0.01	0.10	0.01	2.97	0.01	2.44	0.01
Fluorene	C_{13}	0.24	0.02	0.18	0.02	4.79	0.03	3.19	0.01
Phenanthrene	C_{14}	1.97	0.04	1.53	0.04	3.11	0.02	2.11	0.01
Anthracene	C_{14}	0.70	0.01	0.59	0.03	0.81	0.02	0.66	0.14
Pyrene	C_{16}	0.83	0.05	0.28	0.06	1.01	0.21	0.73	0.07
Fluoranthene	C_{16}	0.33	0.06	0.21	0.06	0.98	0.11	0.38	0. 01

3.7 Conclusion

Groups of compounds identified and quantified in the gas and particle phase include alkanes (n-alkanes and branched alkanes), monocyclic alkanes, bicyclic alkanes, monocyclic aromatics and several PAHs. Monocyclic alkanes, bicyclic alkanes and monocyclic aromatics were separated from UCM and classified as compound homologues in this study to offer a more comprehensive understanding of the components of UCM. For all sampling sites, alkanes were the most abundant hydrocarbons followed by monocyclic alkanes and monocyclic aromatics. The chemical composition of diesel fuel and lubricating oil reported in the literature (Isaacman et al., 2012; Welthagen et al., 2007; Gentner et al., 2012; Alam et al., 2018; Worton et al., 2014; Sakurai et al., 2003) can explain the overwhelming presence of alkanes, monocyclic alkanes and bicyclic alkanes detected in the urban atmospheric samples in the present study. The chemical composition of S/IVOCs was compared between different sampling sites. Chemical composition of S/IVOCs collected at the roof sites (WM and RU) and urban background site (EL) were similar. At the roadside site MR, alkanes were still dominant but accounted for a lesser fraction of the total concentrations due to greater contributions from other compound classes. As expected, concentrations of S/IVOCs at MR were the highest of all sites as it is a heavily trafficked roadside.

The S/IVOC composition of urban air identified in this study was compared with the S/IVOC composition of diesel fuel, lubricating oil and diesel exhaust (gas phase and particle phase separately) reported by Alam et al. (2018), who investigated the isomers set by using the same techniques as in this study. In the gas phase, the alkane classes (acyclic and cyclic) and monocyclic aromatics of $\leq C_{20}$ were most abundant, similar to the corresponding components reported for gas-phase diesel exhaust measured by Alam et al. (2018). In the particle phase,

alkane classes (acyclic and cyclic) and monocyclic aromatics around C_{21}-C_{27} were most abundant, consistent with those reported in lubricating oil and the particle-phase diesel exhaust measured by Alam et al. (2018). The main fraction of heavier SVOCs ($\geq C_{20}$) emitted from gasoline- and diesel-powered engines can be attributed to engine oil (Drozd et al., 2019; Alam et al., 2016b), suggesting these compound observed in the urban air may derive from engine lubricating oil. The PAH concentrations are reported only for compounds for which collection was quantitative. The most abundant PAHs observed in the gas phase were naphthalene (2 rings), anthracene and phenanthrene (3 rings) while the relatively abundant PAHs in the particle phase were fluoranthene and pyrene (4 rings). The similarities found in S/IVOC C_{12}-C_{36} region in urban air and diesel exhaust proved that diesel-powered vehicles could play a crucial role to influence the urban air quality in London.

Chapter 4 Emission sources and transport of S/IVOCs

This chapter discusses the diagnostic ratios of n-alkanes (CPI, %WNA and C_{max}), correlations between traffic indicators (BC, NO_x and benzene) and main S/IVOC classes, spatial distribution of S/IVOC concentrations at the WM-MR-RU sampling sites, and the effect of wind direction on the S/IVOC transport in the street canyon of Marylebone Road. This chapter aims to investigate the contribution of traffic to the S/IVOC concentrations identified at different sites and the transport of S/IVOCs at the WM-MR-RU sampling sites.

4.1 Introduction

Previous studies of the organic chemical composition of particles based on traditional GC analytical techniques have usually regarded n-alkanes as research targets as they can be distinguished from the bulk of unresolved complex mixture (UCM) (Alam et al., 2016b; Schauer et al., 1999; 2002). Diagnostic ratios of n-alkanes have been widely used in previous studies as the homologue distribution is strongly related to the formation mechanism of organic aerosols (Simoneit et al., 2004; Andreou and Rapsomanikis, 2009). The carbon preference index (CPI) and the contribution of wax n-alkanes (%WNA) are critical diagnostic ratios to investigate the emission source of n-alkanes and identify the biogenic contribution from the vegetation. The leaf wax is expected to contribute less to the overall emissions of n-alkanes during this winter-early spring sampling period compared with summer as many local trees are deciduous.

The correlation analysis between traffic indicators (black carbon, NO_x and benzene) and S/IVOCs was carried out in this chapter to investigate the traffic contribution to the S/IVOC

concentrations measured in this study. Fossil fuel combustion is an important source for black carbon (BC) in the urban area of the northern hemisphere while biomass burning can also become the dominant source for BC emission but typically in the tropical area or the southern hemisphere (Pakkanen et al., 2000; Wolff and Cachier, 1998). A number of studies have reported the strong correlation between traffic emission and BC or NO_x concentrations (Watson et al., 1994; Pakkanen et al., 2000; Reche et al., 2011; Charron et al., 2019). BC and NO_x were regarded as indicators for diesel-powered vehicles in this study as substantial emissions of BC and NO_x come from the diesel vehicles in London (Harrison and Beddows, 2017). Approximately 30% of the gasoline mass and 20% of the diesel fuel mass are aromatics (Gentner et al., 2013). It has been reported that the vehicle exhaust is responsible for 70% of benzene near a heavily trafficked road (Kerbachi et al., 2006), and the highest emission is related to the use of gasoline in non-catalytic cars (Sigsby et al., 1987). Benzene was applied to trace the association between the gasoline-powered vehicles and S/IVOC concentrations in this study as gasoline-powered motor vehicles can generate significant quantities of benzene (Harley et al., 2006; Kirchstetter et al., 1996).

Samples were collected at WM and RU simultaneously from 24 January to 19 February 2017, and after that MR sampling was run from 22 March to 18th April 2017. The difference in the sampling period makes less comparability between these sites. The concentrations of organic compounds are typically higher in winter than in summer, attributed to the differences in meteorological parameters as well as the strength of seasonal particulate emissions, such as from residential heating. Besides, the stable weather conditions and a shallow boundary layer in winter contribute to a low atmospheric dispersion. More combustion activities and more inadequate dispersion result in a higher particulate concentration in winter (Gupta et al., 2017).

The significant variation in seasonal concentrations of particles has been reported in several studies (Fu et al., 2008; Pant et al., 2015; Singh et al., 2011; Yadav et al., 2013). In order to have a better understanding of the spatial distribution of S/IVOCs, the initial MR S/IVOC data collected during March-April 2017 were scaled by using BC as a dispersion marker to estimate the MR S/IVOC concentrations during the WM/RU sampling time (January-February 2017). The scaled MR data were used to compare with the WM and RU S/IVOC concentrations to understand the horizontal advection of pollutants from the emission source to the background atmosphere.

Street orientation and the wind conditions strongly influence the airflow within a street canyon. Wind direction is the most crucial factor affecting the flow and mixing processes in the street canyon and the consequent S/IVOC concentrations (arising from emissions within the street canyon) (Kumar et al., 2008). The MR sampling site is located at the southern kerbside of the heavily trafficked Marylebone Road, which is relatively straight and oriented in the west-east direction. The height of the buildings on either side of Marylebone Road is around six storeys, giving the aspect ratio of the street canyon at around 1:1 (Harrison et al., 2019). Typically, winds can set up a single vortex in a regular street canyon with aspect ratio H/W (~1) (H=building height, W=canyon width) when the wind is across the street (wind direction to the canyon axis exceeds 30°) with a wind speed above 1.5 m s^{-1} (DePaul and Sheih, 1985; Kumar et al., 2008). Studies reported that weak counter-rotating secondary vortices might be observed at the street level in deeper street canyons (aspect ratio H/W~2) and third vortices may also be formed in further deeper canyons (aspect ratio H/W~3) (Pavageau et al., 1997; Jeong and Andrews, 2002; Vardoulakis et al., 2003; Pirjola et al., 2012). The vortices are less evident when the wind direction is more parallel to the street axis. The flow can be a combination of

the re-circulating flow and along canyon flows (Kumar et al., 2008; Belcher, 2005). The difference in S/IVOC concentrations during the entire campaign, during southerly wind and northerly wind were compared to investigate the wind effect on the S/IVOC transport in the street canyon of Marylebone Road.

In this study, concentrations of n-alkanes were reported and compared with those reported in the literature. This chapter discusses the diagnostic criteria of n-alkanes as well as the correlation between traffic indicators and S/IVOC groups to identify the traffic contribution to S/IVOC concentrations. Additionally, the spatial distribution of S/IVOC groups at the WM-MR-RU sampling sites and the effect of wind on S/IVOC concentrations were discussed to investigate the horizontal transport of pollutants from traffic (MR) to background atmosphere (RU) and the wind transport of the S/IVOCs in the street canyon of Marylebone Road.

4.2 Concentrations and diagnostic ratios of n-alkanes

The concentrations of grouped alkanes (n+i) ranging from C_{13} to C_{31} in the gas phase and C_{13} to C_{36} in the particle phase have been discussed in Chapter 3. Individual n-alkanes have been separated and identified by GC×GC-ToF-MS in this chapter (Table 4.1). The homologue distribution of n-alkanes correlated well with grouped alkanes (0.5< average R^2 <0.8). The correlation between n-alkanes and total alkanes (n+i) significantly decreased after C_{25} in the gas phase and after C_{31} in the particle phase, indicating that the change in the composition of high molecular weight alkanes (n+i). The number of possible isomers increases with the increase of the number of carbon atom (Goldstein and Galbally, 2007), resulting in a greater contribution of branched alkanes to the high molecular weight alkanes (n+i). Total n-alkanes occupied on average 33% of the total alkanes (n+i) and the branched alkanes accounted for the

rest. Chan et al. (2013) separated and identified linear and branched alkanes ranging from C_{20} to C_{25} emitted from fossil fuel-related sources. The relative ratios of total branched alkanes to linear alkanes reported by Chan et al. (2013) vary greatly from ~1 to >10 between urban sampling sites, which is in broad agreement with this study. Table 4.1 shows the carbon distribution of n-alkanes in the gas phase and the particle phase at four sampling sites. The total concentrations of n-alkanes in the particle phase were lower than the gas phase. The more volatile n-alkanes (C_{13}-C_{18}) were the most abundant homologues in the gas phase while the less volatile n-alkanes (C_{20} to C_{30}) were more abundant in the particle phase, consistent with the carbon distribution of grouped alkanes (n+i). Department for Environment, Food & Rural Affairs (DEFRA) measured n-alkanes ranging from C_2-C_8 at the Marylebone Road (MR) and Eltham (EL) monitoring stations which are the same sampling sites MR and EL used in this study. Figure 4.1 shows the consistency between DEFRA network n-alkanes (C_2-C_8) and GC×GC-MS measured n-alkanes in the gas phase (C_{13}-C_{30}). With the increase of the carbon number, the concentrations of n-alkanes in the gas phase had a downward trend as the low-volatility homologues were partitioning to the particle phase (Figure 4.1).

A summary of the n-alkane concentrations reported in the literature is shown in Table 4.2. The magnitude of n-alkane concentrations measured in this study was similar to that for n-alkanes reported by Cincinelli et al. (2007), Gupta et al. (2017), Nikolova et al. (2016) and Mandalakis et al. (2002) but much lower than those reported by Bi et al. (2003) and Karanasiou et al. (2007). The carbon distribution of n-alkanes in this study (Table 4.1) described a strong similarity to that for n-alkanes measured in Delhi, India (Gupta et al., 2017) and Birmingham, UK (Nikolova et al., 2016) but differed from the gas-phase n-alkane measured in Prato Italy (Cincinelli et al.,

2007) and Athens Greece (Mandalakis et al., 2002), probably due to the different fuel use and road conditions.

Table 4.1: The concentrations, CPI, and %WNA of n-alkanes in the gas and particle phase.

n-alkanes	Gas Phase (ng/m^3)				Particle Phase (ng/m^3)			
Carbon No	WM	RU	MR	EL	WM	RU	MR	EL
C_{13}	19.77	13.91	33.94	40.13	0.90	0.79	1.42	1.23
C_{14}	17.02	10.45	30.31	24.55	1.96	1.59	2.17	2.57
C_{15}	17.03	10.21	37.98	22.15	0.70	0.90	1.55	0.84
C_{16}	16.69	10.35	32.28	16.20	1.13	0.75	3.78	1.84
C_{17}	10.46	6.29	20.72	10.48	0.17	0.31	0.25	0.49
C_{18}	13.78	7.99	29.58	4.84	0.63	0.98	1.37	0.93
C_{19}	3.56	1.64	5.50	1.49	0.92	0.95	3.91	2.05
C_{20}	1.64	0.53	2.42	4.42	0.95	0.97	4.19	1.15
C_{21}	1.36	0.40	2.51	4.57	5.43	2.32	11.87	5.12
C_{22}	1.04	0.43	3.78	5.70	6.85	2.43	13.58	5.04
C_{23}	4.68	2.95	7.48	13.23	5.05	4.16	14.25	4.78
C_{24}	4.01	2.23	7.34	8.28	3.00	2.42	13.22	2.87
C_{25}	2.24	1.33	4.87	6.16	2.78	2.58	8.95	3.98
C_{26}	1.42	0.70	2.68	3.94	2.23	1.83	5.46	3.66
C_{27}	0.71	0.25	1.37	1.99	1.37	1.26	7.75	2.28
C_{28}	0.43	0.16	0.43	1.43	1.10	1.14	6.63	2.19
C_{29}	0.27	0.07	0.18	0.72	2.16	1.58	9.41	1.60
C_{30}	0.23	0.06	0.19	0.56	0.89	1.06	6.53	2.62
C_{31}					0.65	0.83	7.61	0.80
C_{32}					0.63	0.80	8.65	0.06
C_{33}					0.64	0.90	7.75	0.09
C_{34}					0.23	0.67	0.66	0.02
C_{35}					0.35	0.73	0.00	0.12
C_{36}					0.13	0.45	0.00	0.07
$\sum NA$	116.35	69.96	223.57	170.85	40.85	32.41	140.96	46.40
CPI[a]	1.07	1.13	1.05	1.44	1.08	1.17	1.13	1.02
CPI (C_{13}-C_{26})	1.06	1.12	1.04	1.45	0.95	1.10	0.96	1.02
CPI (above C_{25})	1.55	1.80	1.95	1.50	1.59	1.39	1.48	1.03
%WNA[b]	10.93%	11.18%	13.05%	5.59%	18.06%	15.69%	13.68%	20.91%

[a] CPI (C_{13}-C_{30}) for the gas phase and CPI (C_{13}-C_{36}) for the particle phase.
[b] %WNA (C_{13}-C_{30}) for the gas phase and CPI (C_{13}-C_{36}) for the particle phase.
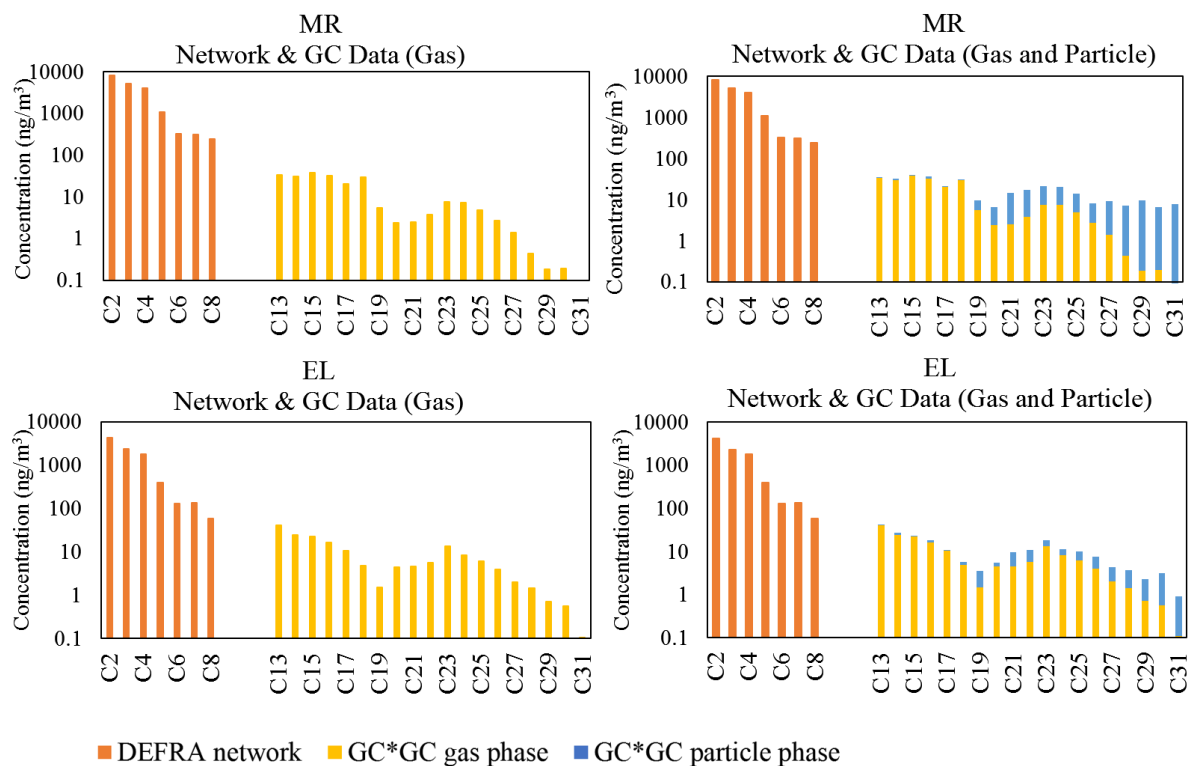
Figure 4.1: Comparison between DEFRA n-alkanes and GC measured n-alkanes in this study. Average concentrations of n-alkanes from DEFRA network (C_2-C_8) and GC×GC-MS (C_{13}-C_{31} in the gas phase and particle phase) at MR from March to April 2017 (top panel) and at EL from Feb to March 2017 (bottom panel).

Table 4.2: A summary of n-alkane concentrations (ng/m^3) in the air samples. Gas and particle indicate the gas phase and particle phase.

Carbon No	Prato Italy (Cincinelli et al., 2007)		Delhi India (Gupta et al., 2017)	Birmingham UK (Nikolova et al., 2016)		Athens Greece (Mandalakis et al., 2002)		Guangzhou, China (Bi et al., 2003)	Athens Greece (Karanasiou et al., 2007)
	Industry area Mar-Nov		Heavily trafficked site Jan-Feb	Busy traffic road (BROS) year 1999/2000		Urban background July		Urban area April	Heavy trafficked central avenue Jun-Jul
	Gas	Particle	Particle (PM$_{10}$)	Gas	Particle	Gas	Particle	Gas and particle	Particle
C$_{13}$								0.51	
C$_{14}$			6			0.83		1.44	
C$_{15}$	3		5			1.83	0.10	2.14	
C$_{16}$	8	<1	4.8	6.42	0.65	3.89	0.15	8.25	
C$_{17}$	16	<1	4	9.32	0.85	4.00	0.09	23.73	
C$_{18}$	23	<1	5	9.36	0.82	5.07	0.10	62.00	87.2±110
C$_{19}$	30	<1	5	9.74	1.32	5.20	0.19	149.28	14.8±6.5
C$_{20}$	32.5	1	6	8.35	1.93	3.92	0.31	226.10	44.6±56.4
C$_{21}$	30.5	1	7.5	6.20	2.63	5.05	0.52	216.23	14.7±6.8
C$_{22}$	24.5	2.5	7.8	3.97	3.25	3.86	0.76	168.07	42.2±46.9
C$_{23}$	18	4.8	12	2.32	2.73	3.97	1.41	117.97	29.8±21.9
C$_{24}$	13	8	17.5	1.59	3.34	2.70	1.50	90.41	57.5±55.3
C$_{25}$	7	14	19	1.20	4.46	2.17	2.71	78.03	55.0±46.7
C$_{26}$	<1	17.5	12	1.00	2.37	1.44	2.35	54.43	65.6±57.8
C$_{27}$	2	22.5	15	1.28	3.61	1.25	5.28	42.97	43.3±36.4
C$_{28}$	1.5	14	11	1.03	1.89	1.13	2.19	32.26	34.0±27.5
C$_{29}$	1.8	18	9	1.24	4.89	1.21	8.25	38.37	25.1±21.0
C$_{30}$	1.5	9	7.5	0.8	2.03	0.98	1.85	25.55	13.6±13.9
C$_{31}$	1.5	18	7.8	0.77	3.60	0.85	8.54	44.05	14.2±15.0
C$_{32}$	1	6	10	0.42	1.32	0.41	1.42	15.89	8.5±14.9
C$_{33}$	<1	6	9.5			0.52	1.23	23.79	10.2±15.8

Several molecular diagnostic parameters were used to distinguish the origin of the n-alkane fraction of organic compounds in the atmosphere. The carbon preference index (CPI) and the contribution of wax n-alkanes (%WNA) are important parameters to distinguish the emission sources of n-alkanes. The carbon preference index (CPI) firstly was defined by Bray and Evans (1961) to investigate the origin of n-alkanes, n-alkanals and n-alkan-2-ones (Simoneit et al., 2004; Andreou and Rapsomanikis, 2009). Carbon preference index (CPI) is the ratio of the summation of odd carbon number homologues over a range to the summation of even carbon number homologues over the same range (Cincinelli et al., 2007; Andreou and Rapsomanikis, 2009; Simoneit, 1999). CPI ratio provides a suitable molecular marker for tracing the organic input of vegetation as plant waxes emit higher molecular weight n-alkanes with odd carbon number predominance. Therefore, n-alkanes from vegetation have higher CPI values (Omar et al., 2007).

In this study, CPI of n-alkanes was calculated based on the following equation,

$$CPI = \frac{Sum\ of\ the\ n-alkanes\ with\ odd\ carbon\ number}{sum\ of\ the\ n-alkanes\ with\ even\ carbon\ number}$$

$$= \frac{\sum(C13-C31)}{\sum(C12-C30)} \qquad\qquad \textit{Equation 4.1}$$

Hydrocarbons emitted from natural sources present CPI of >1 while hydrocarbons emitted from anthropogenic sources (i.e. traffic emission) show CPI values close to or lower than 1 (Simoneit, 1999).

The wax n-alkanes concentration (WNA) is used to estimate the biogenic contribution from the vegetation. WNA for each n-alkane was calculated as followed equation (Simoneit, 1999),

$$WNA\ C_n = C_n\text{-}0.5(C_{n-1} + C_{n+1}) \hspace{3cm} Equation\ 4.2$$

where negative values of WNA C_n were taken as zero. The percentage of total wax n-alkanes to total n-alkanes was calculated followed the equation below (Simoneit, 1999),

$$\%WNA = (\textstyle\sum WAN\ C_n / \sum NA) \times 100\ \% \hspace{2cm} Equation\ 4.3$$

where higher %WNA values indicate a greater contribution from biogenic sources. $\sum WAN\ C_n$ is the total concentration of wax n-alkanes and $\sum NA$ is the total concentration of n-alkanes (Mandalakis et al., 2002; Cincinelli et al., 2007).

The average CPI values were calculated for both the gas and particle phase in each sampling site and can be viewed from Table 4.1. CPI values varied insignificantly at the WM-MR-RU sampling sites in central London. In the gas phase, n-alkanes from C_{13} to C_{31} have been detected in all sampling sites. Average CPI at WM, RU and MR were close to the unity (1.07, 1.13 and 1.05 respectively). Low CPI values and relatively low %WNA (10.93% at WM, 11.18% at RU and 13.05% at MR) specify vehicle emissions in association with the gas phase n-alkanes, and only a minor contribution of n-alkanes originated from epicuticular waxes of terrestrial plants. Gas-phase n-alkanes at the urban background site (EL) had a slightly higher odd carbon number predominance with a CPI value of 1.44 but still close to unity. The lower %WNA (5.59%) at EL shows a lesser contribution of gas-phase n-alkanes originated from plant wax. In the particle phase, n-alkanes from C_{13} to C_{36} have been detected in four sampling sites. CPI values measured for n-alkanes at four sampling sites were close to 1, signifying the major

fraction of particle-phase emissions was attributed to fossil fuel combustion. Although traffic was still the dominant input for the particle-phase alkanes, %WNA values of the particle-phase n-alkanes (18.06% at WM, 15.69% at RU, 13.68% at MR and 20.91% at EL) were higher than the corresponding %WNA values of the gas phase, indicating a greater contribution of biogenic emission sources to the particle-phase n-alkanes. The CPI values above C_{25} are higher than the CPI (C_{13}-C_{26}), especially at WM, RU and MR, suggesting that plant wax made a more significant contribution to the heavier alkanes. The plant wax-derived n-alkanes are typically heavier n-alkanes (above C_{27}) with a strong odd carbon number predominance (Andreou and Rapsomanikis, 2009).

The carbon number of the most abundant alkanes (C_{max}) can also indicate the input source (Mazurek and Simoneit, 1984; Omar et al., 2007). In the gas phase, n-alkanes from C_{13} to C_{31} have been detected with a C_{max} at C_{13}, indicating the characteristic of the fossil fuels residues. In the particle phase, n-alkanes from C_{13} to C_{36} have been detected, and C_{max} values in four sampling sites varied from C_{20} to C_{22}. The low molecular weight C_{max} fits with the interpretation of CPI.

In conclusion, the gas-phase n-alkanes in central London sampling sites (WM-MR-RU) were originated mainly from the vehicular exhaust with a minor contribution from plant waxes, supported by low molecular weight C_{max}, low CPI values, and %WNA. For urban background sampling site EL, there was a lesser fraction of wax n-alkanes in the gas phase, but more in the particle phase compared the WM-MR-RU sampling sites. On the other hand, although traffic was still the dominant input for the particle phase, relatively higher C_{max} and %WAN indicate that more particle-phase n-alkanes were attributed to plant wax compared with the gas phase.

4.3 Correlation between traffic indicators and S/IVOC groups

Correlation analysis was carried out between S/IVOCs (sum of gas and particle phase) with the traffic indicators (BC, NO_x and benzene), and the changes of the correlation coefficient R with the carbon number are shown as Figure 4.2. BC and NO_x were regarded as the traffic indicators of diesel-powered vehicles, as a substantial proportion of BC and NO_x come from diesel vehicles in London (Harrison and Beddows, 2017). As expected, S/IVOC concentrations showed the best correlation with NO_x and BC at the roadside MR, indicating the majority of S/IVOC emissions at MR were attributed to traffic. The buildings prevent the rapid dilution of S/IVOCs emitted from traffic by exchanging with the incoming air in a street canyon. Therefore, traffic emissions can be considered as a dominant source for the pollutants in a street canyon (Wehner et al., 2002). Alkane classes (acyclic and cyclic) correlated well with NO_x and BC, as they were the most abundant observed mass fraction in diesel fuel and lubricating oil (Isaacman et al., 2012; Worton et al., 2014; Sakurai et al., 2003; Alam et al., 2018). Acyclic alkanes (n+i), cyclic alkanes and monocyclic aromatics ranging C_{12} to C_{26} correlated steadily with traffic indicators BC or NO_x with correlation coefficient R up to 0.7, suggesting that BC or NO_x explained around 50% of the variance in the S/IVOC concentrations. The correlation coefficients R of alkanes (n+i) had a slight decrease above C_{26}, suggesting the presence of additional emission sources for high molecular weight alkanes (n+i) at MR, agreed with the CPI results in Table 4.1. Charron et al. (2019) also reported that n-alkanes between C_{19} and C_{26} collected from a near-traffic site had a significant correlation with traffic indicator NO_x and elemental carbon (EC). The n-alkanes emitted from traffic comprise the C_{10}-C_{34} homologues, but n-alkanes ranging from C_{18} to C_{25} are predominant homologues and correspond to the high boiling point components of diesel fuel (Alves et al., 2016). At WM and RU, S/IVOCs ranging from C_{10} to C_{18} also correlated well with BC or NO_x but showed a lower extent than MR. The

diesel vehicle-related S/IVOC concentrations at MR and RU dropped at around C_{18} and tended to be negligible after C_{20}, probably due to the better measurement precision for the lower molecular weight S/IVOC, or possibly due to the traffic source contributing more significantly for $< C_{18}$ compounds.

Diesel vehicles mainly contribute to the emission of unburned diesel fuel (up to C_{20}) and unburned lubricating oil (C_{18} to C_{36}) (Jacobson et al., 2005; Alam et al., 2018) while the gasoline vehicles mainly contribute to the emission of lighter and more volatile molecules (up to C_{12}) (Gentner et al., 2012). The correlation between S/IVOC concentrations and the emission tracer associated with gasoline-powered vehicles (benzene) were also conducted at MR. Benzene is a known toxic contaminant in the ambient air that can be attributed to both gasoline-powered engine (Harley et al., 2006) and diesel-powered engine (Isaacman et al., 2012; Alam et al., 2018). While there is a more complex relationship between the gasoline composition and benzene, as benzene is enriched relative to other aromatics in the exhaust emissions compared to the expectation based on its abundance in unburned gasoline (Harley et al., 2006; Duffy and Nelson, 1996). The additional benzene can be formed in the catalytic converter, especially for the engine under the rich-fuel conditions (Bruehlmann et al., 2005). Benzene may escape from the combustion and oxidative processes in the engine to a greater extent compared with other gasoline components (Kirchstetter et al., 1999; Leppard et al., 1992). Benzene was used to trace the association between the gasoline vehicles and S/IVOCs measured in ambient air. According to the UK emission data, traffic is the dominant source for the traffic tracers used in current study (NO_x, BC and benzene) with minor contibution from other sources that may not affect the roadside air quality significantly, such as waste incineration and chemical industry for benzene, agricultural soil and manure managemnet for NO_x, and waste combustion for BC

(NAEI, 2019). The correlations with benzene for MR are shown in Figure 4.2. Alkane homologues (acyclic and cyclic) and aromatics ranging from C_{12} to C_{18} correlated particularly well with benzene (R=0.7 $\pm$0.14) , but the correlation tended to be weak above C_{18} (R=0.18$\pm$0.2). It suggests that gasoline-powered vehicles mainly contribute to the emission of the low molecular weight compounds, and the much lower correlation for alkanes of > C_{18} for benzene than for BC or NO_x at this site is a clear indication of the predominance of diesel over gasoline emissions for this molecular weight range. It generally agreed with the work of Drozd et al. (2019), who reported monocyclic aromatics ranging from C_{10} to C_{11} accounted for a large fraction of the IVOC emissions in gasoline exhaust. The similarities in S/IVOC profiles in the ambient air of London measured in current study and diesel exhaust measured by Alam et al. (2019b) (average R=0.84) further illustrate the impact of diesel-powered vehicles to the urban air quality. Besides traffic exhaust, other emission sources may also contribute to the S/IVOCs detected in current study, such as tyre and brake lining wear (Rogge et al., 1993; Pant and Harrison, 2013; Kwon and Castaldi, 2012; El Haddad et al., 2009), the use of volatile chemical products (VCPs) (McDonald et al, 2018) and asphalt-related road paving and repair (Khare and Gentner, 2018).
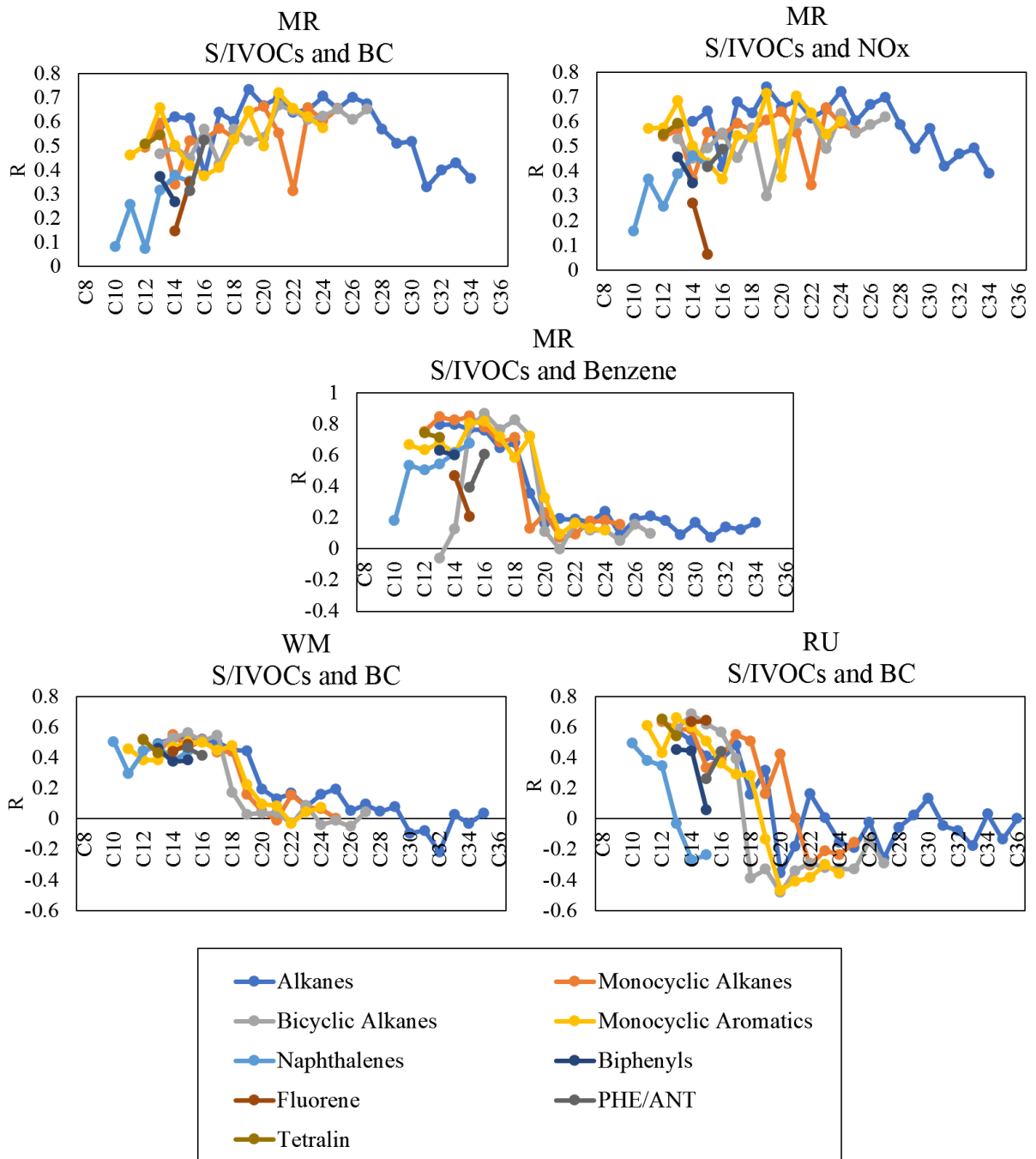
Figure 4.2: Pearson correlation coefficient R between S/IVOCs and traffic indicators at MR, WM and RU.

4.4 Spatial distribution of S/IVOC concentrations at WM-MR-RU

WM-MR-RU sampling sites in central London were applied in this study to investigate the horizontal transport of S/IVOCs from the traffic (roadside site MR) to the cleaner atmosphere of the adjacent park (RU). However, samples were collected during a different period due to a limited number of sampling instruments. Samples were collected at WM and RU simultaneously from 24 Jan to 19 Feb 2017, and after that MR sampling was run from 22 March to 18th April 2017. In order to have a better understanding of the spatial distribution of S/IVOCs, scaling of the initial MR S/IVOC concentrations was applied to estimate the S/IVOC concentrations if MR had been sampled simultaneously with WM/RU (January-February 2017) by taking account of BC as a dispersion marker. In London, BC arises very largely from vehicle traffic (Harrison and Beddows, 2017; Harrison et al., 2019) and the major fraction of BC measured at the roadside site MR is expected to come from traffic emissions. Concentrations of acyclic alkanes (n+i), cyclic alkanes (monocyclic and bicyclic) and monocyclic aromatics ranging C_{12} to C_{28} in the sum of the gas phase and particle phase correlated well steadily with BC at MR during the MR campaign period while there was a weaker correlation for alkanes (n+i) above C_{28} (Figure 4.2). S/IVOCs at MR during the WM/RU sampling campaign were estimated based on the initial MR S/IVOC concentrations multiplied by the ratio of MR BC during the WM/RU sampling period to that during the MR sampling period. Equations were developed as follows,

$$\frac{MR\ S/IVOC_{Jan-Feb}}{MR\ S/IVOC_{Mar-Apr}} = \frac{MR\ BC_{Jan-Feb}}{MR\ BC_{Mar-Apr}} \qquad\qquad Equation\ 4.4$$

Thus,

$$MR\ S/IVOCs_{Jan-Feb}$$

$$= (MR\ BC_{Jan-Feb}/\ MR\ BC_{Mar-Apr})\ *\ MR\ S/IVOCs_{Mar-Apr} \qquad \textit{Equation 4.5}$$

where MR S/IVOCs$_{Jan-Feb}$ is the estimated S/IVOCs at MR (sum of the gas and particle phase) from Jan to Feb 2017 (WM/RU sampling time) while MR BC$_{Jan-Feb}$ is the measured BC at MR from Jan to Feb 2017 (WM/RU sampling time). MR S/IVOCs$_{Mar-Apr}$ is the S/IVOCs measured at MR (sum of the gas and particle phase) from March to April 2017 (MR sampling time); MR BC$_{Mar-Apr}$ is the BC measured at MR from March to April 2017 (MR sampling time).

The concentrations (sum of the gas phase and particle phase) of alkanes, monocyclic alkanes, bicyclic alkanes and monocyclic aromatics at WM and RU during January to February 2017 and estimated concentrations at MR during January to February 2017 are shown in Figure 4.3. The carbon number distribution of hydrocarbons was similar in different sites. Expectedly, SVOC concentrations were the highest at MR as it is a heavily trafficked site. The concentrations of hydrocarbons at WM were higher than RU presumably reflecting a greater distance of RU from the source of emissions.

Results in the current study were compared with a recent gas-phase S/IVOC study (Dunmore et al., 2015) at North Kensington (NK) in London, which is classified as an urban background site by the UK automatic air quality network (Dall'Osto et al., 2011). Dunmore et al. (2015) grouped alkanes, alkenes and cycloalkanes as aliphatic compounds, suggesting approximately 5600 ng/m^3 for C$_{13}$ in January/February. To compare with the NK study (Dunmore et al., 2015), this study summed the gas-phase concentrations of the alkane groups and monocyclic alkane

groups at MR during January-February, reporting a very much lower concentration for C_{13} (282 ng/m^3). The degree of traffic pollution, as represented by the BC concentration was however higher in the Dunmore et al. (2015) study.
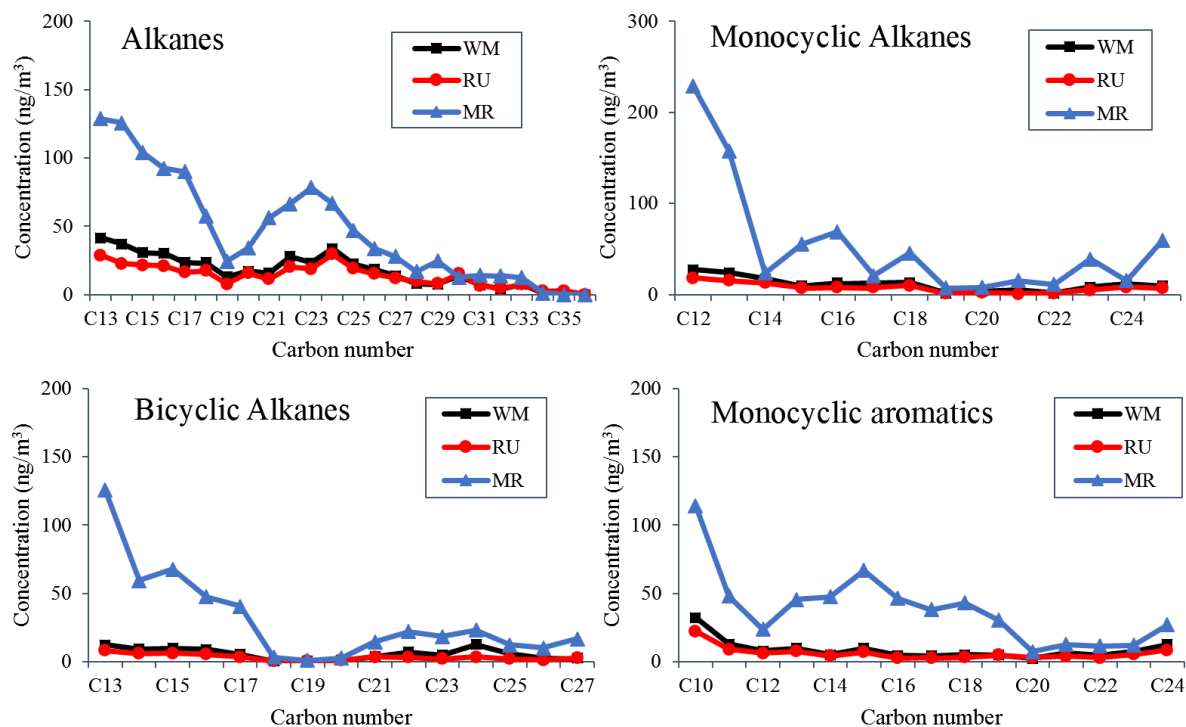
Figure 4.3: Concentrations of S/IVOCs at WM, RU and MR during Jan-Feb 2017. Alkanes (n+i), monocyclic alkanes, bicyclic alkanes and monocyclic aromatics (sum of the gas phase and particle phase) at WM and RU were measured simultaneously from January to February 2017, together with MR data adjusted to match the same period (see text).

4.5 The effect of wind direction in the street canyon of MR

Daily mean wind direction data were used to sort the 24h duration S/IVOC samples into the north wind (N), south wind (S) and undefined wind (Duffy and Nelson, 1996) based on the predominant direction during each sampling interval (See Section 2.1.5). There were 25 daily samples collected at MR, including 8 south wind days, 6 north wind days and 11 mixed-flow days. The average concentrations of the four main S/IVOC groups during the north wind and

south wind have been calculated and compared. In a street canyon, air exchange between the street level and the atmosphere on the rooftop level is limited. The traffic emitted pollutants in the street are not effectively diluted due to the buildings at the roadside. Therefore, the aerosols in the street canyon remain at the street level and result in a high pollutant concentration, especially in winter as a result of a more stable weather condition (Wehner et al., 2002; Gromke et al., 2008).

Figure 4.4 shows the main vortex in street canyon of Marylebone Road (6 traffic lanes) during south wind and north wind, respectively. The pollutants on the street are pushed from the ground level up forwards to the leeward side by the main vortex flow. Small weak vortices may be observed at the bottom side corners of the canyon (Vardoulakis et al., 2003).During the south wind, the sampler at the southern side of Marylebone Road is exposed to the freshly emitted traffic pollutants from the road. Therefore, the concentrations at MR are highest with the south wind when the flow is carrying traffic-produced contaminants efficiently to the MR sampler. During the north wind, the MR sampler is exposed mainly to the incoming air which from the background air from north London, resulting in reduced concentrations of S/IVOCs compared to the average concentrations of the entire campaign. The concentrations of alkanes (n+i) during different wind directions were calculated (Figure 4.5) to investigate the wind effect on the traffic emitted pollutants in the street canyon. The alkane concentrations during the southerly wind were highest, followed by average alkane concentrations during the entire campaign and those during the northerly wind, implying the effect of the vortex on the S/IVOC transport in the street canyon. The hydrocarbon distribution in background north London air was very similar to that in the air heavily polluted by vehicle emissions when the wind was in the southerly sector.
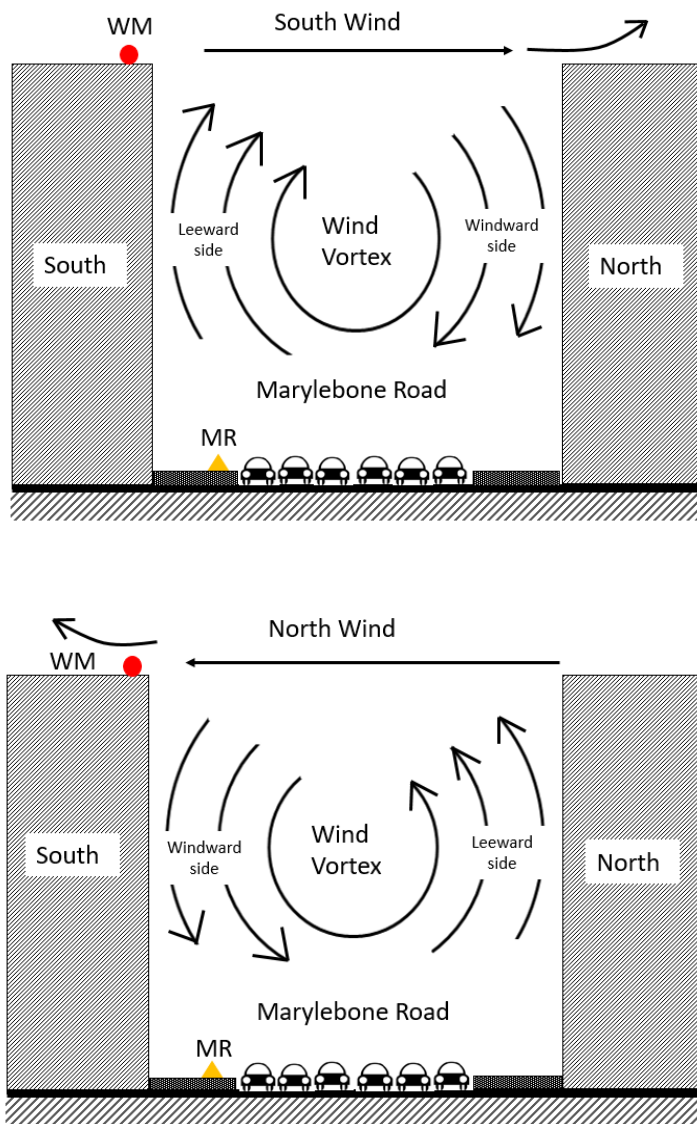
Figure 4.4: A sketch of the wind flows in the street canyon of Marylebone Road (6 traffic lanes) during the southerly wind and northerly wind. The orange triangle marker represents the MR sampling site, and the red round marker represents the WM sampling site (Harrison et al., 2019).
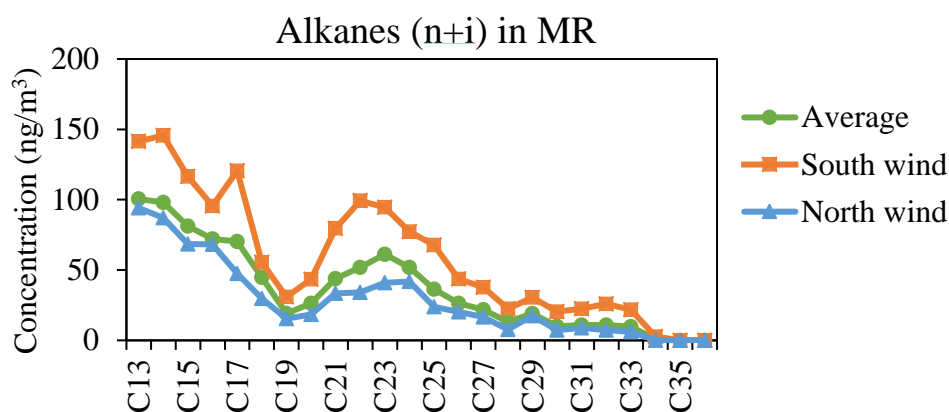
Figure 4.5: The average alkane (n+i) concentrations (sum of the gas phase and particle phase) during the entire MR campaign, southerly wind and northerly wind.

4.6 Conclusion

This chapter reported the concentrations of n-alkanes in the gas phase and particle phase sampled at four sampling sites in London. The magnitude of concentrations and the carbon distribution of n-alkanes measured in this study were consistent with some of the previous studies but differed from the others (Cincinelli et al., 2007; Mandalakis et al., 2002), probably as a result of different fuel use and road conditions. The consistency between the concentrations of low molecular weight n-alkanes measured by DEFRA with those observed in this study (Figure 4.1) gives confidence in the data and illustrates the importance of taking account of compounds of higher molecular weight. With the increase of carbon number, n-alkane concentrations measured by GC× GC (C_{12} to C_{31}) in the gas phase followed the consistent downward tendency with the DEFRA network n-alkanes (C_2-C_8) as the n-alkanes were partitioning from the gas phase to the particle phase.

The diagnostic ratios of n-alkanes (CPI, %WNA, and C_{max}) as well as correlation analysis between S/IVOC groups and traffic indicator suggested that traffic was the major contributor for all four sites with a minor contribution from other sources (i.e., plant wax). Biogenic sources made a slightly higher contribution to those heavier compounds (above C_{25}) and to those measured in the particle phase. More specifically, measured alkanes (acyclic and cyclic) and monocyclic aromatic compounds at MR were mainly attributable to diesel-powered vehicles while a major proportion of the low molecular weight compounds were attributable to the gasoline-powered vehicles.

Direct comparisons of S/IVOCs from MR with those from WM and RU were not carried out due to them being collected in different sampling periods. MR S/IVOC concentrations were scaled by taking account of BC as dispersion marker to assume MR S/IVOCs were collected simultaneously with WM and RU. As expected, concentrations at MR were the highest of all sites as it is a heavily trafficked roadside. The concentration of hydrocarbons at WM was higher than RU as the emissions were diluted more at an increased distance from the traffic emission source. Wind direction can play a crucial role in affecting the flow and consequent S/IVOC concentrations in the street canyon. Winds can typically set up a single vortex in a regular street canyon like Marylebone Road when the wind is across the canyon. The alkane concentrations at MR were highest when the south wind brought the traffic emitted pollutants to the MR sampler, while concentrations were lowest when the north wind brought background air from north London.

Chapter 5 Estimation of the S/IVOC emission factors at the roadside site MR

This chapter describes the estimation processes and results of emission factors (EFs) of the main S/IVOC groups identified at the roadside site MR. Then, a comparison between the estimated n-alkane EFs and those estimated in the literature is carried out.

5.1 Introduction

Road traffic associated emissions are known to make a significant contribution to total particles and vapour concentrations in the urban areas. It is important to understand the characteristics of S/IVOC emissions from vehicles, especially in megacities like London. Measurements on laboratory-based diesel engines (Schauer et al., 1999; Perrone et al., 2014) allow the determination of exhaust emissions under controlled test conditions, but these tests often cover a limited set of vehicles due to the high costs. These tests cannot fully represent the large variation in engine types and driving modes in different environments (Charron et al., 2018), and are not able to give an accurate estimation on the effect of dilution on the gas/particle partitioning of S/IVOCs (Kim et al., 2016), and do not include non-exhaust emissions (Pant and Harrison, 2013). Therefore, estimates deriving from concentration measurements in real-world are considered to offer a realistic simulation for the emission factors, which currently comprise both tunnel and roadside measurements (Hwa et al., 2002; Kawashima et al., 2006; He et al., 2008). The emission factors of S/IVOC groups at MR in 2017 were estimated in this chapter to investigate the vehicle emissions from Marylebone Road (MR). The estimated emission factors of n-alkanes were compared with other published data.

5.2 Calculation processes of the S/IVOC emission factors

NO_x emission factor at MR during the MR campaign 2017 was estimated by scaling the NO_x emission factor at MR in 2002/2003 reported by Jones and Harrison (2006). NO_x is usually regarded as a traffic indicator in London (Harrison and Beddows, 2017; Harrison et al., 2019), especially for the roadside monitoring site MR. The emission factors of S/IVOC groups at MR during the MR campaign 2017 were estimated from the ratio of their emissions to NO_x emissions at MR during the MR campaign 2017. Emissions of pollutants at MR can be estimated by the concentrations measured at MR after subtraction of the background concentrations. Details of calculation processes are shown in this section.

Light-duty vehicles occupied approximately 91% of all vehicles passing Marylebone Road while heavy-duty vehicles accounted for the rest 9%. MR is a congested urban street canyon where vehicle speeds vary greatly over short distances (Jones and Harrison, 2006) and the traffic flow is over 80,000 vehicles per day. Jones and Harrison (2006) estimated the fleet-average emission factor of NO_x at Marylebone Road in 2002/2003 from fleet composition and published emission factors. The NO_x emission factors for heavy duty and light duty (veh^{-1} km^{-1}), the mean number of vehicles (h^{-1}) and the total number of vehicles (h^{-1}) at Marylebone Road in 2002/2003 were listed as followings (Jones and Harrison, 2006),

EF (NO_x) = 5.19 g (as NO_2) veh^{-1} km^{-1} for heavy duty
EF (NO_x) = 0.59 g (as NO_2) veh^{-1} km^{-1} for light duty

Mean number of vehicles (h^{-1}) = 297 heavy duty
2951 light duty

Total number of vehicles (h^{-1}) =3284

It leads the composite emission factor of NO_x can be calculated as followings,

Composite emission factor $= (5.19 \times 297 + 0.59 \times 2951) \div 3248$

$= 1.010$ g (NO_x as NO_2) veh^{-1} km^{-1}

The emission factor of NO_x at MR during the MR campaign 2017 was estimated based on the composite emission factor of NO_x at MR in 2002/2003 (Jones and Harrison, 2006). Daily mean Heathrow wind direction data were applied to sort the entire campaign into days during the northerly wind and southerly wind, and the details were shown as Section 4.5. Figure 4.4 shows the south wind carries the traffic-emitted pollutants efficiently to the MR sampler while the north wind brings the air from the urban background of north London. The differences in the pollutant concentrations during southerly wind and northerly wind were used to estimate the emissions from MR. Table 5.1 shows the NO_x emissions at MR in 2002 and 2003 respectively (Jones and Harrison, 2006), and the mean NO_x emission value during the period of 2002/2003. To estimate the NO_x emission at Marylebone Road during the MR Campaign 2017, this study regarded the average NO_x concentration during southerly wind (326 µg m^{-3}) as the concentration measured at Marylebone Road while the NO_x concentration during the northerly wind (130 µg m^{-3}) as the background level. The emission from MR was estimated as the MR concentration after subtraction of the background concentration (Table 5.1).

95

Table 5.1: The NO_x concentrations at MR and background, and the NO_x emissions from MR (the differences between MR and background concentrations). 2002 and 2003 data come from Jones and Harrison (2006).

Concentration ($\mu g\ m^{-3}$)	2002	2003	2002/2003 Mean	MR Campaign 2017
Marylebone Road (NO_x)	300	314	307	326
Background (NO_x)	66	74	70	130
Emission at MR (NO_x)	234	240	237	196

Based on 2002/2003 data, NO_x EF during the MR Campaign 2017 can be calculated as follows,

EF (NO_x) during the MR Campaign 2017

$$= \text{EF (NO}_x \text{ in 2002/2003) x } \frac{\text{Emission from MR (NOx)in 2017}}{\text{Emission from MR (NOx)in 2002/2003}}$$

$$= 1.010 \text{ x } \frac{196}{237}$$

$$= 0.84 \text{ g (NO}_x \text{ as NO}_2\text{) veh}^{-1} \text{ km}^{-1}$$

The NO_x emission factor at Marylebone Road was estimated as 0.84 g veh^{-1} km^{-1}, based upon the mean NO_x concentrations during the MR sampling period.

S/IVOC EFs were scaled from the NO_x EF at MR during the MR campaign 2017 based on the following equations,

$$S/IVOC\ _{MR\ EF}\ /NO_x\ _{MR\ EF} = S/IVOC\ _{MR\ emission}\ /NO_x\ _{MR\ emission.} \qquad Equation\ 5.1$$

$$S/IVOC\ _{MR\ EF} = NO_x\ _{MR\ EF} \times (S/IVOC\ _{MR\ emission}\ /NO_x\ _{MR\ emission}) \qquad Equation\ 5.2$$

where S/IVOC $_{MR\ EF}$ and NO_x $_{MR\ EF}$ represent the S/IVOC and NO_x emission factors at MR respectively. S/IVOC $_{MR\ emission}$ and NO_x $_{MR\ emission}$ represent the S/IVOC and NO_x emissions per vehicle per kilometre from the MR.

An example of the calculation processes of the C_{13} n-alkane EF (sum of gas and particle phase) at MR during the MR Campaign 2017 was shown as below, and Table 5.2 shows the data that be involved into the calculation. Figure 5.1 shows the difference in n-alkane concentrations during the northerly wind and southerly wind.

EF (C_{13} n-alkanes in gas and particle) at MR 2017 can be calculated based on NO_x at MR 2017:

$$\text{EF (}C_{13}\text{ n-alkanes in gas and particle)} = NO_{x\ EF} \times \frac{C13\ n-alkanes\ MR\ increment}{NOx\ MR\ increment}$$

$$= 0.84 \times \frac{0.011}{196} = 4.7 \times 10^{-5} \text{g veh}^{-1}\text{ km}^{-1}$$

$$= 47\ \mu\text{g veh}^{-1}\text{ km}^{-1} \text{ at MR in 2017}$$

Table 5.2: The emissions of NO_x and C_{13} n-alkane (sum of gas phase and particle phase) from MR in 2017. The emission concentrations (traffic increment) from MR can be estimated as MR concentrations after subtraction of the background concentration.

Pollutants	MR Campaign 2017	Information	Concentration (μg m^{-3})
NO_x	Marylebone Road	NO_x concentrations during the south wind	326
	Background	NO_x concentrations during the north wind	130
	Traffic increment	Difference between the south wind and south wind	196
C_{13} n-alkane	Marylebone Road	C_{13} n-alkanes concentrations during the south wind	0.046
	Background	C_{13} n-alkanes concentrations during the north wind	0.035
	Traffic increment	Difference between the south wind and south wind	0.011
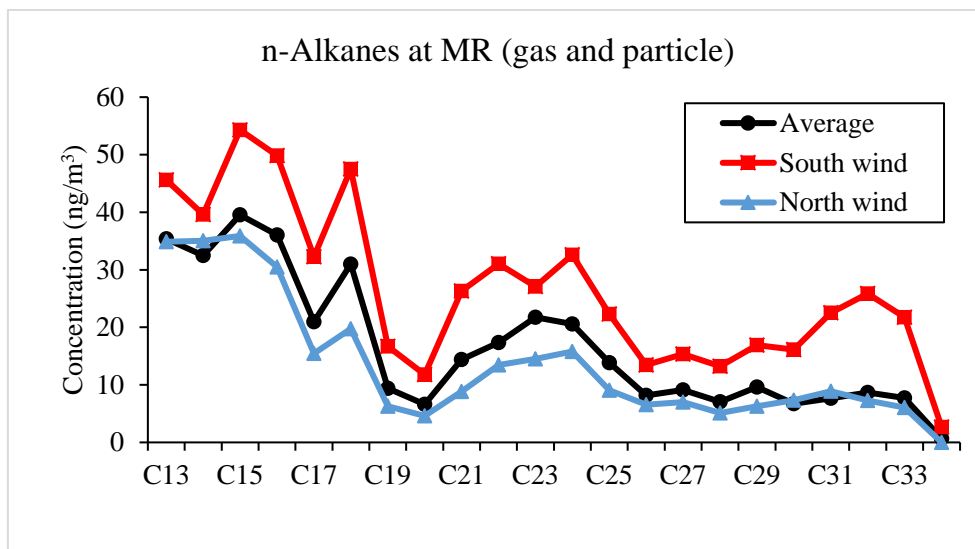
Figure 5.1: The average n-alkane concentrations at MR (sum of gas phase and particle phase) during the entire MR campaign, southerly and northerly winds.

5.3 Emission factors of the main S/IVOC groups

The emission factors of S/IVOC groups identified at MR were estimated. 92% of the gas phase emissions and 99.5 % of the particle phase emissions were contributed by four main classes of compounds, including alkanes, monocyclic alkanes, bicyclic alkanes and monocyclic aromatics (Figure 5.2). Alkane, an abundant S/IVOC class in gasoline, diesel fuel and lubricant oil, was identified as a major component in the particle-phase organic compounds from vehicle emissions (Rogge et al., 1993a; He et al., 2008; Schauer et al., 1999). Particle-phase alkanes (n+i) had the highest total emission factor among all particle-phase compound classes in this study, with a total emission factor of alkanes from C_{13} to C_{31} in the gas phase estimated as 1306 $\mu g\ veh^{-1}\ km^{-1}$, with 1744 $\mu g\ veh^{-1}\ km^{-1}$ from C_{13} to C_{36} in the particle phase. The emissions of monocyclic alkanes, bicyclic alkanes, monocyclic aromatics and naphthalene were more abundant in the gas phase than in the particle phase. Monocyclic alkanes from C_{12} to C_{18} were

detected in the gas phase emissions with a total emission factor of 988 µg veh^{-1} km^{-1} while C_{12} to C_{25} were detected in the particle phase with a total emission factor of 562 µg veh^{-1} km^{-1}. Emission factors of bicyclic alkanes were 511 µg veh^{-1} km^{-1} (C_{13} to C_{17}) in the gas phase and 446 µg veh^{-1} km^{-1} (C_{13} to C_{27}) in the particle phase. Emission factors of monocyclic aromatics were 592 µg veh^{-1} km^{-1} (C_{10} to C_{19}) in the gas phase and 308 µg veh^{-1} km^{-1} (C_{10} to C_{24}) in the particle phase. Naphthalene was the most abundant individual compound among the measured PAHs. Alkyl-naphthalenes were defined as a compound class in this work, and emission factors were estimated based on their total carbon number. The summed emission factors of naphthalenes (C_{11} to C_{16}) were 129 µg veh^{-1} km^{-1} in the gas phase and 15 µg veh^{-1} km^{-1} in the particle phase.
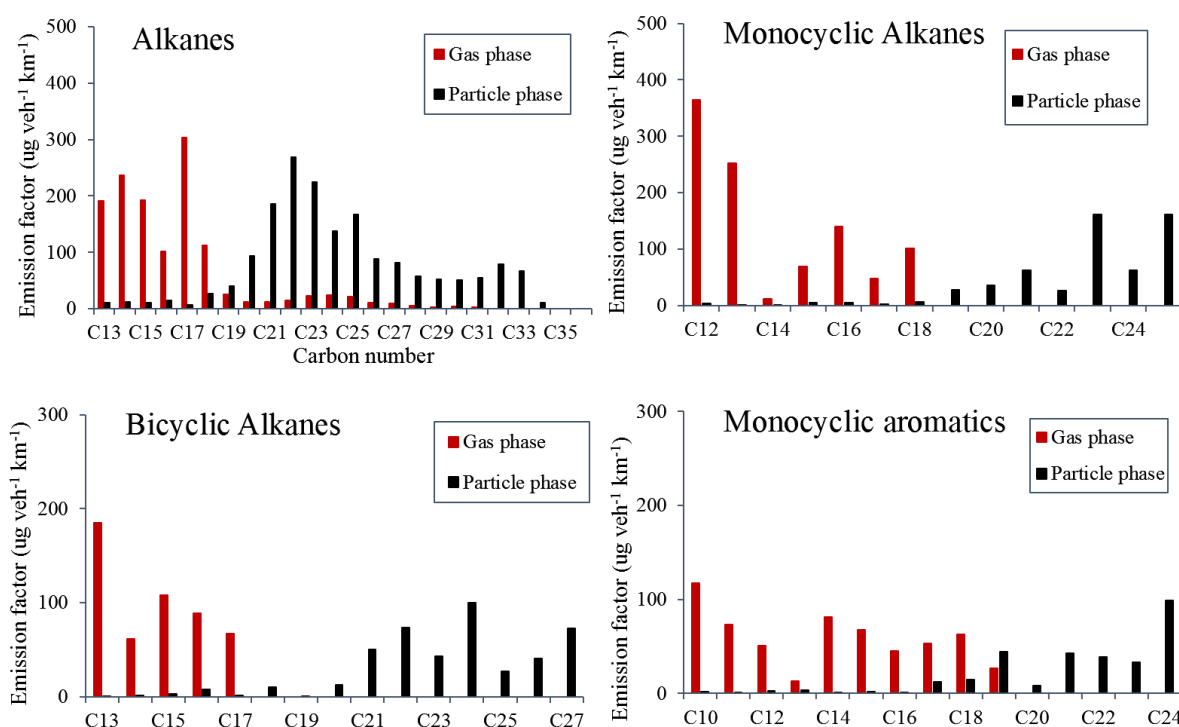
Figure 5.2: Emission factors of alkanes (n+i), monocyclic alkanes, bicyclic alkanes and monocyclic aromatics in the gas phase and particle phase at MR.

5.4 Comparison of n-alkane EFs with the literature

A few tunnel and roadside measurements have been reported which present the emission factors of individual organic compounds in real-world conditions (Hwa et al., 2002; Kawashima et al., 2006; He et al., 2008; Staehelin et al., 1998). Very few studies have reported the emission factors of the heavier hydrocarbons (above C_{12}), leading to a lack of information for a comprehensive comparison. The most frequently reported compounds are n-alkanes, so the n-alkane EFs estimated in the current study were compared with those reported in earlier studies. Table 5.3 shows the n-alkane emission factors reported in this study and three previous studies, including the Zhujiang Tunnel study in China (He et al., 2008), the roadside study of Route 467 in Fujisawa, Japan (Kawashima et al., 2006) and the roadside study of Grenoble Ring Road in Grenoble, France (Charron et al., 2019). The background information on these studies can be seen in Table 5.4, including sampling date, vehicle speed, traffic volume and the proportion of light-duty vehicles (LDVs) and heavy-duty vehicles (HDVs). The emission factors of n-alkanes measured in the gas phase in this study were markedly lower than in the roadside study in Japan (Kawashima et al., 2006). The emission factors of the particle-phase n-alkanes ranging from C_{19}-C_{26} showed a good agreement with the tunnel study in China (He et al., 2008) and the roadside study in France (Charron et al., 2019), all of which showed a broad peak at around C_{21}-C_{25}. Higher particle-phase emissions of long-chain n-alkanes (above C_{27}) were detected in this study compared with the Zhujiang Tunnel study in China (He et al., 2008). Also included in Table 5.3 are the emission factors for particle-phase hydrocarbons measured on a chassis dynamometer for passenger cars of Euro 3, Euro 4, and Euro 4 with a particle trap (Charron et al., 2019). The on-road emission factors measured both in this work and by previous work in Table 5.3 are close to, or exceed the values for Euro 3 vehicles, despite the fact that most vehicles would have been built to more recent Euro standards at the time of sampling, and many

would be fitted with a diesel particle filter (DPF). This suggests a major contribution from the heavy-duty vehicles and/or many high emission vehicles with malfunctions in their emissions control devices or an unrepresentative test cycle in the laboratory work.

Factors which influence the emission factors include the road conditions, vehicle type, vehicle speed and driving mode, and the composition of fuel and oil in use. Vehicle fleet composition varies appreciably between countries. There are far fewer light-duty diesel-powered vehicles in China and Japan than in the EU. Gasoline-powered engines are typically used in light-duty vehicles (LDVs) whilst diesel-powered engines are dominant in heavy-duty vehicles (HDVs) because diesel engines have greater fuel efficiency and torque compared to gasoline engines. However, the market of the small vehicle has been shifted to diesel-powered vehicles in recent year, especially in several European countries including the UK (Ntziachristos et al., 2017; EMEP/EEA, 2016). Diesel vehicles represented 40% of the vehicles in the UK in 2017 (Fleet News, 2018) while accounted for 72% of vehicles in France in 2011 (Charron et al., 2019). In contrast, light-duty gasoline vehicles represent a large percentage of the Chinese vehicle fleet, and the share increased rapidly from less than 50% in 2002 to 70% in 2009 (Huo et al., 2012). In Japan, the ratio of diesel-powered small trucks to gasoline-powered vehicles was 8.1% (Kawashima et al., 2006). Gentner et al. (2012) measured the carbon distribution of straight and branched chain alkanes from gasoline- and diesel-powered vehicles, finding a predominant contribution of gasoline combustion to the lighter alkanes (up to C_{12}). Diesel emissions are mainly comprised of heavier aliphatic hydrocarbons containing primarily unburned fuel (up to C_{20}) and unburned lubricating oil (C_{18} to C_{36}) (Alam et al., 2016b). Therefore, greater emissions of light alkanes might be expected in the gas phase in Japan as gasoline-powered vehicles dominate the market. The composition of lubricants may explain the difference in the long chain

n-alkane (above C_{27}) emissions in this study and the Zhujiang Tunnel study in China (He et al., 2008).

Table 5.3: Summary of emission factors of n-alkanes ($\mu g\ veh^{-1}\ km^{-1}$) in the near-road measurements (IQR:25th and 75th percentiles) and lab tests.

Carbon No	Roadside of Marylebone Road, London, UK 2017		Zhujiang Tunnel, China (He et al., 2008)	Roadside of Route 467, Japan (Kawashima et al., 2006)	Roadside of Grenoble Ring Road, France IQR emission significantly related to traffic (Charron et al., 2019)	Diesel passenger cars (lab tested) median concentration (Charron et al., 2019)		
	Gas phase	Particle phase	Particle phase (PM$_{2.5}$ emissions)	Gas phase	Particle phase	Particle phase		
						E3	E4	E4 + PF
C$_{13}$	43.26	2.50		540				
C$_{14}$	17.83	1.60		260				
C$_{15}$	75.66	2.84		380				
C$_{16}$	76.12	8.40	4.11	250				
C$_{17}$	70.53	1.10	10.7					
C$_{18}$	112.63	5.61	6.69					
C$_{19}$	23.81	20.58	14.9		2.0-8.3	17.4	4.7	0.92
C$_{20}$	10.19	20.42	24.9		5.2-18.9	25.4	5.1	2.8
C$_{21}$	9.27	65.22	40.5		19.9-62.4	31.5	5.8	2.8
C$_{22}$	14.37	60.64	61.6		29.8-81.4	22.1	4.9	2.2
C$_{23}$	22.43	35.61	68.7		30.6-70.3	16.8	4.2	1.1
C$_{24}$	23.92	47.58	57.9		26.1-52.5	11.1	3.5	0.2
C$_{25}$	19.50	36.93	36.4		12.5-34.2	6.1	1.9	n.d.
C$_{26}$	8.04	21.19	13.4		9.3-21.9	3.6	1.2	n.d.
C$_{27}$	4.21	31.52	7.79					
C$_{28}$	0.92	33.68	5.62					
C$_{29}$	0.58	44.66	3.55					
C$_{30}$	0.43	33.69	1.79					
C$_{31}$	0.05	54.63	0.17					
C$_{32}$		79.05	0.062					
C$_{33}$		60.90						
C$_{34}$		11.42						

Note: E3 is Euro 3, E4 is Euro 4 and PF is a diesel particle filter.

Table 5.4: A summary of sampling date, vehicle speed, traffic volume, the proportion of light-duty vehicles (LDVs) and heavy-duty vehicles (HDVs) for the near-road emission factor measurements.

Study	City and Country	Date	Speed (km h^{-1})	Traffic volume (vehicle h^{-1})	Proportion of LDVs (%) and HDVs (%)
Marylebone Road (Current study)	London UK	Feb-March 2017	-	Over 3000	91% LDVs 9% HDVs
Zhujiang Tunnel (He et al., 2008)	China	Sep 2014	40-50	1812 (542-2348)	80.2% LDVs 19.8% HDVs
Route 467 (Kawashima et al., 2006)	Fujisawa Japan	2003	22 (11-53)	1387 (1170-1530)	81.3% LDVs 12.3% HDVs 6.5% Motorcycles
Grenoble Ring Road (Charron et al., 2019)	Grenoble France	Sep 2011	80 (52-94)	2708-3958	95% LDVs 5%HDVs

5.5 Conclusion

The emission factors of NO$_x$ and S/IVOC groups at the roadside site MR were estimated based on published data (Jones and Harrison, 2006) to investigate the emissions from the heavily trafficked Marylebone Road. The four main class of compounds, including alkanes (n+i), monocyclic alkanes, bicyclic alkanes and monocyclic aromatics contributed to 92% of the gas phase emission and 99.5 % of the particle phase emission at MR.

Emission factors of n-alkanes in this study were compared with those estimated from three past studies: a tunnel study in China (He et al., 2008), a roadside study in Japan (Kawashima et al., 2006) and a roadside study in France (Charron et al., 2019). This study showed a good agreement with the tunnel study in China (He et al., 2008) and the roadside study in France (Charron et al., 2019). The gas-phase n-alkanes in the roadside study in Japan (Kawashima et

al., 2006) were significantly higher than in this study, probably caused by variations in the vehicle type and the composition of fuel/oil in use, as well as the road conditions and vehicle speed.

Chapter 6 Gas-particle partitioning and potential SOA formation

This chapter discusses the gas-particle partitioning of individual n-alkanes based on Pankow's gas-particle partitioning theory. Also, this chapter estimates the primary reactivity between OH radicals and the main S/IVOC classes identified in this study, and the potential formation of secondary organic aerosol (SOA) from these S/IVOC groups.

6.1 Introduction

Semi-volatile and intermediate volatility organic compounds (S/IVOCs) are compounds that can partition between the gas phase and particle phase in the atmosphere. The partitioning of S/IVOCs is an important process that affects many concerns, such as the formation of secondary organic particles and the role of organic aerosols in climate change (Arp et al., 2008). Gas/particle (G/P) partitioning varies with changing atmospheric conditions, and the partitioning equilibrium is generally reached resulting from the concentration and composition of particulate matter, the vapour pressure of the compound, and the temperature and relative humidity of the environment (Yamasaki et al., 1982; Pankow and Bidleman, 1992). G/P partitioning also affects a compound's atmospheric fate, its permanence in the air, its deposition, and its transformation and transport (Bidleman et al., 1986; Pankow and Bidleman, 1992; Mader and Pankow, 2001; Sangiorgi et al., 2014). Different chemical groups have variable vapour pressures, and may present different G/P partitioning coefficients due to their diverse interaction with soot and organic matter (Kaupp and McLachlan, 1999; Arp et al., 2008; He and Balasubramanian, 2009; Williams et al., 2010b; Sangiorgi et al., 2014).

A great number of studies have been processed over the last two decades to clarify the factors governing the gas/particle partitioning. However, fewer papers have focused on other semi-volatile organic compound classes compared to PAHs; therefore, it is difficult to extend the partitioning models to the S/IVOCs other than PAHs due to the lack of knowledge. n-Alkanes are always regarded as the research objective in the studies of the G/P partitioning of S/IVOCs because they have a similar vapour pressure (10^{-6} to 10^{-13} atm) to PAHs but diverse physical-chemical properties and emission sources (Sangiorgi et al., 2014). A handful of studies discussed the partitioning of n-alkanes (Leal-Granadillo et al., 2000; Mandalakis et al., 2002; Bi et al., 2003; Cincinelli et al., 2007). This study discussed the partitioning of measured n-alkanes at four sites based on Pankow's gas-particle partitioning theory (Pankow and Bidleman, 1992; Pankow, 1994).

Large quantities of gas-phase S/IVOCs contribute to ozone and other secondary pollutant generation following the reaction with OH radicals (mainly during daylight hours). For the majority of the tropospheric organic compounds in the gas phase, reaction with the OH radicals is the dominant loss process (Kwok and Atkinson, 1995). The lifetime of these chemicals in the troposphere plays a crucial role in the transportation of compounds to remote regions (Bidleman et al., 1990). The mechanism and the rate coefficients k_{OH} for the reactions between OH radicals and alkanes (acyclic and cyclic) as well as aromatics have been discussed and evaluated in the literature (Atkinson, 2003; Atkinson, 1986b; 1997; Atkinson and Arey, 2003). The primary OH reactivity with alkane homologues and monocyclic aromatics were considered and estimated in this study.

Recent studies have proposed that low-volatile organic vapour can lead to the significant production of secondary organic aerosol (SOA), but this reactant is not included in many model studies (Presto et al., 2010; Robinson et al., 2007; Lim and Ziemann, 2005; Lim and Ziemann, 2009b). The traditional gas chromatography-mass spectrometry (GC-MS) cannot separate the vast majority of S/IVOCs adequately and presents them as an unresolved complex mixture (UCM). Alkane classes (linear, branched and cyclic) and aromatic compounds account for the major fraction of the unresolved complex mixture (UCM) (Robinson et al., 2007; Isaacman et al., 2012; Jathar et al., 2012; Mao et al., 2009; van Deursen et al., 2000) while S/IVOC UCM contributes to a substantial fraction of SOA formation (Zhao et al., 2014). The larger hydrocarbons (above C_{12}) identified in this research represent a substantial part of what is referred to as unspeciated chemicals in other studies, so the contribution of different traffic emitted S/IVOC groups to the potential SOA formation can be more accurately estimated by using our data.

Many of studies shows that structure and chain length of alkanes affect their SOA yields (Lim and Ziemann, 2005; Lim and Ziemann, 2009a; Lim and Ziemann, 2009b; Lim and Ziemann, 2009c; Lipsky and Robinson, 2006; Presto et al., 2010; Presto et al., 2009; Lambe et al., 2012; Tkacik et al., 2012). Chain length leads to the difference in SOA yields through its influence on the volatility of formed products (Lim and Ziemann, 2005; Pye and Pouliot, 2012), and the structure of alkanes (linear, branched, cyclic or cyclic+branched) affects the yields through the competition between isomerisation and decomposition of alkoxy radical (Lim and Ziemann, 2009b; Atkinson, 2007; Pye and Pouliot, 2012). Isomerisation process can lead to further functionalisation and low-volatile products while decomposition would compete with isomerisation and decrease the SOA yields for those alkanes with adjacent branch alkoxy

radical. Regarding those alkanes with large ring (i.e., cyclooctane, cyclodecane), decomposition leads to the generation of open-ring products with an addition carbonyl group, resulting in higher SOA yields than linear alkanes with same carbon number (Pye and Pouliot, 2012). The reaction of alkanes and OH radicals under the high NO_x conditions result in highly oxidised products (Lim and Ziemann, 2009b; Russell et al., 2011). Photooxidation of long-chain alkanes may present an important contribution to SOA formation due to their relatively long lifetimes with OH reaction at typical atmospheric OH concentrations (from several hours to days) (Yee et al., 2012). Several recent studies have worked on the oxidation of alkanes in the absence of NO_x to estimate the SOA formation after longer times (i.e., after 12h) (Yee et al., 2012; Lambe et al., 2012; Loza et al., 2014).

Monocyclic aromatics also play an important role in atmospheric chemistry processes, acting as precursors of tropospheric ozone (Atkinson and Arey, 2003) and secondary organic aerosol (SOA) (Dechapanya et al., 2003a; b). For monocyclic aromatics, the mechanisms of SOA formation have not been fully understood (Ng et al., 2007). Few studies worked on the molecular composition of SOA from the oxidation of aromatics (Jang and Kamens, 2001; Kleindienst et al., 2004). Light aromatics are traditionally regarded as important precursors for SOA formation. SOA yields of some light aromatics have been established based on the level of nitrogen oxides (NO_x), and the target aromatics were mainly m-xylene, toluene, and benzene (Song et al., 2005; Presto et al., 2005; Ng et al., 2007; Song et al., 2007). The SOA yields were estimated under high NO_x conditions and low NO_x conditions where peroxyl radicals (RO_2) react primarily with NO and react primarily with HO_2, respectively (Ng et al., 2007; Loza et al., 2014). Similar to alkane classes, SOA yields of aromatics are sensitive with

the presence of NO_x, and the observed SOA yields were higher in the absence of NO_x in the literature (Ng et al., 2007; Song et al., 2005; Henze et al., 2008).

6.2 Gas-particle partitioning

A critical consideration in understanding and modeling the atmospheric transport and removal of semi-volatile organic components is the distribution of these substances between the gas (or vapour) and particle phases (G/P) (Foreman and Bidleman, 1990). Many studies about the G/P partitioning of semi-volatile organics have involved simple physical adsorption mechanism (Liang et al., 1997; May et al., 2013). Organic vapour can absorb into organic liquid or onto the surface of soot, and the relative contribution of this mechanism depends on the proportion of the sorptive material (Roth et al., 2005). Studies have identified that absorption is the dominant gas-particle partitioning mechanism in the atmosphere (Roth et al., 2005; Liang et al., 1997).

6.2.1   Pankow's gas-particle partitioning theory

Locally released organic compounds need to equilibrate to the particles present and ambient temperature. Gas to particle adsorption begins when relatively clean particles enter the contaminated air. The distribution of a semi-volatile compound between the gas phase and particle phase in the atmosphere is defined by using partition coefficient Kp (Pankow and Bidleman, 1992; Pankow, 1994),

$$Kp= (F/TSP)/A. \qquad\qquad Equation\ 6.1$$

where F and A are the chemical concentrations (ng/m^3) in the particle phase and the gas phase respectively. TSP is the total suspended particle concentration (ug/m^3), and TSP was estimated based on the concentrations of PM_{10} divided by 0.8 for the urban traffic. The average mass

concentration (ug/m^3) of PM$_{10}$ was calculated based on the hourly data offered by DEFRA North Kensington monitoring site (an urban background monitoring site in London).

Partitioning to the particulate matter increases with the increase of *Kp* (Pankow and Bidleman, 1992). For a given sample at a given temperature, *Kp* tends to be correlated with the sub-cooled liquid vapour pressure (*VPt*, torr) according to the following equation (Pankow, 1994),

$$LogKp=m_r log(VPt)+b_r \hspace{4cm} Equation\ 6.2$$

when *Log Kp* is regressed against the vapour pressure (*VPt*), negative slopes (*m$_r$*) are generally observed, presenting an association of the target compound with aerosol particles decreases with the increase of vapour pressure (Yamasaki et al., 1982; Gustafson and Dickhut, 1996; Harner and Bidleman, 1998; Lohmann et al., 2000; Fernández et al., 2002; Cincinelli et al., 2007). *Kp* is temperature dependent; therefore *VPt* used in such regression must pertain to the temperature during the sampling. The temperature applied was from Met Office (2006).

The vapour pressure values were calculated by UManSysProp v1.0 (UManSysProp, 2016), which is an online tool to estimate the vapour pressure of organic compounds at a given temperature by selecting a list of methods. The technique of UManSysProp v1.0 was explained by Topping et al. (2016), and methods provided by the tool were reviewed by Barley and McFiggans (2010) and O'Meara et al. (2014). This study selected the vapour pressure method provided by Compernolle et al. (2011) as it is close to the lab results of the FASTER vapour pressure study (Alam et al., 2019a).

6.2.2 Variability on slope (m_r) and intercept (b_r)

Theory predicts slope m_r value should be near to -1 under equilibrium conditions for either adsorptive or absorptive partitioning (Pankow and Bidleman, 1992; Pankow, 1994). The values of *log Kp* were regressed upon *log (VPt)* for all n-alkanes (C_{13} to C_{29}) at a given day in the London Campaign 2017 (Table 6.1-6.4). The slopes (m_r) of these regressions ranged from -0.13 to -0.42 with an average R^2 of 0.68±0.16 for WM, ranged from -0.20 to -0.42 with an average R^2 of 0.77±0.09 for RU, ranged from -0.22 to -0.54 with an average R^2 of 0.71± 0.11 for MR, and ranged from -0.10 to -0.40 with an average R^2 of 0.52± 0.15 for EL.

This study reported a good fit to the regression relationship between *log kp* versus *log(VPt)* for n-alkanes, but slopes were shallower than the theoretical value of -1 according to equilibrium conditions. The m_r values at MR were relatively closer to the theoretical value of -1 compared with other sites. A previous FASTER study (Lyu et al., 2019) reported the calculated *log kp* versus *log(VPt)* for alkanals (C_{10}-C_{14}), alkan-2-ones(C_{10}-C_{18}) and alkan-3-ones(C_{10}-C_{16}) for each day collected at four sites in the London Campaign 2017, and showed the best fit to the regression equation was at MR. It is not easy to explain the differences among sites. One possible explanation could be that gas-particle partitioning was closer to equilibrium at MR as the increased particle surface area at MR enhanced the kinetics of gas-particle exchange (Lyu et al., 2019). The difference in ambient temperature (0.4-11.4 ℃ during WM/RU measurements, 4.1-12.7 ℃ during EL measurements, and 8.2-15.5℃ during MR measurements) might be one of the reasons causing the difference in the slope values m_r among sites.

The gas-phase n-alkanes were partitioning to the particle phase with the increase of the carbon number (Figure 4.1). The fraction of gas-phase n-alkanes decreased gradually from C_{13} to C_{22}

with a small peak at the C_{23} to C_{29}, probably because diesel-related hydrocarbon emissions are overwhelming in the gas phase (Dunmore et al., 2015). The analysis of n-alkane partitioning was divided into two groups, including C_{13} to C_{22} and C_{23} to C_{29} (Table 6.1-6.4). There were weaker correlations expressed as R^2 values for divided groups rather than the total carbon range of C_{13} to C_{29}, probably due to the lower analytical precision.

There are noticeable differences in reported m_r values in the literature. Some are close to the theoretical value of -1 while significant deviations have also been reported. Many reasons have been discussed to explain the variability of slope m_r, and these deviations do not always indicate disequilibrium (Terzi and Samara, 2004). Recently, a few studies worked on the gas-particle partitioning of n-alkanes (Mandalakis et al., 2002; Cincinelli et al., 2007; Karanasiou et al., 2007) and PAHs (Mandalakis et al., 2002; Callén et al., 2008; Fernández et al., 2002; Gaga and Ari, 2011), showing significantly shallower m_r values ranging around -0.5 (Lyu et al., 2019). Slopes shallower than -0.6 are characteristics of absorption into the organic matter, while those steeper than -1 are generally interpreted to be attributed to adsorption on particle surfaces (Fernández et al., 2002; Callén et al., 2008). Other reasons associated with the shallow slopes have been discussed by Terzi and Samara (2004) and Callén et al. (2008), such as (a) chemical reaction in the ambient air (b) presence of nonexchangeable S/IVOCs fractions on particulate matter (c) slow gas-to-particle sorption of the heavier compounds with lower volatility (d) pollution sources close to the sampling site, so that the produced compounds have no time to cool down and pass to the particle phase (e) difference in energy terms (i.e. activity coefficients, adsorption sites and enthalpies) that affected by the chemical composition of the particles. Regarding the temperature variations during the sampling, there is no clear evidence indicating the fluctuations in temperature are responsible for shallower slopes. Steeper slopes can be

observed in the study that the temperature changed higher than 10 ℃, while shallow slopes were shown in the study that temperature fluctuations were lower than 6 ℃ (Callén et al., 2008).

There is some compound to compound similarity in intercept b_r (Pankow and Bidleman, 1992; Pankow, 1994). The values of b_r varied from day to day, but most of them were in the range of -2 to -5 for n-alkanes from C_{13} to C_{29} (Table 6.1-6.4). The factors that affect the slope m_r also affect the intercept b_r. Values of b_r mainly depend on the properties associated with the particles. The number of adsorption sites and chemical interactions on the particle surface are the main factors that affect b_r values for adsorptive partitioning, while the activity coefficient of the absorbing compound in organic components and the fraction of organic components on the particle surface affect b_r values for absorptive partitioning (Pankow and Bidleman, 1992; Pankow, 1994; Terzi and Samara, 2004).

Table 6.1: Analysis of n-alkane partitioning, all compounds, daily data at WM.

Date	Total C$_{13}$ to C$_{29}$			Group1 C$_{13}$ to C$_{22}$			Group 2 C$_{23}$ to C$_{29}$		
	Slope m_r	Intercept b_r	R^2	Slope m_r	Intercept b_r	R^2	Slope m_r	Intercept b_r	R^2
26/01/2017	-0.33	-4.81	0.84	-0.09	-3.92	0.04	-0.34	-4.84	0.64
27/01/2017	-0.28	-4.18	0.81	-0.26	-4.10	0.28	-0.40	-5.22	0.72
28/01/2017	-0.24	-2.67	0.65	-0.34	-3.00	0.46	-0.37	-3.89	0.77
29/01/2017	-0.33	-3.35	0.77	-0.21	-2.98	0.26	-0.09	-1.21	0.10
03/02/2017	-0.42	-3.21	0.69	-0.50	-3.50	0.59	-0.12	-1.00	0.21
04/02/2017	-0.23	-3.18	0.86	-0.14	-2.91	0.24	-0.18	-2.68	0.34
05/02/2017	-0.35	-3.26	0.75	-0.53	-3.99	0.71	-0.35	-3.50	0.92
06/02/2017	-0.13	-2.67	0.32	-0.22	-3.03	0.49	0.04	-1.18	0.00
07/02/2017	-0.29	-4.32	0.75	-0.14	-3.81	0.10	-0.41	-5.41	0.48
08/02/2017	-0.23	-3.51	0.66	-0.34	-3.96	0.50	-0.06	-1.98	0.10
09/02/2017	-0.33	-3.72	0.80	-0.40	-4.02	0.60	-0.16	-2.27	0.68
10/02/2017	-0.26	-4.05	0.64	0.13	-2.67	0.24	-0.33	-4.42	0.64
11/02/2017	-0.39	-4.74	0.59	-0.45	-4.97	0.40	-0.02	-1.66	0.04
12/02/2017	-0.23	-4.18	0.70	-0.05	-3.61	0.02	-0.10	-2.95	0.14
13/02/2017	-0.31	-4.22	0.75	-0.34	-4.39	0.39	-0.13	-2.60	0.30
14/02/2017	-0.24	-4.45	0.70	0.07	-3.38	0.07	-0.61	-7.69	0.84
15/02/2017	-0.32	-3.24	0.77	-0.36	-3.39	0.54	-0.31	-3.13	0.42
16/02/2017	-0.34	-3.65	0.73	-0.34	-3.67	0.41	-0.11	-1.69	0.39
17/02/2017	-0.14	-3.86	0.30	0.02	-3.27	0.00	-0.52	-7.32	0.65
18/02/2017	-0.31	-4.30	0.85	-0.06	-3.47	0.03	-0.37	-4.75	0.68
19/02/2017	-0.20	-2.58	0.37	-0.36	-3.21	0.56	0.17	0.54	0.05

Table 6.2: Analysis of n-alkane partitioning, all compounds, daily data at RU.

Date	Total C_{13} to C_{29}			Group1 C_{13} to C_{22}			Group 2 C_{23} to C_{29}		
	Slope m_r	Intercept b_r	R^2	Slope m_r	Intercept b_r	R^2	Slope m_r	Intercept b_r	R^2
27/01/2017	-0.27	-2.98	0.70	-0.34	-3.26	0.43	-0.13	-1.69	0.37
28/01/2017	-0.25	-2.79	0.69	0.09	-1.61	0.10	-0.40	-4.07	0.45
29/01/2017	-0.20	-1.90	0.51	-0.36	-2.52	0.57	-0.07	-0.89	0.04
03/02/2017	-0.33	-3.21	0.82	-0.28	-3.04	0.49	-0.31	-2.99	0.48
04/02/2017	-0.26	-2.58	0.72	-0.50	-3.52	0.90	-0.15	-1.85	0.57
05/02/2017	-0.31	-3.28	0.65	-0.52	-4.19	0.64	0.03	-0.18	0.02
06/02/2017	-0.40	-4.24	0.76	-0.17	-3.35	0.15	-0.88	-8.58	0.77
07/02/2017	-0.36	-4.59	0.80	-0.37	-4.52	0.49	-0.86	-9.17	0.90
08/02/2017	-0.26	-3.54	0.73	-0.21	-3.39	0.24	-0.22	-3.13	0.21
09/02/2017	-0.31	-4.36	0.86	-0.16	-3.79	0.13	-0.32	-4.37	0.80
10/02/2017	-0.40	-4.10	0.91	-0.26	-3.58	0.32	-0.38	-3.87	0.83
11/02/2017	-0.35	-4.41	0.85	-0.40	-4.60	0.56	-0.31	-4.10	0.34
12/02/2017	-0.32	-4.45	0.86	-0.18	-3.99	0.15	-0.19	-3.16	0.72
13/02/2017	-0.35	-4.80	0.79	-0.40	-5.05	0.55	-0.02	-1.80	0.01
14/02/2017	-0.27	-4.29	0.79	-0.34	-4.45	0.60	-0.50	-6.31	0.77
15/02/2017	-0.34	-3.87	0.89	-0.30	-3.72	0.40	-0.41	-4.43	0.72
16/02/2017	-0.30	-3.87	0.78	-0.07	-3.15	0.02	-0.19	-2.88	0.45
17/02/2017	-0.25	-4.10	0.75	-0.18	-3.81	0.19	-0.51	-6.41	0.71
18/02/2017	-0.26	-3.81	0.71	-0.05	-3.10	0.01	-0.36	-4.61	0.70
19/02/2017	-0.42	-3.67	0.83	-0.49	-3.91	0.62	-0.41	-3.65	0.81

Table 6.3: Analysis of n-alkane partitioning, all compounds, daily data at MR.

Date	Total C_{13} to C_{29}			Group1 C_{13} to C_{22}			Group 2 C_{23} to C_{29}		
	Slope m_r	Intercept b_r	R^2	Slope m_r	Intercept b_r	R^2	Slope m_r	Intercept b_r	R^2
22/03/2017	-0.22	-2.62	0.59	-0.25	-2.72	0.33	-0.36	-3.94	0.79
23/03/2017	-0.38	-4.21	0.67	-0.57	-4.83	0.79	-0.85	-8.63	0.72
24/03/2017	-0.38	-4.31	0.76	-0.48	-4.69	0.63	-0.38	-4.36	0.37
25/03/2017	-0.40	-4.21	0.72	-0.53	-4.66	0.63	-0.56	-5.74	0.57
26/03/2017	-0.32	-3.73	0.67	-0.45	-4.20	0.59	-0.46	-5.09	0.51
27/03/2017	-0.52	-4.92	0.87	-0.52	-4.86	0.62	-0.70	-6.46	0.89
28/03/2017	-0.36	-2.94	0.65	-0.55	-3.62	0.57	-0.21	-1.78	0.16
29/03/2017	-0.50	-3.89	0.78	-0.55	-3.96	0.59	-1.02	-8.40	0.93
30/03/2017	-0.46	-3.95	0.83	-0.51	-4.08	0.67	-0.70	-5.99	0.73
31/03/2017	-0.33	-3.19	0.68	-0.52	-3.85	0.68	-0.40	-3.95	0.41
01/04/2017	-0.37	-4.12	0.77	-0.51	-4.59	0.63	-0.48	-5.16	0.81
02/04/2017	-0.36	-4.29	0.78	-0.56	-5.03	0.76	-0.28	-3.73	0.43
03/04/2017	-0.25	-3.71	0.41	-0.41	-4.19	0.46	-0.72	-7.94	0.60
04/04/2017	-0.35	-3.24	0.50	-0.44	-3.52	0.51	-0.79	-7.05	0.36
05/04/2017	-0.49	-4.33	0.88	-0.64	-4.87	0.78	-0.42	-3.84	0.71
07/04/2017	-0.44	-5.15	0.76	-0.60	-5.75	0.64	-0.31	-4.14	0.36
08/04/2017	-0.51	-4.88	0.78	-0.65	-5.37	0.68	-0.51	-4.95	0.41
09/04/2017	-0.54	-4.60	0.76	-0.67	-5.07	0.62	-0.42	-3.65	0.27
10/04/2017	-0.39	-3.86	0.68	-0.70	-4.98	0.73	-0.35	-3.73	0.40
11/04/2017	-0.47	-4.46	0.75	-0.72	-5.41	0.78	-0.23	-2.55	0.12
12/04/2017	-0.40	-3.69	0.79	-0.44	-3.81	0.53	-0.56	-5.15	0.81
13/04/2017	-0.33	-3.67	0.76	-0.44	-4.09	0.73	-0.25	-3.05	0.20
14/04/2017	-0.46	-4.46	0.68	-0.60	-4.99	0.51	-0.41	-4.18	0.34
15/04/2017	-0.31	-3.30	0.51	-0.64	-4.53	0.85	-0.26	-3.09	0.09
16/04/2017	-0.30	-3.02	0.67	-0.44	-3.51	0.60	-0.38	-3.84	0.59
18/04/2017	-0.30	-3.43	0.68	-0.42	-3.92	0.57			

Table 6.4: Analysis of n-alkane partitioning, all compounds, daily data at EL.

Date	Total C$_{13}$ to C$_{29}$			Group1 C$_{13}$ to C$_{19}$			Group 2 C$_{20}$ to C$_{29}$		
	Slope m_r	Intercept b_r	R^2	Slope m_r	Intercept b_r	R^2	Slope m_r	Intercept b_r	R^2
23/02/2017	-0.30	-2.91	0.67	-0.37	-3.03	0.33	-0.45	-4.19	0.70
24/02/2017	-0.25	-3.07	0.69	-0.52	-3.83	0.65	-0.47	-5.04	0.89
25/02/2017	-0.10	-1.67	0.40	-0.40	-2.63	0.64	-0.06	-1.38	0.24
26/02/2017	-0.19	-2.18	0.41	-0.52	-3.29	0.51	-0.04	-1.05	0.02
27/02/2017	-0.12	-2.23	0.16	-0.32	-3.05	0.33	0.05	-0.77	0.01
28/02/2017	-0.40	-4.43	0.63	-0.04	-3.04	0.02	-0.92	-8.66	0.79
01/03/2017	-0.22	-2.80	0.66	-0.36	-3.34	0.51	-0.06	-1.46	0.06
02/03/2017	-0.28	-2.79	0.71	-0.54	-3.69	0.61	-0.18	-2.07	0.50
03/03/2017	-0.16	-3.20	0.63	-0.27	-3.54	0.40	-0.23	-3.82	0.38
04/03/2017	-0.12	-2.52	0.31	-0.41	-3.47	0.48	-0.11	-2.45	0.16
06/03/2017	-0.17	-3.00	0.55	-0.33	-3.54	0.29	-0.04	-1.94	0.09
07/03/2017	-0.16	-2.16	0.54	-0.47	-3.20	0.79	-0.07	-1.52	0.12
08/03/2017	-0.21	-3.09	0.66	-0.43	-3.81	0.45	-0.16	-2.74	0.59
16/03/2017	-0.19	-3.64	0.41	-0.59	-4.90	0.62	-0.51	-6.50	0.73
17/03/2017	-0.17	-3.03	0.31	-0.44	-3.75	0.75	-0.69	-7.64	0.52
18/03/2017	-0.17	-3.19	0.59	-0.39	-3.82	0.60	-0.38	-4.93	0.75
19/03/2017	-0.18	-3.18	0.51	-0.47	-3.95	0.61	-0.57	-6.43	0.80

6.3 Primary OH reactivity

6.3.1 Estimation of k_OH coefficients

A structure-reactivity approach was developed by Atkinson (1986b) and Kwok and Atkinson (1995) to calculate the reaction coefficients k_{OH} for the reaction between organic compounds and OH radicals in the gas phase. During the reaction, a number of separate OH radical reaction processes occur. These processes can be dealt with individually and the rate coefficients can be summed. The total OH radical rate coefficient can be calculated based on the following equation (Kwok and Atkinson, 1995),

$k_{total}= k$ (H atom abstraction from $C - H$ and $O - H$ bonds)

$+k$ (OH radical addition to $> C = C <$ and $- C \equiv C -$ bonds)

$+ k$ (OH radical addition to aromatic rings)

$+k$ (OH radical interaction with $- NH2, > NH, > N-, -SH,$ and $- S -$ groups)

Equation 6.3

As alkanes only have C–H bonds, the calculation is based upon the estimation of –CH$_3$, –CH$_2$– and >CH–.

k (CH$_3$ −X) $=k_{prim}$F(X)   *Equation 6.4*

k ($X - CH_2 -Y$) $=k_{sec}$F(X) F(Y)   *Equation 6.5*

k ($X - CH <^Y_Z$)$=k_{tert}$F(X) F(Y) F (Z)   *Equation 6.6*

k_{prim}, k_{sec} and k_{tert} are group rate constants for H-atom abstraction from $-CH_3, -CH_2-$ and

$X-CH<^Y_Z$ respectively (Kwok and Atkinson, 1995).

An example of n-butane is given below,

$$CH_3 - CH_2 - CH_2 - CH_3$$
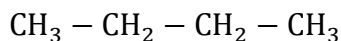
$$k_{butane} = \{k_{prim}F(-CH_2-) + k_{sec}F(-CH_3) \ F(-CH_2-) + k_{sec}F(-CH_3) \ F(-CH_2-)$$

$$+ k_{prim}F(-CH_2-)\}$$

If add one more carbon atom, k_{OH} of n-pentane can be given as following,

$$CH_3 - CH_2 - CH_2 - CH_2 - CH_3$$
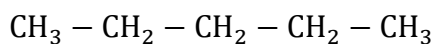
$$k_{add} = k_{sec}F(-CH_2-) \ F(-CH_2-)$$

$$k_{pentane} = k_{butane} + k_{add}$$

$$= \{k_{prim}F(-CH_2-) + k_{sec}F(-CH_3) \ F(-CH_2-) + k_{sec}F(-CH_2-)F(-CH_2-) + k_{sec}F(-CH_3) \ F(-CH_2-) + k_{prim}F(-CH_2-)\}$$

Kwok and Atkinson (1995) suggested the values of $F(-CH_2-)$ and k_{sec} as below,

$F(-CH_2-) = F(>CH-) = F(>C<) = 1.23$ at 298K

$k_{sec} = 0.934 \times 10^{-12}$ cm^3 molecule^{-1}s^{-1} at 298K

Thus,

$$k_{add} = k_{sec}\text{F}(-CH_2-)\text{F}(-CH_2-) = 0.934 \times 10^{-12} \times 1.23 \times 1.23$$

$$= 1.4 \times 10^{-12} \text{ cm}^3 \text{ molecule}^{-1}\text{s}^{-1} \text{ at 298K}$$

This method allows the k_{OH} rate coefficient to be estimated based on the structure-activity relationship. The rate coefficients of n-alkanes can be estimated according to $k_{Cn+1} = k_{add} + k_{Cn}$, where C_n is the n-alkane with the number of n carbon atoms.

Atkinson (2003) recently summarised the rate coefficient data for hydroxyl radical reaction with n-alkane from C_3 to C_{13}. The rate coefficients $k_{OH} \times 10^{12}$ (cm^3 molecule^{-1}s^{-1}) were plotted as a function of the number of carbon atoms, the number of hydrogen atoms and the number of hydrogen atoms minus 6 (representing the terminal methyl groups) respectively. It suggested an excellent fit to a linear relationship between k_{OH} and carbon number or hydrogen number of n-alkanes. Episuite (EPI, 2017) extended an estimation method used by AOPWIN based upon the structure-reactivity methods developed by Atkinson and co-workers (Atkinson, 1986b; 1987; 1986a; Kwok and Atkinson, 1995; Atkinson, 1991; Atkinson and Carter, 1984; Biermann et al., 1985) to provide a comprehensive estimation on the reaction coefficients k_{OH} for alkanes and aromatics.

To calculate the primary OH reactivity with S/IVOCs, the rate coefficients k_{OH} of hydrocarbon groups need to be assigned to an individual compound as a surrogate. The rate coefficients k_{OH} of these S/IVOC surrogates were estimated based on their structure-activity by Episuite (EPI, 2017) and are shown in Table 6.5. Due to the lack of isomer speciation and the corresponding

kinetic data for hydrocarbons above C$_9$, this study applied the k_{OH} coefficients of straight-chain alkanes to estimate the primary OH reactivity of grouped alkanes (n+i) with corresponding carbon number. The measured rate coefficients k_{OH} of branched alkanes are generally similar to or slower than n-alkanes, based on the location and degree of the branching (Dunmore et al., 2015). Application of the n-alkanes k_{OH} to the entire alkane groups suggested a slight overestimate of the OH reaction. The k_{OH} values of alkyl-cyclohexane and alkyl-benzenes were applied to estimate the OH reactivity of cyclic alkanes (monocyclic and bicyclic) and monocyclic aromatics respectively.

Table 6.5: A summary of rate coefficients $k \times 10^{11}$ (cm^3 molecule^{-1} s^{-1}) for the reaction of OH radicals with the chemical groups identified in this study (EPI, 2017).

Species	Carbon No	$k_{OH} \times 10^{11}$	k_{OH} surrogate
Alkanes	C_{13}	1.53	n-Tridecane
Alkanes	C_{14}	1.68	n-Tetradecane
Alkanes	C_{15}	1.82	n-Pentadecane
Alkanes	C_{16}	1.96	n-Hexadecane
Alkanes	C_{17}	2.1	n-Heptadecane
Alkanes	C_{18}	2.24	n-Octadecane
Alkanes	C_{19}	2.38	n-Nonadecane
Alkanes	C_{20}	2.52	n-Eicosane
Alkanes	C_{21}	2.67	n-Heneicosane
Alkanes	C_{22}	2.81	n-Docosane
Alkanes	C_{23}	2.95	n-Tricosane
Alkanes	C_{24}	3.09	n-Tetracosane
Alkanes	C_{25}	3.23	n-Pentacosane
Alkanes	C_{26}	3.37	n-Hexacosane
Alkanes	C_{27}	3.51	n-Heptacosane
Alkanes	C_{28}	3.65	n-Octacosane
Alkanes	C_{29}	3.8	n-Nonacosane
Alkanes	C_{30}	3.94	n-Triacontane
Alkanes	C_{31}	4.08	n-Hentriacontane
Monocyclic alkanes/Bicyclic alkanes	C_{12}	1.76	Cyclohexane, hexyl-
Monocyclic alkanes/Bicyclic alkanes	C_{13}	1.91	Cyclohexane, heptyl-
Monocyclic alkanes/Bicyclic alkanes	C_{14}	2.05	Cyclohexane, octyl-
Monocyclic alkanes/Bicyclic alkanes	C_{15}	2.19	Cyclohexane, nonyl-
Monocyclic alkanes/Bicyclic alkanes	C_{16}	2.33	Cyclohexane, decyl-
Monocyclic alkanes/Bicyclic alkanes	C_{17}	2.47	Cyclohexane, undecyl-
Monocyclic alkanes	C_{18}	2.61	Cyclohexane, dodecyl-
Monocyclic alkanes	C_{19}	2.75	Cyclohexane, tridecyl-
Monocyclic alkanes	C_{20}	2.89	Cyclohexane, tetradecyl-
Monocyclic alkanes	C_{21}	3.04	Cyclohexane, pentadecyl-
Monocyclic alkanes	C_{22}	3.18	Cyclohexane, hexadecyl-
Monocyclic alkanes	C_{23}	3.32	Cyclohexane, heptadecyl-
Monocyclic alkanes	C_{24}	3.46	Cyclohexane, octadecyl-
Monocyclic alkanes	C_{25}	3.6	Cyclohexane, nonadecyl-
Monocyclic aromatics	C_{10}	1.62	Benzene, butyl
Monocyclic aromatics	C_{11}	1.01	Benzene, pentyl
Monocyclic aromatics	C_{12}	1.15	Benzene, hexyl
Monocyclic aromatics	C_{13}	1.3	Benzene, heptyl
Monocyclic aromatics	C_{14}	1.44	Benzene, octyl
Monocyclic aromatics	C_{15}	1.58	Benzene, nonyl
Monocyclic aromatics	C_{16}	1.72	Benzene, decyl

Monocyclic aromatics	C_{17}	1.86	Benzene, undecyl
Monocyclic aromatics	C_{18}	2	Benzene, dodecyl
Monocyclic aromatics	C_{19}	2.14	Benzene, tridecyl

6.3.2 OH radical reactivity

The OH radical reactivity with S/IVOCs is the driving force for the formation of O_3 and many other secondary pollutants. The primary hydrocarbon OH reactivity can be calculated by following equations (Dunmore et al., 2015),

$$S^{-1} = ([VOC]\ (ppb) \times 10^{-9} \times [M]) \times k_{OH}\ (298K) \qquad \text{Equation 6.7}$$

$$\text{Where } [M] = \left(\frac{Pressure\ (mbar) \times 10^{-4}}{(8.314 \times (273.15 + temperature))}\right) \times 6.022 \times 10^{23} \qquad \text{Equation 6.8}$$

Figure 6.1 shows the gas-phase concentrations and primary OH reactivity of alkanes (n+i), monocyclic alkanes, bicyclic alkanes and monocyclic aromatics at the roadside site MR and roof site RU. Alkanes (n+i) were the most abundant class in the gas phase emission (31% at MR and 44% at RU) followed by monocyclic alkanes (29% at MR and 24% at RU), monocyclic aromatics (23% at MR and 21% at RU) and bicyclic alkanes (16% at MR and 10% at RU). Cyclic alkanes reacted faster with OH radicals than alkanes (n+i) and monocyclic aromatics with the same carbon number, shown as higher rate coefficients k_{OH} in Table 6.5. Monocyclic and bicyclic alkanes made the overwhelming contribution to OH reactivity at MR (60%) and RU (51%). As expected, OH reactivity of the summed S/IVOC groups at roadside site MR was the greatest among the four sampling sites, followed by the urban background site EL and then the two roof sites. Whalley et al. (2016) measured the total OH reactivity at an urban background site in central London during a summer campaign. For the organics and inorganics they studied, NO_x and the carbonyl class of VOCs made the dominant contribution to the

average OH reactivity in the ambient atmosphere (18.1 s^{-1}). The hydroxyl radical reactivity with the organic classes identified in this study only accounted for a minor fraction of the magnitude of the total OH reactivity that Whalley et al. (2016) reported.
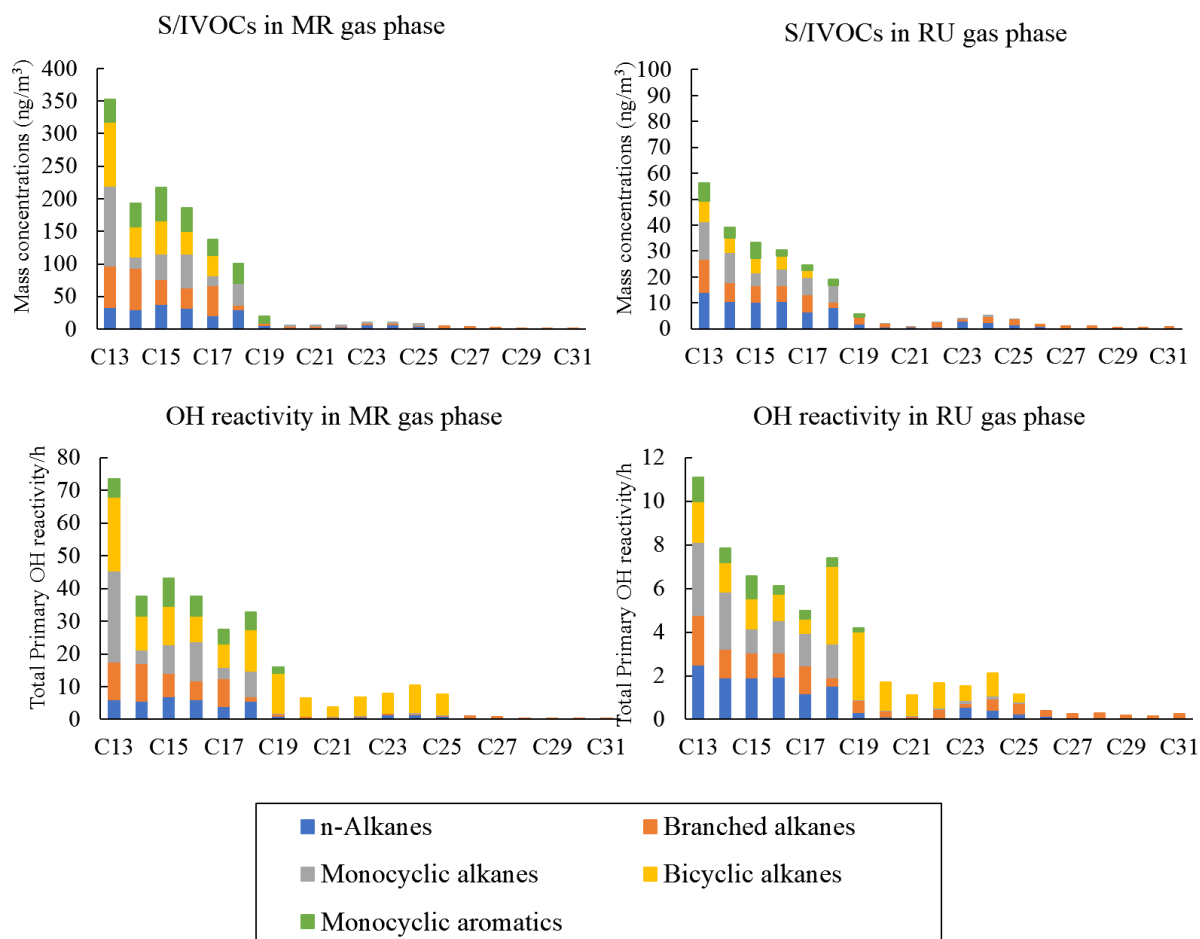
Figure 6.1: The mass concentrations of S/IVOCs and primary hydrocarbon OH reactivity grouped by carbon number at MR and RU.

6.4 Potential SOA formation

SOA is typically generated only from the oxidation of gaseous reactive organic compounds above C$_7$ as the vapour pressures of the oxidation products must be sufficiently low to enable

the gas-phase organics to partition to the particle phase (Odum et al., 1997). The potential SOA formation contributed by S/IVOC groups were estimated based on the corresponding SOA yields (Presto et al., 2010; Ng et al., 2007). The SOA yields applied in this study were measured in previous chamber studies. The organic aerosol mass C_{OA} at roadside site MR and background roof site RU derived from the average organic matter concentrations at MR and North Kensington station (NK) respectively. Organic matter (OM) concentrations at MR and NK were estimated based on organic carbon (OC) from DEFRA network dataset (https://uk-air.defra.gov.uk/networks/). The average concentration of organic carbon (OC) at MR during the MR sampling period (March-April) was 4700 ng/m^3; therefore, organic matter (OM) was approximately 6.6 ug/m^3 if the typical OM/OC ratio of 1.4 was applied (Grosjean and Friedlander, 1975; White and Roberts, 1977; Polidori et al., 2008). Turpin and Lim (2001) argued that increased oxidised organics (i.e. formed by the photochemical reactions) can enhance the OM/OC ratio and suggested the ratio of 1.6 ± 0.2 for urban environments while 2.1 ± 0.2 for rural areas based on the published data. The OM/OC ratio may vary based on the location and season, and a number of studies have reported the OM/OC measurements for several locations over the world (Kiss et al., 2002; El-Zanan et al., 2005; Reff et al., 2007; Takegawa et al., 2005; Polidori et al., 2008). The average concentration of organic carbon (OC) at NK during the WM/RU sampling period (Jan-Feb) was 5180 ng/m^3; therefore, organic matter (OM) was around 7.3 ug/m^3 if the typical OM/OC ratio of 1.4 was applied. For simplicity, the organic aerosol mass C_{OA} for MR and RU were estimated as 7 ug m^{-3}. According to the UK NO$_x$ emission interactive map from the National Atmospheric Emissions Inventory (NAEI) (https://naei.beis.gov.uk/emissionsapp/), the area within the London Orbital Motorway M25 can be regarded as the high NO$_x$ emission area while the area outside of the M25 is regarded as low NO$_x$ emission area. With a distance of 20-30 km between the MR-RU-WM sampling area

and M25, and a minimum wind speed of 1.5 m s^{-1} during the sampling period, there was

assumed to be 6 h of SOA formation under the high-NO$_x$ regime. Hence, the SOA yields under

high NO$_x$ conditions were applied to estimate the SOA formation in the first 6 h and SOA yields

under low NO$_x$ conditions for SOA formation at 12 h and 36 h.

The potential SOA formation generated by the oxidation of gas-phase SOA precursor was

estimated by the following equation (Chan et al., 2009),

$$\Delta M_{SOA,i} = [HCi] \times (1 - e^{-k_{OH,i}[OH]\Delta t}) \times Y_i \qquad \text{Equation 6.9}$$

where *[HCi]* is the measured concentration of gas-phase SOA precursor *i* (ng m^{-3}); $k_{OH,i}$ is the

rate coefficient of the reaction of OH radicals with SOA precursor *i* (cm^3 molecule $^{-1}$ s^{-1}); $[OH]$

is the concentration of OH radicals; Δt is the OH radical exposure time (s); and Y_i is the SOA

yield of the SOA precursor *i*, defined as the mass of SOA formed divided by mass of

hydrocarbon reacted.

6.4.1 SOA yields under high NO$_x$ conditions

To estimate the reaction between hydrocarbons and OH radicals in the first 6h, this study took

the SOA yields from previous chamber studies under high NO$_x$ conditions with the organic

aerosol mass C$_{OA}$ of 7 ug m^{-3}. The mechanism on the formation of multi-generation product

from the oxidation of alkanes (linear, branched, and cyclic) in the presence of NO$_x$ have been

discussed in past studies (Lim and Ziemann, 2005; 2009a; 2009c). SOA yields for low

molecular weight alkanes (C$_7$-C$_{25}$) with the linear, branched and cyclic structure under high

NO$_x$ conditions were measured by chamber studies (Lim and Ziemann, 2005; Lim and Ziemann,

2009b; Presto et al., 2010; Tkacik et al., 2012). SOA yields reported in these high NO$_x$ studies

may not represent the highest possible yields as they were measured after 50-85% of alkanes have oxidised (Loza et al., 2014).

Under high NO_x conditions, SOA yields increase with the increase of the carbon number for the series of n-alkanes and cyclic alkanes due to their decreasing volatility and thus the reaction products (Presto et al., 2010; Lim and Ziemann, 2009b; Lim and Ziemann, 2005). Besides, SOA yields were found to increase with the presence of the cyclic structure and decrease with the presence of branches on the carbon chain (Loza et al., 2014). Past studies developed slightly different rules to estimate the SOA yields based on the carbon number and structure of alkanes. For instance, Aumont et al. (2012) suggested SOA yields could increase by about 10% for each carbon atom added to the carbon chain for C_8–C_{14} alkanes and this increase levels off for heavier alkanes. Zhao et al. (2014) assumed the SOA yields for n-alkanes after C_{17} were same as C_{17}, and SOA yields for cyclic alkanes were same as the linear alkanes with the same carbon number. Eluri et al. (2018) suggested Cx branched alkanes can be assigned to a C_{X-2} linear alkane as a surrogate while Cx cyclic alkanes can be assigned to a C_{X+2} linear alkane as a surrogate based on the work of Lim and Ziemann (2009b) and Tkacik et al. (2012).

In this study, SOA yields for n-alkanes ranging from C_{12} to C_{17} under high NO_x conditions were taken from Presto et al. (2010), and SOA yields for n-alkanes higher than n-heptadecane were estimated using the assumption that the SOA yields of n-alkanes change log-linearly with the carbon number. Pye and Pouliot (2012) developed a method to estimate the SOA yields for alkanes of varying length and structure for all NO_x regimes, and linear n-dodecane was chosen as a surrogate (Table 6.6).

Table 6.6: Ratio of alkane SOA yields to n-dodecane SOA yield when n-dodecane was regarded as 1 (Pye and Pouliot, 2012).

	Cyclic	Linear	Branched
C_{12}	2.3	1	0.5
C_{13}	3.7	2.6	1.3
C_{14}	5.2	2.9	1.5
C_{15}	6.6	4.4	2.2
C_{16}	6.6	5	2.5
C_{17}	6.6	5.6	2.8

Branched and cyclic alkane groups were assigned to linear n-alkanes as surrogates to model the potential formation of SOA. For the reaction in the first 6h, 2×10^6 molecule cm^{-3} was taken as OH concentration (Chan et al., 2009) as it is equivalent to around 0.25 days of daytime atmospheric processing (Presto et al., 2010). A summary of the SOA mass yields of speciated hydrocarbon classes under high NO_x conditions was shown in Table 6.7.

Table 6.7: SOA mass yields of speciated S/IVOCs for high NO_x conditions at the OA concentration of 7 µg/m³.

Carbon No	n-Alkanes	Branched alkanes	Cyclic alkanes	Monocyclic aromatic
C_{10}				0.07[e]
C_{11}				0.07[e]
C_{12}			0.16[d]	0.07[e]
C_{13}	0.18[a]	0.09[c]	0.26[d]	0.07[e]
C_{14}	0.25[a]	0.13[c]	0.36[d]	0.07[e]
C_{15}	0.30[a]	0.15[c]	0.46[d]	0.07[e]
C_{16}	0.33[a]	0.17[c]	0.55[b]	0.07[e]
C_{17}	0.36[a]	0.18[c]	0.63[b]	0.07[e]
C_{18}	0.43[b]	0.21[c]	0.71[b]	0.07[e]
C_{19}	0.47[b]	0.24[c]	0.78[b]	0.07[e]
C_{20}	0.51[b]	0.26[c]	0.85[b]	
C_{21}	0.55[b]	0.28[c]	0.91[b]	
C_{22}	0.59[b]	0.30[c]	0.98[b]	
C_{23}	0.63[b]	0.31[c]	1.04[b]	
C_{24}	0.66[b]	0.33[c]	1.10[b]	
C_{25}	0.70[b]	0.35[c]	1.15[b]	
C_{26}	0.73[b]	0.36[c]		
C_{27}	0.76[b]	0.38[c]		
C_{28}	0.79[b]	0.39[c]		
C_{29}	0.82[b]	0.41[c]		
C_{30}	0.84[b]	0.42[c]		
C_{31}	0.87[b]	0.43[c]		

[a] Presto et al. (2010)

[b] SOA yields of alkane classes change log-linearly with the carbon number (Presto et al., 2010; Tkacik et al., 2012).

[c] Branched alkanes were estimated as half of the value for linear alkanes (Pye and Pouliot, 2012).

[d] Estimated by using n-alkanes as surrogates (Pye and Pouliot, 2012).

[e] Assumed to be the same as toluene (Ng et al., 2007).

6.4.2 SOA formation under high NO_x conditions

The predicted SOA formed by the photooxidation of the four main gas-phase chemical classes measured at the roadside site MR in 3h is shown as Figure 6.2. Although monocyclic aromatics accounted for a substantial fraction (over 20%) of the gas-phase emissions in this study, these compounds contributed to only a small fraction (around 5%) of the SOA formed in the first 3h of photooxidation due to their relatively low SOA yields and slow oxidation rates. This is

consistent with the estimation results of the SOA formation from diesel exhaust suggested by Chan et al. (2009), who reported light aromatics contributed to a much smaller fraction of SOA formation than their fraction in the total emission. Alkane classes were important contributors to SOA formation, and SOA yields of a given carbon number followed the order cyclic> linear>branched alkanes (Loza et al., 2014). Although alkanes (n+i) were the most abundant class in the primary gas-phase emission, monocyclic alkanes made the most significant contribution to SOA formation (39%) in the first 3h due to their substantial primary emission and more significant SOA yields. Bicyclic alkanes contributed to 26% of the SOA formation, followed by n-alkanes (20%) and branched alkanes (10%) at 3h at MR.
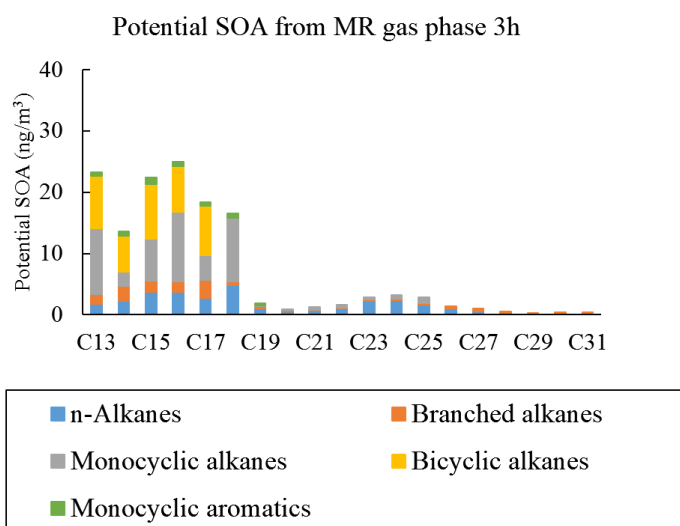
Figure 6.2: The potential SOA formation in the 3h at MR.

6.4.3 SOA yields under low NO$_x$ conditions

To estimate the SOA formation from hydrocarbons in ambient air over longer timescales (after the first 6h), this study assumed the time at 12h and 36h is sufficiently long, allowing 95-100% of the hydrocarbons to react with OH radicals (if ignore the chemical reaction during night-time and deposition of gas-phase hydrocarbons) (Chan et al., 2009). After such a long time, hydrocarbons in ambient air are supposed to be transported from the emission source to more remote regions, where the NO$_x$ level is lower (Henze et al., 2008; Chan et al., 2009). Although much attention has been paid to the SOA formation from alkane classes under high NO$_x$ conditions, few studies reported the SOA yields of alkane classes in the absence of NO$_x$. Yee et al. (2012) developed the photooxidation mechanism and multiple generations of dodecane (C$_{12}$H$_{26}$) under low NO$_x$ conditions, and a later study of Yee et al. (2013) extended the mechanism to C$_{12}$ cyclic and branched alkanes. Lambe et al. (2012) measured the SOA yields for linear C$_{10}$ and C$_{15}$ n-alkanes under OH exposure of up to 2×10^{12} molecules cm^{-3} s, simulating the SOA yields over multiple days of atmospheric oxidation. They reported the maximum SOA yields of C$_{10}$ n-alkanes (0.39) and C$_{15}$ n-alkanes (0.69) were measured at OH exposure of 1.4×10^8 and 9.7×10^7 molecules cm^{-3} h, and SOA concentrations of 231 and 100 µgm^{-3} for C$_{10}$ and C$_{15}$ n-alkanes respectively. Loza et al. (2014) reported SOA yields for C$_{12}$ linear, cyclic and branched alkanes under both high-and low-NO$_x$ conditions. They measured SOA yields after 30-36h irradiation for which the reaction with OH radicals has consumed at least 95% of the initial alkanes, and the corresponding OH exposure was $(6–12) \times 10^7$ molecule cm^{-3} h. However, the SOA yield of C$_{12}$ n-alkane reported by Loza et al. (2014) was less than that of C$_{10}$ n-alkane reported by Lambe et al. (2012) at similar OH exposure although SOA yield of C$_{12}$ n-alkane is expected to lie between those for C$_{10}$ and C$_{15}$ n-alkanes.

Studies suggest that SOA yields under low NO_x conditions increases with the increase of carbon number (Lambe et al., 2012) and follow the order: cyclic> linear ~branched alkanes (Loza et al., 2014). This study derived the SOA yield of n-dodecane under low NO_x conditions at the OA concentration of 7 $\mu g/m^3$ from Loza et al. (2014), and then estimated those of alkanes with linear, branched and cyclic structures based on n-dodecane as a surrogate by the method developed by Pye and Pouliot (2012). Under low NO_x conditions, aromatic compounds are expected to produce more SOA due to higher mass yields (Henze et al., 2008; Ng et al., 2007; Xu et al., 2015). The SOA yields of monocyclic aromatics under low NO_x conditions were estimated based on the toluene yield under high NO_x conditions (Ng et al., 2007) and the branching ratio for toluene between the high- and low- NO_x pathway (Henze et al., 2008). The estimation of SOA yields in the absence of NO_x are shown in Table 6.8. For the reaction at 30-36h, OH exposures were estimated as $(6-12) \times 10^7$ molecule cm^{-3} h (Loza et al., 2014).

Table 6.8: SOA mass yields of speciated S/IVOCs for low NO_x conditions at the OA concentration of 7 µg/m³.

Carbon No	n-alkanes	Branched alkanes	Cyclic alkanes	Monocyclic aromatic
C_{10}				0.22[e]
C_{11}				0.22[e]
C_{12}			0.24[b]	0.22[e]
C_{13}	0.28[a]	0.28[d]	0.39[b]	0.22[e]
C_{14}	0.31[b]	0.31[d]	0.55[b]	0.22[e]
C_{15}	0.47[b]	0.47[d]	0.70[b]	0.22[e]
C_{16}	0.53[b]	0.53[d]	0.83[b]	0.22[e]
C_{17}	0.59[b]	0.59[d]	0.95[c]	0.22[e]
C_{18}	0.69[c]	0.69[d]	1.07[c]	0.22[e]
C_{19}	0.77[c]	0.77[d]	1.18[c]	0.22[e]
C_{20}	0.84[c]	0.84[d]	1.29[c]	0.22[e]
C_{21}	0.90[c]	0.90[d]	1.39[c]	0.22[e]
C_{22}	0.97[c]	0.97[d]	1.48[c]	0.22[e]
C_{23}	1.03[c]	1.03[d]	1.57[c]	0.22[e]
C_{24}	1.09[c]	1.09[d]	1.66[c]	0.22[e]
C_{25}	1.15[c]	1.15[d]	1.75[c]	
C_{26}	1.20[c]	1.20[d]	1.83[c]	
C_{27}	1.25[c]	1.25[d]	1.90[c]	
C_{28}	1.30[c]	1.30[d]		
C_{29}	1.35[c]	1.35[d]		
C_{30}	1.40[c]	1.40[d]		
C_{31}	1.44[c]	1.44[d]		

[a] Derived from Loza et al. (2014)

[b] Derived from n-dodecane and the method developed by Pye and Pouliot (2012).

[c] SOA yields of alkane classes change log-linearly with the carbon number.

[d] SOA yields of branched were set to be the same as n-alkanes (Loza et al., 2014)

[e] Estimation based on the toluene yield under high NO_x conditions (Ng et al., 2007) and the ratio between high- and low- NO_x pathway (Henze et al., 2008).

6.4.4 SOA formation under low NO$_x$ conditions

After the first 6h, SOA formation was estimated based on the mass concentrations of hydrocarbons and the SOA yields under low NO$_x$ conditions. Figure 6.3 shows the SOA formation at 12h and the maximum potential SOA formation after 36 h if all particle-associated material had entered the vapour phase and been available for oxidation. The particle associated S/IVOCs will progressively evaporate and be oxidised with atmospheric dilution caused by the lack of equilibrium between the gas and the particle phase, creating substantial amounts of low-volatility gas-phase compounds (Robinson et al., 2007). Primary particle associated S/IVOCs may potentially contribute a considerable amount of SOA formed from C$_{20}$-C$_{27}$ semi-volatile hydrocarbons (Figure 6.3). The SOA formation from the sum of gas phase and particle phase S/IVOCs at 36h was estimated to present the maximum potential SOA formation, and the realistic SOA formation likely lies between this and the SOA formed by gas phase compounds only. Gas-phase cyclic alkanes still made the overwhelming contribution (54%-55%) to the SOA formation at 12-36h. Gas-phase monocyclic aromatics made a greater contribution to SOA formation (9%-11%) at 12-36h compared with their contribution in the first 3h due to higher SOA yields under low NO$_x$ conditions (Loza et al., 2014; Henze et al., 2008, Ng et al., 2007). At 36h, particle-phase branched alkanes (33%) made the greatest contribution to SOA formation, followed by monocyclic alkanes (26%) and bicyclic alkanes (22%), n-alkanes (18%) and monocyclic aromatics (3%) (Figure 6.3). Figure 6.4 shows the changes in SOA formation from the oxidation of the semi-volatile hydrocarbons with the time at RU. In the first 6h, SOA formation from RU gas-phase showed a steady increase with the time under high NO$_x$ conditions, and then a more significant increase after 6h due to higher SOA yields under low NO$_x$ conditions. The total potential SOA formation at 36 hours based upon the RU data

amounts (both gas and particle phase) was around 0.4 µg m^{-3}, which is only a small contribution to overall SOA measured in background London of around 2.9 µg m^{-3} (Yin et al., 2015).
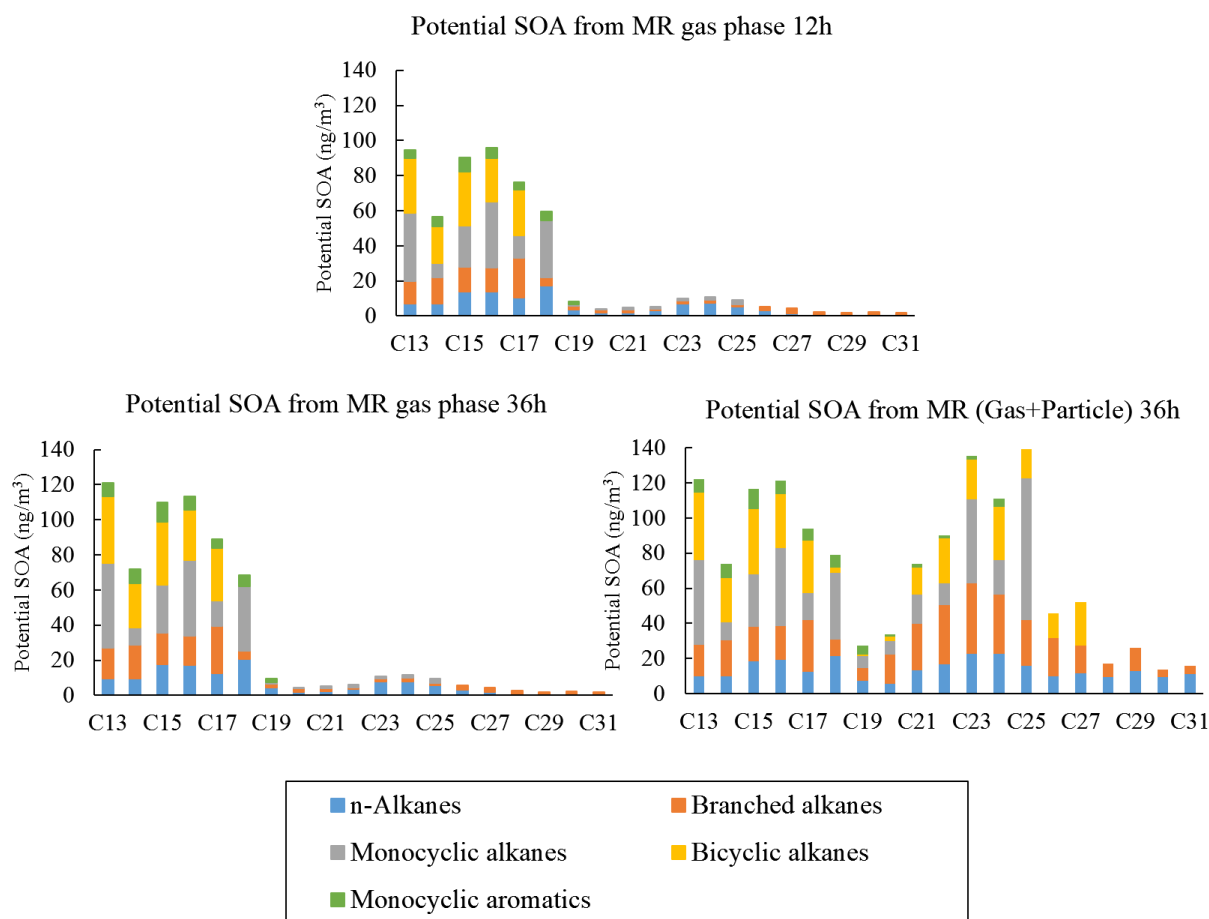
Figure 6.3: The potential SOA formation at 12h and 36h at MR.
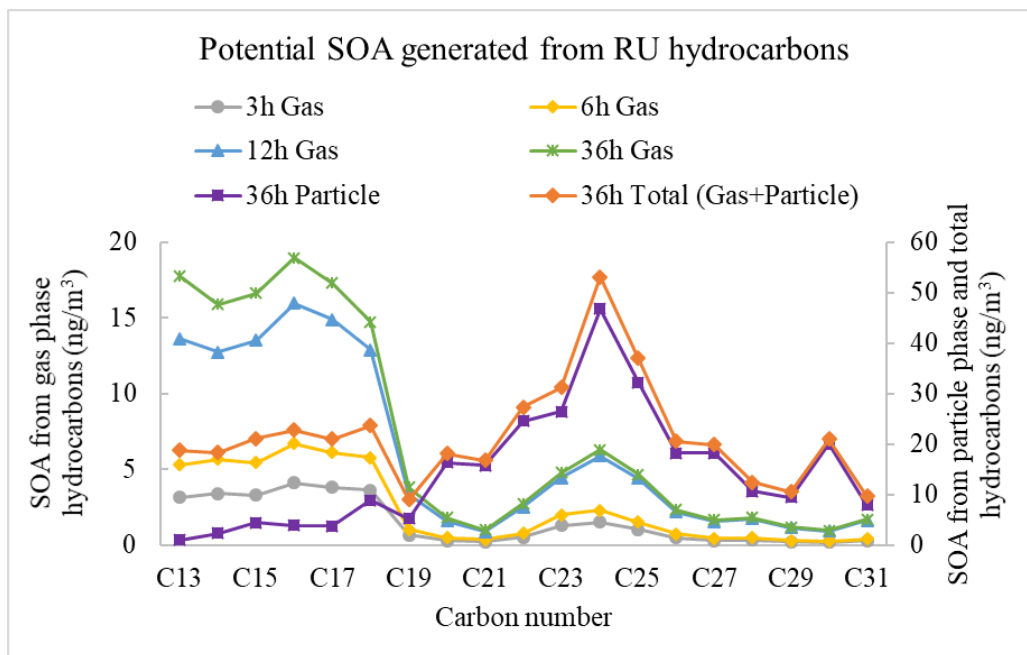
Figure 6.4: Potential SOA generated from the gas phase in the first 3h, 6h, 12h and 36h (first y-axis) and generated from the particle phase and total (gas+particle phase) at 36h (secondary y-axis).

6.5 Conclusion

The partitioning of n-alkanes between the gas phase and the particle phase was examined in this study, showing *Log Kp* correlated well with *Log(VPt)* but with shallower slopes (m_r) at around -0.5 for the regression. The slopes observed in London are broadly similar to other studies of n-alkanes (Mandalakis et al., 2002; Cincinelli et al., 2007; Karanasiou et al., 2007). Many reasons have been discussed to explain the deviation of slopes m_r from the theoretical value of -1. The reason for the shallow slopes is uncertain, but disequilibrium is a possibility due to the proximity of our sites to traffic sources.

The primary OH reactivity and the formation of secondary organic aerosol (SOA) were considered and estimated in this chapter. Alkanes (n+i), cyclic alkanes and aromatics are

important classes of S/IVOCs that react with OH radicals, leading to SOA formation. Roadside site MR had the fastest OH reactivity followed by the rooftop sites WM and RU, due to their lower concentrations. Cyclic alkanes contributed overwhelmingly to the OH reactivity estimated in this study due to their relatively high rate coefficients k_{OH}. The SOA yields under high NO_x conditions were applied to estimate the SOA formation in the first 6h and SOA yields under low NO_x conditions for the SOA formation after 6h. In the first 6h, monocyclic alkanes made the greatest contribution to the SOA formation due to their significant SOA yields and substantial primary emissions. Monocyclic aromatics contributed to only a small fraction of the SOA formation as a result of low SOA yields and slow oxidation rates although they accounted for a more substantial percentage of gas-phase emissions. At 36h, primary particle-phase S/IVOCs were considered into the SOA formation estimation to evaluate the maximum SOA formation. The total estimated SOA formation at RU at 36h (0.4 µg m^{-3}) only made a small contribution to overall SOA in background London (2.9 µg m^{-3}) measured by Yin et al. (2015).

Chapter 7 Overall conclusion

Traffic emitted particles have gained interest in the last decades as many studies have reported the link between particle exposure and cardiovascular health outcomes (Rissler et al., 2012; Fan et al., 2006; Masiol et al., 2012). The gasoline fuel-related organic compounds are mainly in the carbon range below C_{12}, while diesel fuel emissions are mainly in the range from C_8 to C_{25} (Gentner et al., 2012). There are many uncertainties on the composition and behaviour of S/IVOCs in the carbon number range above C_{12}. Firstly, conventional gas chromatography-mass spectrometry (GC-MS) is not able to separate the vast majority of S/IVOC mass and presents them as an unresolved complex mixture (UCM). The UCM is often observed in samples related with the use of fossil fuel (Nelson et al., 2006; Frysinger et al., 2003; Ventura et al., 2008), and accounts for more than 80% of the semi-volatile hydrocarbons emitted from diesel and gasoline-powered engines (Schauer et al., 2002; 1999; Chan et al., 2013). Secondly, a comprehensive understanding of the S/IVOC chemical composition has not been addressed. The carbon range of S/IVOC $\geq C_{12}$ is mainly from diesel-powered vehicles rather than gasoline-powered vehicles in the traffic-relative air samples. Very few studies worked on the abundance of heavier molecular weight hydrocarbons ($\geq C_{12}$), whilst there is a significant increase in the use of diesel vehicles in the UK. Besides, most of the work based on GC techniques only paid attention to a limited range of homologous series that can be distinguished from UCM, such as n-alkanes and PAHs. Thirdly, semi-volatile organic compounds (SVOCs) and intermediate volatility organic compounds (IVOCs) can partition between the gas and particle phase under ambient conditions. Many past studies measured S/IVOCs in the gas phase (Kawashima et al., 2006) or particle phase only (He et al., 2008; Charron et al., 2019; Gupta et al., 2017; Karanasiou et al., 2007) due to their study design or the limit of the sampling instruments. Fourthly, the semi-volatile components of particles can play an important role in photochemical

smog formation and contribute to the formation of secondary organic aerosol (SOA). The specific contribution of S/IVOCs species to SOA formation has not been addressed due to the lack of detailed composition information for these species.

To answer these questions, this study designed an in-house auto-sampler to collect both the gas phase and particle phase of air samples at four sampling sites in central London (UK), including the roadside site at the heavily trafficked Marylebone Road (MR), two rooftop sites (WM and RU) near MR, and an urban background site Eltham (EL) during different times from January to April 2017. A thermal desorption coupled to comprehensive two-dimensional gas chromatography time-of-flight mass spectrometry (TD-GC×GC-ToF-MS) combined with the mapping and grouping methodology was applied to classify, identify and quantify the S/IVOC classes. The aims of this study mainly include (a) provide a comprehensive understanding of the chemical composition of the traffic emitted S/IVOCs above C_{12}; (b) further investigate the behaviour of S/IVOC species based on the detailed S/IVOC composition. Four key research directions built the four discussion chapters (Chapter 3-6) of this thesis.

Chapter 3 mainly reports S/IVOC composition and the average concentrations of the main chemical classes. This study identified and quantified S/IVOCs ranging from C_{10} to C_{36} in both the gas phase and particle phase, and the main S/IVOC classes identified include C_{13}-C_{36} alkanes (n+i) (the sum of n-alkanes and branched alkanes), C_{12}-C_{25} monocyclic alkanes, C_{13}-C_{27} bicyclic alkanes and C_{10}-C_{24} monocyclic aromatics. Abundant acyclic alkanes (linear and branched) and cyclic alkanes (monocyclic and bicyclic) were observed in the urban atmospheric samples, can be explained by the chemical composition of diesel fuel and lubricating oil reported in the literature (Isaacman et al., 2012; Welthagen et al., 2007; Gentner et al., 2012;

Alam et al., 2018; Worton et al., 2014; Sakurai et al., 2003). The S/IVOC composition of urban air was compared with the composition of diesel fuel, lubricating oil and diesel exhaust reported by Alam et al. (2018), who applied the same analysis techniques as used in this study. S/IVOC groups identified in urban air were most abundant at $\leq C_{20}$ in the gas phase, similar to the composition of gas-phase diesel exhaust. S/IVOC groups identified in urban air were most abundant at around C_{21}-C_{27} in the particle phase, consistent with the carbon distribution reported for lubricating oil and the particle-phase diesel exhaust. SVOCs above C_{20} related to gasoline powered- and diesel powered-engines can mainly be attributed to engine oil (Drozd et al., 2019; Alam et al., 2016b), suggesting the most abundant S/IVOCs observed in the particle phase may derive from engine lubricating oil. The high similarities between the composition of urban air samples and those of diesel emissions indicated diesel-powered vehicles were the most probable potential sources for the S/IVOC groups identified in this study.

Chapter 4 further investigates the emission sources and dilution of S/IVOCs at the sampling sites, especially the street canyon of Marylebone Road. The magnitude of n-alkane concentrations and their carbon number distribution were compared with previous studies and DEFRA network data, giving confidence in the data and showing the importance of taking account of these high molecular weight compounds. Molecular diagnostic parameters of n-alkanes (CPI, %WNA, and C_{max}) as well the correlation analysis of S/IVOCs and traffic indicators suggested the traffic emission was the most important source for all four sites with a minor contribution from other sources, such as plant wax. More specifically, the majority of the S/IVOC concentrations were attributed to diesel-powered vehicles while a fraction of the low molecular weight compounds might be attributed to gasoline exhaust, consistent with the findings in Chapter 3. The magnitude of S/IVOC concentrations followed the order:

MR >WM>RU, as the distance increases from the traffic emissions. The effect of wind direction on the dispersion of traffic emitted pollutants in the street canyon MR showed that wind could set up a single vortex in a regular street like Marylebone Road during the crosswind (north wind and south wind).

Chapter 5 estimates the emission factors (EFs) for n-alkanes and the main S/IVOC groups at the roadside site MR. The estimated EFs of n-alkanes were compared with three published studies, including a tunnel study in China (He et al., 2008), a roadside study in Japan (Kawashima et al., 2006) and a roadside study in France (Charron et al., 2019). It suggested that the EF variations in different studies may mainly be explained by the vehicle type and composition of the fuel used in the sampling countries, and also other factors, such as road conditions and vehicle speed.

Chapter 6 discusses the G/P partitioning of n-alkanes, and estimates the OH reactivity and SOA formation from the main S/IVOC groups. *Log Kp* correlated well with *Log(VPt)* but with shallower slopes (m_r) at around -0.5 for the regression, broadly similar to other studies of n-alkanes (Mandalakis et al., 2002; Cincinelli et al., 2007; Karanasiou et al., 2007). Many reasons have been discussed for the shallow slopes, and disequilibrium could be a possible explanation due to the proximity of the sampling sites to traffic sources. Large quantities of gas-phase S/IVOCs can contribute to the generation of secondary pollutants following the reaction with hydroxyl radicals. The primary OH reactivity and potential SOA concentrations from the main S/IVOC groups identified in this study only accounted for a small fraction of the total OH reactivity reported by Whalley et al. (2016) and the overall SOA formation reported by Yin et al. (2015) for the background London. Cyclic alkanes made a substantial contribution to the

OH reactivity and SOA formation due to their relatively high rate coefficients k_{OH}, significant SOA yields and substantial primary emissions. Monocyclic aromatics contributed a lesser fraction of SOA formation compared with their primary gas-phase emissions due to their low SOA yields and slow oxidation rates.

The main advantages/contributions of this study are summarised. First, this study aims at the organic compounds with carbon range above C_{12} as a substantial part of them is referred to as unspeciated chemicals in other studies. The more precise and comprehensive chemical composition of traffic emitted S/IVOCs can provide comparative and fundamental information for future studies (i.e. urban air studies or further modeling work). Second, the mapping chromatogram method allows quantification of the isomer set groups and accounts for approximately 78% of the total ion current of the chromatogram. As a part of FASTER study, previous work in the engine lab identified and quantified the S/IVOC groups of diesel fuel, lubricating oil and diesel exhaust by using the same techniques as in this study (Alam et al., 2018), allowing a comprehensive comparison between the urban air samples with the diesel emissions. Third, this study contributes to more accurate estimations of S/IVOC behaviour based on detailed chemical composition, such as OH reactivity and SOA formation.

The major limitation of this study design is that the sampling at WM/RU, MR and EL were not run simultaneously as there were only two self-designed in-house auto-samplers. Therefore, direct comparisons of S/IVOC concentrations from MR with those from WM/RU and EL were not carried out. Spatial distribution of S/IVOCs at WM-MR-RU was accessed through scaling the MR S/IVOC concentrations by applying BC as a dispersion maker to assume MR S/IVOCs were collected simultaneously with WM and RU. Sampling at four sites simultaneously would

allow more convenient and accurate analysis, but it is a challenge to achieve due to many limits, such as the costs and management of time. The significant variations in seasonal particle concentrations have been discussed in the literature (Fu et al., 2008; Pant et al., 2015; Singh et al., 2011; Yadav et al., 2013). The concentrations of organic compounds in winter are typically higher than summer due to a number of reasons, such as the more stable weather conditions, a shallow boundary layer and extra emissions from heating in winter (Gupta et al., 2017). Sampling for one month is not adequate but measuring S/IVOCs for at least a full year would be useful to define the seasonal as well as spatial patterns. Also, it might be useful to work on the variations in the daily S/IVOC concentrations, such as investigation on the differences in compound concentrations between the weekdays and weekends. A number of studies have compared the emission of organic compounds during the weekdays and weekends as the traffic load might be more massive during weekdays compared with weekends (Gentner et al., 2013; Li et al., 2016; Ho et al., 2009; Grover et al., 2008; Zhao et al., 2014).

This study mainly focuses on acyclic alkanes (linear and branched), cyclic alkanes (monocyclic and bicyclic) and monocyclic aromatics, as they are the major fraction of the diesel related emissions. The main compound groups occupied over 90% of the S/IVOCs identified while the other compound groups identified are C_{11}-C_{16} naphthalenes, C_{12}-C_{13} tetralins, C_{13}-C_{15} biphenyls, C_{14}-C_{15} fluorenes and C_{15}-C_{16} phenanthrenes/anthracenes, contributing 7% of the total S/IVOCs identified at MR and 2% at WM, RU and EL. Future work can be carried out to analyse and discuss the behaviour of these compound groups. Besides, current methods have been designed to cover as much as ion current on the chromatogram, but 22% of the ion current has not been identified. Lyu et al. (2019) further identified alkanals (C_{10}-C_{14}), alkan-2-ones (C_{10}-C_{18}) and alkan-3-ones (C_{10}-C_{16}) for the London Campaign 2017. Exploring the chromatogram might be

able to identify other oxidised compounds or more individual compounds and isomer sets based on the method system built by this study.

.

The FASTER project ran CPC (condensation particle counter) to provide the total particle number count at RU and WM in the London Campaign 2017 (Harrison et al., 2019; Harrison et al., 2018). The concentration variations of the particle-associated SVOCs in time can be compared with the total particle number. The cluster analysis combined with the analysis of inter-group correlations in clusters might be a good method to investigate the patterns of the dataset (Schnelle-Kreis et al., 2005). Besides, measuring meteorological data may provide new findings or explanation for the S/IVOC results. Detailed meteorological data (i.e., wind speed and temperature) may explain the variations in daily S/IVOC concentrations to some extent. The current studies about the SOA formation are mainly based on chamber experiments and numerical models whereas the field measurements might provide a broader view of the S/IVOC behaviour. All the sampling sites selected by this study are at the roadside or in the urban background. A future campaign of S/IVOC measurements at a rural site can be carried out to look at how S/IVOC concentrations differ from those collected in the urban area and the grow-in of more oxidised compounds.

Appendix A. S/IVOC concentrations

Table S1. The concentrations of grouped chemicals (ng/m^3) at four sampling sites in the London Campaign 2017.

Name and total carbon number		WM		RU		MR		EL	
		Gas phase	Particle phase	Gas phase	Particle phase	Gas phase	Particle phase	Gas phase	Particle phase
Monocyclic aromatics	C_{10}	31.75	0.39	22.09	0.36	87.40	1.73	56.11	0.60
	C_{11}	12.64	0.24	8.73	0.20	36.99	0.59	11.02	0.52
	C_{12}	7.72	0.22	6.03	0.33	17.61	0.98	3.26	0.71
	C_{13}	9.35	0.60	6.99	0.66	34.49	1.08	6.17	1.37
	C_{14}	4.78	0.29	4.08	0.23	36.63	0.45	12.85	0.36
	C_{15}	9.18	0.81	6.15	0.90	50.66	1.57	19.16	1.31
	C_{16}	4.02	0.60	2.16	0.51	35.41	0.75	17.00	0.85
	C_{17}	3.64	0.78	2.08	0.85	24.93	4.71	12.57	1.42
	C_{18}	4.09	0.99	2.29	1.05	29.07	4.65	16.04	1.82
	C_{19}	1.81	3.03	0.97	3.90	10.28	13.32	5.71	4.85
	C_{20}		2.31		2.95		5.78		3.18
	C_{21}		6.64		4.17		9.95		7.71
	C_{22}		4.91		2.89		8.95		5.09
	C_{23}		7.43		5.41		9.38		8.91
	C_{24}		12.57		8.49		21.00		13.43
Bicyclic alkanes	C_{13}	12.12	0.10	8.08	0.09	97.62	0.34	39.67	0.27
	C_{14}	9.14	0.23	5.83	0.23	45.28	1.05	14.54	0.51
	C_{15}	9.66	0.21	5.98	0.20	51.39	1.55	20.31	0.47
	C_{16}	8.65	0.27	5.33	0.22	34.25	2.90	13.58	0.42
	C_{17}	4.90	0.53	2.93	0.52	31.05	0.54	15.09	0.93

Bicyclic alkanes	C_{18}		0.53		0.51		2.51		1.08
	C_{19}		0.74		0.68		0.76		1.07
	C_{20}		1.12		1.03		2.02		1.68
	C_{21}		3.82		3.57		11.29		7.60
	C_{22}		7.11		3.30		17.18		7.74
	C_{23}		4.80		2.03		14.39		5.95
	C_{24}		12.68		3.35		18.16		7.65
	C_{25}		5.60		2.04		9.60		3.63
	C_{26}		2.69		1.34		7.82		2.76
	C_{27}		2.57		2.54		13.03		3.21
Biphenyls	C_{13}	0.30	0.01	0.22	0.01	1.78	0.00	0.94	0.01
	C_{14}	0.07	0.00	0.07	0.00	0.49	0.01	0.22	0.00
	C_{15}	0.01	0.00	0.01	0.00	0.13	0.02	0.00	0.00
Alkanes	C_{13}	38.89	2.38	26.52	2.22	97.14	3.35	61.26	3.81
	C_{14}	30.94	5.97	17.56	5.04	93.60	4.48	48.59	8.89
	C_{15}	26.15	4.49	16.42	5.05	75.96	5.24	22.15	6.98
	C_{16}	24.98	5.36	16.33	4.55	63.42	8.57	23.11	9.09
	C_{17}	20.50	2.96	12.93	3.22	66.59	3.64	21.90	6.87
	C_{18}	17.23	6.09	9.98	7.26	36.98	7.71	13.81	10.12
	C_{19}	9.36	3.45	4.49	3.13	8.74	10.25	4.41	7.66
	C_{20}	5.06	11.92	2.04	13.71	4.65	21.77	14.54	20.63
	C_{21}	2.35	13.45	0.74	10.40	4.33	39.55	8.13	21.80
	C_{22}	4.36	23.58	2.43	17.73	4.72	47.12	7.13	42.65
	C_{23}	5.85	17.39	3.69	15.16	9.35	51.75	16.54	26.76
	C_{24}	6.81	26.93	4.69	24.73	9.17	42.73	16.58	39.49
	C_{25}	6.01	16.27	3.75	15.12	6.09	30.32	13.91	26.50
	C_{26}	3.78	14.59	1.94	13.18	4.56	21.70	9.28	33.26
	C_{27}	2.81	10.92	1.32	10.74	3.65	18.09	6.79	16.54

Alkanes	C_{28}	2.42	5.38	1.38	8.19	2.00	11.07	4.88	19.33
	C_{29}	1.64	6.02	0.88	6.96	1.36	17.73	3.20	9.35
	C_{30}	1.60	11.86	0.70	14.32	1.71	8.16	3.54	24.77
	C_{31}	1.46	5.54	1.18	5.49	1.38	9.52	3.27	9.34
	C_{32}		4.09		4.65		10.82		10.27
	C_{33}		7.43		7.46		9.69		10.73
	C_{34}		1.05		2.24		0.82		2.01
	C_{35}		1.54		2.73		0.00		0.22
	C_{36}		0.00		0.00		0.00		0.00
Monocyclic alkanes	C_{12}	26.60	0.80	17.24	0.77	176.44	1.90	97.18	1.57
	C_{13}	23.38	0.53	14.75	0.51	122.96	0.08	65.58	0.79
	C_{14}	15.39	1.85	11.59	1.21	17.84	0.63	6.12	2.98
	C_{15}	6.88	2.45	4.88	2.53	39.17	3.71	19.53	4.64
	C_{16}	10.64	2.09	6.53	1.38	52.51	1.27	25.29	3.28
	C_{17}	11.74	1.17	6.69	1.22	15.24	0.94	6.89	2.22
	C_{18}	10.42	2.83	6.88	2.94	34.04	1.51	16.51	5.79
	C_{19}	0.50	1.01	0.14	0.97	0.64	5.05	0.33	2.97
	C_{20}	0.63	2.82	0.08	2.26	0.34	5.77	0.34	2.73
	C_{21}	1.59	3.04	0.23	0.39	0.90	10.99	0.74	8.10
	C_{22}	0.53	1.04	0.27	1.28	0.96	7.58	0.49	1.29
	C_{23}	0.70	7.41	0.63	4.09	0.67	29.53	0.25	13.17
	C_{24}	0.85	10.56	0.71	7.51	1.07	10.69	0.18	14.19
	C_{25}	0.63	8.70	0.22	6.53	1.44	44.86	0.12	17.49
Fluorene	C_{14}	0.24	0.00	0.16	0.00	1.92	0.00	1.32	0.00
	C_{15}	0.09	0.00	0.06	0.00	0.70	0.16	0.30	0.00
Naphthalene	C_{11}	0.70	0.08	0.62	0.11	17.82	1.37	2.33	0.16
	C_{12}	0.43	0.05	0.34	0.05	13.85	0.46	1.56	0.07
	C_{13}	0.55	0.59	0.38	0.41	19.63	2.42	1.54	0.78

Naphthalene	C_{14}	0.34	0.24	0.21	0.26	15.24	1.86	1.05	0.33
	C_{15+16}	0.96	0.59	0.16	0.25	36.07	2.37	5.04	0.75
Phenanthrene/Anthracene	C_{15}	0.09	0.00	0.07	0.00	0.87	0.00	1.83	0.00
	C_{16}	0.07	0.01	0.04	0.01	0.51	0.00	0.18	0.01
Tetralin	C_{12}	4.24	0.01	2.53	0.01	26.57	0.01	5.85	0.01
	C_{13}	3.30	0.01	1.81	0.02	27.21	0.01	7.03	0.02

Table S2. The concentrations of individual chemical compounds (ng/m^3) at four sampling sites in the London Campaign 2017.

Group	Name	Carbon No	WM		RU		MR		EL	
			Gas	Particle	Gas	Particle	Gas	Particle	Gas	Particle
Alkyl-cyclohexane	Cyclohexane, hexyl-	C$_{12}$	4.77	0.09	3.01	0.08	10.45	0.13	3.66	0.14
	Cyclohexane, heptyl-	C$_{13}$	5.42	0.25	3.25	0.16	14.21	0.04	4.13	0.35
	Cyclohexane, octyl-	C$_{14}$	2.53	0.32	1.68	0.21	8.10	0.17	2.01	0.39
	Cyclohexane, nonyl-	C$_{15}$	1.95	0.47	1.28	0.39	6.27	0.37	2.14	0.70
	Cyclohexane, decyl-	C$_{16}$	1.85	0.42	0.99	0.36	3.55	0.77	1.87	0.86
	Cyclohexane, undecyl-	C$_{17}$	1.83	0.04	0.89	0.06	1.26	0.25	0.50	0.12
	Cyclohexane, dodecyl-	C$_{18}$	0.94	0.00	0.50	0.02	1.70	0.26	0.49	0.10
	Cyclohexane, tridecyl-	C$_{19}$	0.50	0.00	0.14	0.00	0.64	0.41	0.33	0.00
	Cyclohexane, tetradecyl-	C$_{20}$	0.63	0.02	0.08	0.00	0.34	0.29	0.34	0.00
	Cyclohexane, pentadecyl-	C$_{21}$	1.59	0.07	0.23	0.00	0.90	0.16	0.74	0.00
	Cyclohexane, hexadecyl-	C$_{22}$	0.53	0.02	0.27	0.00	0.96	0.55	0.49	0.00
	Cyclohexane, heptadecyl-	C$_{23}$	0.70	0.06	0.63	0.00	0.67	3.19	0.25	0.01
	Cyclohexane, octadecyl-	C$_{24}$	0.85	1.08	0.71	0.83	1.07	3.15	0.18	1.18
	Cyclohexane, nonadecyl-	C$_{25}$	0.63	1.19	0.22	1.05	1.44	4.68	0.12	1.54
Alkyl-benzene	Butylbenzene	C$_{10}$	0.00	0.02	0.03	0.00	16.76	0.00	14.42	0.01
	Hexylbenzene	C$_{12}$	1.23	0.00	0.73	0.01	3.73	0.01	1.67	0.01
	Octylbenzene	C$_{14}$	0.29	0.01	0.24	0.01	1.57	0.03	0.98	0.02
	Decylbenzene	C$_{16}$	0.29	0.02	0.18	0.03	1.99	0.15	0.48	0.03
	Dodecylbenzene	C$_{18}$	0.17	0.59	0.15	0.68	0.60		0.78	
Tetralins	Tetralin	C$_{10}$	1.00	0.00	0.53	0.00	1.14	0.00	0.37	0.00
	5-Methyltetralin	C$_{11}$	0.51	0.00	0.33	0.00	0.89	0.01	0.29	0.00
	1,4-Dimethyltetralin	C$_{12}$	0.45	0.00	0.16	0.00	0.47	0.00	0.13	0.00
	2,5,8-Trimethyltetralin	C$_{13}$	0.30	0.00	0.19	0.00	0.36	0.00	0.15	0.00

	2,2,5,7-Tetramethyltetralin	C_{14}	0.15	0.00	0.05	0.00	0.17	0.03	0.04	0.10
Alkyl-naphthalene	Naphthalene, 1-methyl-	C_{11}	1.64	0.01	1.29	0.00	0.00	0.00	0.00	0.01
	Naphthalene, 1-ethyl-	C_{12}	0.11	0.01	0.07	0.00	0.00	0.01	0.00	0.00
	Naphthalene, 1-propyl-	C_{13}	0.04	0.00	0.03	0.00	0.00	0.03	0.00	0.00
	Naphthalene, 1-hexyl-	C_{16}	0.01	0.00	0.00	0.00	0.00	0.03	0.00	0.01

Appendix B. CLIC expression

This section here defines the CLIC expressions for the descriptive criteria for compound class identification used in this study. These expressions are presented for illustrative purposes. Different rules would be required for different chemical samples and different GC×GC conditions. Examples of the CLIC expression used for tetralin, biphenyl, fluorene and phenanthrene/anthracene in this study are illustrated as following.

Tetralin-C_1

(Ordinal (131) =1) & (relative (146)>15) & (relative (118)>15

Criteria: Base peak 131 and with two of peaks from set greater than 15% relative intensity.

Biphenyls-C_1

(Ordinal (168) =1) & (ordinal (167) =2) & (Relative (168)>90) & (Relative (167) <85) & (Relative (152) <30

Criteria: Base peak 168 and the second largest peak 167. Peaks set of 168 is greater than 90% relative intensity. Peak 167 is smaller than 85% relative intensity and peak 152 is smaller than 30% relative intensity.

Fluorene-C_1

((ordinal (165) =1) & (ordinal (180) =2) & (Relative (165) >90) & (Relative (180)>50) |
((ordinal (180) =1) & (ordinal (165) =2) & (Relative (180)>90) & (Relative (165)>85)

Criteria: (1) Base peak 165 and the second largest peak 180 with peak165 greater than 90% relative intensity and peak 180 greater than 50 % relative intensity. (2) Or base peak 180 and the second largest peak 165 with peak 180 greater than 90% relative intensity and peak 165 greater than 85% relative intensity.

Phenanthrene/Anthracene-C_1

(Ordinal (192) =1) & (ordinal (191) =2) & (Relative (192)>90) & (Relative (191)>30

Criteria: (1) Base peak 192 and the second largest peak 191 with peak 192 greater than 90% relative intensity and peak 191 greater than 30 % relative intensity.

Appendix C. List of publications

In the following a list of all publications stemming from this thesis is given:

XU, R., ALAM, M. S., STARK, C. & HARRISON, R. M. 2019. Composition and Emission Factors of Traffic- Emitted Intermediate Volatility and Semi-Volatile Hydrocarbons (C_{10}-C_{36}) at a Street Canyon and Urban Background Sites in Central London, UK. *Submitted to Atmospheric Environment.*

XU, R., ALAM, M. S., STARK, C. & HARRISON, R. M. 2019. Behaviour of Traffic Emitted Semi-Volatile and Intermediate Volatility Organic Compounds Within the Urban Atmosphere. *Submitted to Science of the Total Environment.*

Co-author publications

HARRISON, R. M., BEDDOWS, D., ALAM, M. S., SINGH, A., BREAN, J., <u>XU, R.,</u> KOTTHAUS, S. & GRIMMOND, S. 2019. Interpretation of particle number size distributions measured across an urban area during the FASTER campaign. *Atmospheric Chemistry and Physics,* 19**,** 39-55.

HARRISON, R. M., ROB MACKENZIE, A., XU, H., ALAM, M. S., NIKOLOVA, I., ZHONG, J., SINGH, A., ZERAATI-REZAEI, S., STARK, C., BEDDOWS, D. C., LIANG, Z., <u>XU, R.</u> & CAI, X. 2018. Diesel exhaust nanoparticles and their behaviour in the atmosphere. *Proceedings of the Royal Society A,* 474**,** 20180492.

LYU, R., ALAM, M. S., STARK, C., <u>XU, R.,</u> SHI, Z., FENG, Y. & HARRISON, R. M. 2019a. Aliphatic carbonyl compounds (C_8–C_{26}) in wintertime atmospheric aerosol in London, UK. *Atmospheric Chemistry and Physics,* 19**,** 2233-2246.

LYU, R., SHI, Z., ALAM, M. S., WU, X., LIU, D., VU, T. V., STARK, C., <u>XU, R.,</u> FU, P. & FENG, Y. 2019b. Alkanes and aliphatic carbonyl compounds in wintertime $PM_{2.5}$ in Beijing, China. *Atmospheric Environment,* 202**,** 244-255.

ZHONG, J., NIKOLOVA, I., CAI, X., MACKENZIE, A. R., ALAM, M. S., <u>XU, R.,</u> SINGH, A. & HARRISON, R. M. 2019a. Implementation of traffic-induced multicomponent ultrafine particles microphysics in WRF v3.6.1 large eddy simulation model: General behaviour from idealised scenarios at the neighbourhood-scale. *Atmospheric Environment.* 117213.

ZHONG, J., NIKOLOVA, I., CAI, X., MACKENZIE, A. R., ALAM, M. S., <u>XU, R.,</u> SINGH, A. & HARRISON, R. M. 2019b. Neighbourhood-scale dispersion of traffic-induced ultrafine particles in central London: A WRF large eddy simulation. *Submitted to Environmental pollution.*

Reference

ALAM, M. S., LIANG, Z., ZERAATI-REZAEI, S., STARK, C., XU, H., MACKENZIE, A. R. & HARRISON, R. M. 2017. Mapping and quantifying isomer sets of hydrocarbons in diesel fuel, lubricating oil and diesel exhaust samples using GC&GC-ToFMS. *Atmospheric Measurement Techniques Discussions*, 1-32.

ALAM, M. S., NIKOLOVA, I., SINGH, A., MACKENZIE, A. & HARRISON, R. M. 2019a. Experimental vapour pressures of eight n-alkanes (C_{17}, C_{18}, C_{20}, C_{22}, C_{24}, C_{26}, C_{28} and C_{31}) measured at ambient temperatures. *Atmospheric Environment,* 213, 739-745.

ALAM, M. S., STARK, C. & HARRISON, R. M. 2016a. Using variable ionization energy time-of-flight mass spectrometry with comprehensive GCxGC To identify isomeric species. *Analytical Chemistry,* 88, 4211-20.

ALAM, M. S., WEST, C. E., SCARLETT, A. G., ROWLAND, S. J. & HARRISON, R. M. 2013. Application of 2D-GCMS reveals many industrial chemicals in airborne particulate matter. *Atmospheric Environment,* 65, 101-111.

ALAM, M. S., ZERAATI-REZAEI, S., LIANG, Z., STARK, C., XU, H., MACKENZIE, A. R. & HARRISON, R. M. 2018. Mapping and quantifying isomer sets of hydrocarbons ($\geqslant$ C_{12}) in diesel exhaust, lubricating oil and diesel fuel samples using GC×GC-ToF-MS. *Atmospheric Measurement Techniques,* 11, 3047-3058.

ALAM, M. S., ZERAATI-REZAEI, S., STARK, C. P., LIANG, Z., XU, H. & HARRISON, R. M. 2016b. The characterisation of diesel exhaust particles–composition, size distribution and partitioning. *Faraday Discussions,* 189, 69-84.

ALAM, M. S., ZERAATI-REZAEI, S., XU, H. & HARRISON, R. M. 2019b. Characterisation of gas and particulate phase organic emissions (C_9-C_{37}) from a diesel engine and the effect of abatement devices. *Environmental Science & Technology,* 53(19) 11345-11352.

ALVES, C. A. 2008. Characterisation of solvent extractable organic constituents in atmospheric particulate matter: an overview. *Anais da Academia Brasileira de Ciências,* 80, 21-82.

ALVES, C. A., OLIVEIRA, C., MARTINS, N., MIRANTE, F., CASEIRO, A., PIO, C., MATOS, M., SILVA, H. F., OLIVEIRA, C. & CAMÕES, F. 2016. Road tunnel, roadside, and urban background measurements of aliphatic compounds in size-segregated particulate matter. *Atmospheric Research,* 168, 139-148.

ANDREOU, G. & RAPSOMANIKIS, S. 2009. Origins of n-alkanes, carbonyl compounds and molecular biomarkers in atmospheric fine and coarse particles of Athens, Greece. *Science of the Total Environment,* 407, 5750-5760.

ARP, H. P. H., SCHWARZENBACH, R. P. & GOSS, K.-U. 2008. Ambient gas/particle partitioning. 2: The influence of particle source and temperature on sorption to dry terrestrial aerosols. *Environmental Science & Technology,* 42, 5951-5957.

ARSENE, C., VIONE, D., GRINBERG, N. & OLARIU, R. I. 2011. GC×GC-Ms hyphenated techniques for the analysis of volatile organic compounds in air. *Journal of Liquid Chromatography & Related Technologies,* 34, 1077-1111.

ATKINSON, R. 1986a. Estimations of OH radical rate constants from H‑atom abstraction from C-H and O-H bonds over the temperature range 250‑1000K. *International Journal of Chemical Kinetics,* 18, 555-568.

ATKINSON, R. 1986b. Kinetics and mechanisms of the gas-phase reactions of the hydroxyl radical with organic compounds under atmospheric conditions. *Chemical Reviews,* 86, 69-201.

ATKINSON, R. 1987. A structure‑activity relationship for the estimation of rate constants for the gas‑phase reactions of OH radicals with organic compounds. *International Journal of Chemical Kinetics,* 19**,** 799-828.

ATKINSON, R. 1991. Kinetics of the gas-phase reactions of a series of organosilicon compounds with hydroxyl and nitrate (NO_3) radicals and ozone at 297+-2 K. *Environmental Science & Technology,* 25**,** 863-866.

ATKINSON, R. 1997. Gas-phase tropospheric chemistry of volatile organic compounds: 1. Alkanes and alkenes. *Journal of Physical Chemical Reference Data,* 26**,** 215-290.

ATKINSON, R. 2003. Kinetics of the gas-phase reactions of OH radicals with alkanes and cycloalkanes. *Atmospheric Chemistry and Physics,* 3**,** 2233-2307.

ATKINSON, R. 2007. Rate constants for the atmospheric reactions of alkoxy radicals: An updated estimation method. *Atmospheric Environment,* 41**,** 8468-8485.

ATKINSON, R. & AREY, J. 2003. Atmospheric degradation of volatile organic compounds. *Chemical Reviews,* 103**,** 4605-4638.

ATKINSON, R. & CARTER, W. P. 1984. Kinetics and mechanisms of the gas-phase reactions of ozone with organic compounds under atmospheric conditions. *Chemical Reviews,* 84**,** 437-470.

AUMONT, B., VALORSO, R., MOUCHEL-VALLON, C., CAMREDON, M., LEE-TAYLOR, J. & MADRONICH, S. 2012. Modeling SOA formation from the oxidation of intermediate volatility n-alkanes. *Atmospheric Chemistry Physics,* 12**,** 7577-7589.

BAHREINI, R., MIDDLEBROOK, A., DE GOUW, J., WARNEKE, C., TRAINER, M., BROCK, C., STARK, H., BROWN, S., DUBE, W. & GILMAN, J. 2012. Gasoline emissions dominate over diesel in formation of secondary organic aerosol mass. *Geophysical Research Letters,* 39.

BAILEY, J. & EGGLESTON, S. 1993. The contribution of gasoline fuelled vehicle exhaust to the UK speciated hydrocarbon inventory. *Science of the Total Environment,* 134**,** 263-271.

BARLEY, M. & MCFIGGANS, G. 2010. The critical assessment of vapour pressure estimation methods for use in modelling the formation of atmospheric organic aerosol. *Atmospheric Chemistry and Physics,* 10**,** 749-767.

BELCHER, S. E. 2005. Mixing and transport in urban areas. *Philosophical Transactions of the Royal Society of London A: Mathematical, Physical and Engineering Sciences,* 363**,** 2947-2968.

BI, X., SHENG, G., PENG, P. A., CHEN, Y., ZHANG, Z. & FU, J. 2003. Distribution of particulate-and vapor-phase n-alkanes and polycyclic aromatic hydrocarbons in urban atmosphere of Guangzhou, China. *Atmospheric Environment,* 37**,** 289-298.

BIDLEMAN, T., ATLAS, E. L., KNAP, A. H., ATKINSON, R., MILLER, J., BONSANG, B., RUDOLPH, J., BURNS, K., TANABE, S. & KEENE, W. C. 1990. *The long-range transport of organic compounds*, Springer.

BIDLEMAN, T. F., BILLINGS, W. N. & FOREMAN, W. T. 1986. Vapor-particle partitioning of semivolatile organic compounds: estimates from field collections. *Environmental Science & Technology,* 20**,** 1038-1043.

BIERMANN, H. W., MAC LEOD, H., ATKINSON, R., WINER, A. M. & PITTS, J. N. 1985. Kinetics of the gas-phase reactions of the hydroxyl radical with naphthalene, phenanthrene, and anthracene. *Environmental Science & Technology,* 19**,** 244-248.

BLUMBERG, L. M., DAVID, F., KLEE, M. S. & SANDRA, P. 2008. Comparison of one-dimensional and comprehensive two-dimensional separations by gas chromatography. *Journal of Chromatography A,* 1188**,** 2-16.

BRUEHLMANN, S., FORSS, A.-M., STEFFEN, D. & HEEB, N. V. 2005. Benzene: a secondary pollutant formed in the three-way catalyst. *Environmental Science & Technology,* 39**,** 331-338.

BURCAT, A., DIXON-LEWIS, G., FRENKLACH, M., HANSON, R. K., SALIMIAN, S., TROE, J., WARNATZ, J. & ZELLNER, R. 2012. Combustion Chemistry. *Edit by Gardiner, W. J., Springer-Verlag New York Inc., New York, NY, USA.*

CALLÉN, M., DE LA CRUZ, M., LÓPEZ, J., MURILLO, R., NAVARRO, M. & MASTRAL, A. 2008. Some inferences on the mechanism of atmospheric gas/particle partitioning of polycyclic aromatic hydrocarbons (PAH) at Zaragoza (Spain). *Chemosphere,* 73**,** 1357-1365.

CAPPA, C., ZHANG, X., LOZA, C., CRAVEN, J., LEE, Y. & SEINFELD, J. 2013. Application of the statistical oxidation model (SOM) to secondary organic aerosol formation from photooxidation of C_{12} alkanes. *Atmospheric Chemistry and Physics,* 13**,** 1591-1606.

CARR, D., VON EHRENSTEIN, O., WEILAND, S., WAGNER, C., WELLIE, O., NICOLAI, T. & VON MUTIUS, E. 2002. Modeling annual benzene, toluene, NO_2, and soot concentrations on the basis of road traffic characteristics. *Environmental Research,* 90**,** 111-118.

CARSLAW, D. C., BEEVERS, S. D., TATE, J. E., WESTMORELAND, E. J. & WILLIAMS, M. L. 2011. Recent evidence concerning higher NO_x emissions from passenger cars and light duty vehicles. *Atmospheric Environment,* 45**,** 7053-7063.

CHAN, A. W. H., ISAACMAN, G., WILSON, K. R., WORTON, D. R., RUEHL, C. R., NAH, T., GENTNER, D. R., DALLMANN, T. R., KIRCHSTETTER, T. W., HARLEY, R. A., GILMAN, J. B., KUSTER, W. C., DE GOUW, J. A., OFFENBERG, J. H., KLEINDIENST, T. E., LIN, Y. H., RUBITSCHUN, C. L., SURRATT, J. D., HAYES, P. L., JIMENEZ, J. L. & GOLDSTEIN, A. H. 2013. Detailed chemical characterization of unresolved complex mixtures in atmospheric organics: Insights into emission sources, atmospheric processing, and secondary organic aerosol formation. *Journal of Geophysical Research: Atmospheres,* 118**,** 6783-6796.

CHAN, A. W. H., KAUTZMAN, K., CHHABRA, P., SURRATT, J., CHAN, M., CROUNSE, J., KÜRTEN, A., WENNBERG, P., FLAGAN, R. & SEINFELD, J. 2009. Secondary organic aerosol formation from photooxidation of naphthalene and alkylnaphthalenes: implications for oxidation of intermediate volatility organic compounds (IVOCs). *Atmospheric Chemistry and Physics,* 9**,** 3049-3060.

CHARRON, A., POLO-REHN, L., BESOMBES, J.-L., GOLLY, B., BUISSON, C., CHANUT, H., MARCHAND, N., GUILLAUD, G. & JAFFREZO, J.-L. 2019. Identification and quantification of particulate tracers of exhaust and non-exhaust vehicle emissions. *Atmospheric Chemistry and Physics,* 19(7)**,** 5187-5207.

CHIRICO, R., DECARLO, P., HERINGA, M., TRITSCHER, T., RICHTER, R., PRÉVÔT, A., DOMMEN, J., WEINGARTNER, E., WEHRLE, G. & GYSEL, M. 2010. Impact of aftertreatment devices on primary emissions and secondary organic aerosol formation potential from in-use diesel vehicles: results from smog chamber experiments. *Atmospheric Chemistry and Physics* 10.

CHOW, J. C., WATSON, J. G., FUJITA, E. M., LU, Z., LAWSON, D. R. & ASHBAUGH, L. L. 1994. Temporal and spatial variations of $PM_{2.5}$ and PM_{10} aerosol in the Southern California air quality study. *Atmospheric Environment,* 28**,** 2061-2080.

CINCINELLI, A., BUBBA, M. D., MARTELLINI, T., GAMBARO, A. & LEPRI, L. 2007. Gas-particle concentration and distribution of n-alkanes and polycyclic aromatic hydrocarbons in the atmosphere of Prato (Italy). *Chemosphere,* 68**,** 472-8.

COLLINS, J. F., BROWN, J. P., ALEXEEFF, G. V. & SALMON, A. G. 1998. Potency equivalency factors for some polycyclic aromatic hydrocarbons and polycyclic aromatic hydrocarbon derivatives. *Regulatory Toxicology and Pharmacology,* 28**,** 45-54.

COMPERNOLLE, S., CEULEMANS, K. & MÜLLER, J.-F. 2011. EVAPORATION: a new vapour pressure estimation methodfor organic molecules including non-additivity and intramolecular interactions. *Atmospheric Chemistry and Physics,* 11**,** 9431-9450.

DALL'OSTO, M., THORPE, A., BEDDOWS, D. C. S., HARRISON, R. M., BARLOW, J. F., DUNBAR, T., WILLIAMS, P. I. & COE, H. 2011. Remarkable dynamics of nanoparticles in the urban atmosphere. *Atmospheric Chemistry and Physics,* 11**,** 6623-6637.

DALLUGE, J., RIJN, M. V., BEENS, J., VREULS, R. J. J. & BRINKMAN, U. A. T. 2002. Comprehensive two-dimensional gas chromatography with time-offlight mass spectrometric detection applied to the determination of pesticides in food extracts. *Journal of Chromatography A,* 965**,** 207–217.

DECHAPANYA, W., EUSEBI, A., KIMURA, Y. & ALLEN, D. T. 2003a. Secondary organic aerosol formation from aromatic precursors. 1. Mechanisms for individual hydrocarbons. *Environmental Science & Technology,* 37**,** 3662-3670.

DECHAPANYA, W., EUSEBI, A., KIMURA, Y. & ALLEN, D. T. 2003b. Secondary organic aerosol formation from aromatic precursors. 2. Mechanisms for lumped aromatic hydrocarbons. *Environmental Science & Technology,* 37**,** 3671-3679.

DEPAUL, F. & SHEIH, C. 1985. A tracer study of dispersion in an urban street canyon. *Atmospheric Environment* 19**,** 555-559.

DROZD, G. T., ZHAO, Y., SALIBA, G., FRODIN, B., MADDOX, C., OLIVER CHANG, M. C., MALDONADO, H., SARDAR, S., WEBER, R. J., ROBINSON, A. L. & GOLDSTEIN, A. H. 2019. Detailed speciation of intermediate volatility and semivolatile organic compound emissions from gasoline vehicles: effects of cold-starts and implications for secondary organic aerosol formation. *Environmental Science & Technology,* 53**,** 1706-1714.

DUFFY, B. L. & NELSON, P. F. 1996. Non-methane exhaust composition in the Sydney Harbour Tunnel: A focus on benzene and 1, 3-butadiene. *Atmospheric Environment,* 30**,** 2759-2768.

DUNMORE, R., HOPKINS, J., LIDSTER, R., LEE, J., EVANS, M., RICKARD, A., LEWIS, A. & HAMILTON, J. 2015. Diesel-related hydrocarbons can dominate gas phase reactive carbon in megacities. *Atmospheric Chemistry and Physics,* 15**,** 9983-9996.

EL-ZANAN, H. S., LOWENTHAL, D. H., ZIELINSKA, B., CHOW, J. C. & KUMAR, N. J. C. 2005. Determination of the organic aerosol mass to organic carbon ratio in IMPROVE samples. *Chemosphere,* 60**,** 485-496.

ELURI, S., CAPPA, C. D., FRIEDMAN, B., FARMER, D. K. & JATHAR, S. H. 2018. Modeling the formation and composition of secondary organic aerosol from diesel exhaust using parameterized and semi-explicit chemistry and thermodynamic models. *Atmospheric Chemistry and Physics,* 18**,** 13813-13838.

EMEP/EEA 2016. Technical guidance to prepare national emission inventories, EEA Report No 21/016, European Environment Agency, Denmark. *Air Pollutant Emission Inventory Guidebook 2016.*

EPI. 2017. *EPI Suite™ - Estimation Program Interface v4.11* [Online]. Available: https://www.epa.gov/tsca-screening-tools/download-epi-suitetm-estimation-program-interface-v411 [Accessed 18 Jan 2019].

EXXONMOBIL 2014. The Outlook for Energy: A view to 2040. *Tech. rep., Exxon Mobil Corporation, Texas.*

EYZAT, P. & GUIBET, J.-C. 1968. A new look at nitrogen oxides formation in internal combustion engines. *SAE Transactions,* 481-500.

FAN, Z., MENG, Q., WEISEL, C., SHALAT, S., LAUMBACH, R., OHMAN-STRICKLAND, P., BLACK, K., RODRIGUEZ, M. & BONANNO, L. 2006. Acute short-term exposures to $PM_{2.5}$ generated by vehicular emissions and cardiopulmonary effects in older adults. *Epidemiology,* 17**,** S213-S214.

FERNANDES, M. B., BRICKUS, L. S., MOREIRA, J. & CARDOSO, J. 2002. Atmospheric BTX and polyaromatic hydrocarbons in Rio de Janeiro, Brazil. *Chemosphere,* 47**,** 417-425.

FERNÁNDEZ, P., GRIMALT, J. O. & VILANOVA, R. M. 2002. Atmospheric gas-particle partitioning of polycyclic aromatic hydrocarbons in high mountain regions of Europe. *Environmental Science & Technology,* 36**,** 1162-1168.

FLEET NEWS. 2018. *Record number of diesel cars now on Britain's roads, says RAC Foundation* [Online]. Available: https://www.fleetnews.co.uk/news/manufacturer-news/2018/04/16/diesel-cars-reach-record-number-in-britain [Accessed 07/02/2019].

FOREMAN, W. T. & BIDLEMAN, T. F. 1990. Semivolatile organic compounds in the ambient air of Denver, Colorado. *Atmospheric Environment. Part A. General Topics,* 24**,** 2405-2416.

FRASER, M. P., CASS, G. R. & SIMONEIT, B. R. 1998. Gas-phase and particle-phase organic compounds emitted from motor vehicle traffic in a Los Angeles roadway tunnel. *Environmental Science & Technology,* 32**,** 2051-2060.

FRYSINGER, G. S., GAINES, R. B., XU, L. & REDDY, C. M. 2003. Resolving the unresolved complex mixture in petroleum-contaminated sediments. *Environmental Science & Technology,* 37**,** 1653-1662.

GAGA, E. O. & ARI, A. 2011. Gas–particle partitioning of polycyclic aromatic hydrocarbons (PAHs) in an urban traffic site in Eskisehir, Turkey. *Atmospheric Research,* 99**,** 207-216.

GENTNER, D. R., HARLEY, R. A., MILLER, A. M. & GOLDSTEIN, A. H. 2009. Diurnal and seasonal variability of gasoline-related volatile organic compound emissions in Riverside, California. *Environmental Science & Technology,* 43**,** 4247-4252.

GENTNER, D. R., ISAACMAN, G., WORTON, D. R., CHAN, A. W., DALLMANN, T. R., DAVIS, L., LIU, S., DAY, D. A., RUSSELL, L. M. & WILSON, K. R. 2012. Elucidating secondary organic aerosol from diesel and gasoline vehicles through detailed characterization of organic carbon emissions. *Proceedings of the National Academy of Sciences,* 109**,** 18318-18323.

GENTNER, D. R., WORTON, D. R., ISAACMAN, G., DAVIS, L. C., DALLMANN, T. R., WOOD, E. C., HERNDON, S. C., GOLDSTEIN, A. H. & HARLEY, R. A. 2013. Chemical composition of gas-phase organic carbon emissions from motor vehicles and implications for ozone production. *Environmental Science & Technology,* 47**,** 11837-11848.

GOLDSTEIN, A. H. & GALBALLY, I. E. 2007. Known and unexplored organic constituents in the earth's atmosphere. *Environmemental Science & Technology,* MARCH 1**,** 1515-1521.

GORDON, T. D., TKACIK, D. S., PRESTO, A. A., ZHANG, M., JATHAR, S. H., NGUYEN, N. T., MASSETTI, J., TRUONG, T., CICERO-FERNANDEZ, P. & MADDOX, C. 2013. Primary gas-and particle-phase emissions and secondary organic aerosol production from gasoline and diesel off-road engines. *Environmental Science & Technology,* 47**,** 14137-14146.

GRIESHOP, A. P., MIRACOLO, M. A., DONAHUE, N. M. & ROBINSON, A. L. 2009. Constraining the volatility distribution and gas-particle partitioning of combustion aerosols using isothermal dilution and thermodenuder measurements. *Environmental Science & Technology,* 43**,** 4750-4756.

GROMKE, C., BUCCOLIERI, R., DI SABATINO, S. & RUCK, B. 2008. Dispersion study in a street canyon with tree planting by means of wind tunnel and numerical investigations–evaluation of CFD data with experimental data. *Atmospheric Environment,* 42**,** 8640-8650.

GROSJEAN, D. & FRIEDLANDER, S. K. 1975. Gas-particle distribution factors for organic and other pollutants in the Los Angeles atmosphere. *Journal of the Air Pollution Control Association,* 25**,** 1038-1044.

GROVER, B. D., EATOUGH, N. L., WOOLWINE, W. R., CANNON, J. P., EATOUGH, D. J. & LONG, R. W. J. A. E. 2008. Semi-continuous mass closure of the major components of fine particulate matter in Riverside, CA. 42**,** 250-260.

GUPTA, S., GADI, R., MANDAL, T. K. & SHARMA, S. K. 2017. Seasonal variations and source profile of n-alkanes in particulate matter (PM_{10}) at a heavy traffic site, Delhi. *Environ Monit Assess,* 189**,** 43.

GUSTAFSON, K. E. & DICKHUT, R. M. 1996. Particle/gas concentrations and distributions of PAHs in the atmosphere of southern Chesapeake Bay. *Environmental Science & Technology,* 31**,** 140-147.

HAMILTON, J., WEBB, P., LEWIS, A., HOPKINS, J., SMITH, S. & DAVY, P. 2004. Partially oxidised organic components in urban aerosol using GCXGC-TOF/MS. *Atmospheric Chemistry and Physics,* 4**,** 1279-1290.

HAMILTON, J. F. & LEWIS, A. C. 2003. Monoaromatic complexity in urban air and gasoline assessed using comprehensive GC and fast GC-TOF/MS. *Atmospheric Environment,* 37**,** 589-602.

HARLEY, R. A., HOOPER, D. S., KEAN, A. J., KIRCHSTETTER, T. W., HESSON, J. M., BALBERAN, N. T., STEVENSON, E. D. & KENDALL, G. R. 2006. Effects of reformulated gasoline and motor vehicle fleet turnover on emissions and ambient concentrations of benzene. *Environmental Science & Technology,* 40**,** 5084-5088.

HARNER, T. & BIDLEMAN, T. F. 1998. Octanol− air partition coefficient for describing particle/gas partitioning of aromatic compounds in urban air. *Environmental Science & Technology,* 32**,** 1494-1502.

HARRISON, R. M., BEDDOWS, D., ALAM, M. S., SINGH, A., BREAN, J., XU, R., KOTTHAUS, S. & GRIMMOND, S. 2019. Interpretation of particle number size distributions measured across an urban area during the FASTER campaign. *Atmospheric Chemistry and Physics,* 19**,** 39-55.

HARRISON, R. M. & BEDDOWS, D. C. 2017. Efficacy of recent emissions controls on road vehicles in Europe and implications for public health. *Scientific Reports,* 7**,** 1152.

HARRISON, R. M., BEDDOWS, D. C. & DALL'OSTO, M. 2011. PMF analysis of wide-range particle size spectra collected on a major highway. *Environmental Science & Technology,* 45**,** 5522-5528.

HARRISON, R. M., JONES, A. M., BEDDOWS, D. C. S., DALL'OSTO, M. & NIKOLOVA, I. 2016. Evaporation of traffic-generated nanoparticles during advection from source. *Atmospheric Environment,* 125**,** 1-7.

HARRISON, R. M., ROB MACKENZIE, A., XU, H., ALAM, M. S., NIKOLOVA, I., ZHONG, J., SINGH, A., ZERAATI-REZAEI, S., STARK, C., BEDDOWS, D. C., LIANG, Z., XU, R. & CAI, X. 2018. Diesel exhaust nanoparticles and their behaviour in the atmosphere. *Proceedings of the Royal Society A,* 474**,** 20180492.

HE, J. & BALASUBRAMANIAN, R. 2009. A study of gas/particle partitioning of SVOCs in the tropical atmosphere of Southeast Asia. *Atmospheric Environment,* 43**,** 4375-4383.

HE, L.-Y., HU, M., ZHANG, Y.-H., HUANG, X.-F. & YAO, T.-T. 2008. Fine particle emissions from on-road vehicles in the Zhujiang Tunnel, China. *Environmental Science & Technology,* 42**,** 4461-4466.

HEALD, C. L., JACOB, D. J., PARK, R. J., RUSSELL, L. M., HUEBERT, B. J., SEINFELD, J. H., LIAO, H. & WEBER, R. J. 2005. A large organic aerosol source in the free troposphere missing from current models. *Geophysical Research Letters,* 32.

HENZE, D., SEINFELD, J., NG, N., KROLL, J., FU, T.-M., JACOB, D. J. & HEALD, C. 2008. Global modeling of secondary organic aerosol formation from aromatic hydrocarbons: high-vs. low-yield pathways. *Atmospheric Chemistry and Physics,* 8**,** 2405-2420.

HO, K., HO, S. S. H., LEE, S., CHENG, Y., CHOW, J. C., WATSON, J. G., LOUIE, P. K. K. & TIAN, L. 2009. Emissions of gas-and particle-phase polycyclic aromatic hydrocarbons (PAHs) in the Shing Mun Tunnel, Hong Kong. *Atmospheric Environment,* 43**,** 6343-6351.

HUO, H., YAO, Z., ZHANG, Y., SHEN, X., ZHANG, Q., DING, Y. & HE, K. 2012. On-board measurements of emissions from light-duty gasoline vehicles in three mega-cities of China. *Atmospheric Environment,* 49**,** 371-377.

HWA, M.-Y., HSIEH, C.-C., WU, T.-C. & CHANG, L.-F. W. 2002. Real-world vehicle emissions and VOCs profile in the Taipei tunnel located at Taiwan Taipei area. *Atmospheric Environment,* 36**,** 1993-2002.

ISAACMAN, G., WILSON, K. R., CHAN, A. W., WORTON, D. R., KIMMEL, J. R., NAH, T., HOHAUS, T., GONIN, M., KROLL, J. H. & WORSNOP, D. R. 2012. Improved resolution of hydrocarbon structures and constitutional isomers in complex mixtures using gas chromatography-vacuum ultraviolet-mass spectrometry. *Analytical chemistry,* 84**,** 2335-2342.

JACOBSON, M., KITTELSON, D. & WATTS, W. 2005. Enhanced coagulation due to evaporation and its effect on nanoparticle evolution. *Environmental Science & Technology,* 39**,** 9486-9492.

JANG, M. & KAMENS, R. M. 2001. Characterization of secondary aerosol from the photooxidation of toluene in the presence of NO_x and 1-propene. *Environmental Science & Technology,* 35**,** 3626-3639.

JATHAR, S. H., MIRACOLO, M. A., PRESTO, A. A., DONAHUE, N. M., ADAMS, P. J. & ROBINSON, A. L. 2012. Modeling the formation and properties of traditional and non-traditional secondary organic aerosol: problem formulation and application to aircraft exhaust. *Atmospheric Chemistry and Physics,* 12**,** 9025-9040.

JEONG, S. J. & ANDREWS, M. J. 2002. Application of the k–ε turbulence model to the high Reynolds number skimming flow field of an urban street canyon. *Atmospheric Environment,* 36**,** 1137-1145.

JIMENEZ, J., CANAGARATNA, M., DONAHUE, N., PREVOT, A., ZHANG, Q., KROLL, J. H., DECARLO, P. F., ALLAN, J. D., COE, H. & NG, N. 2009. Evolution of organic aerosols in the atmosphere. *Science,* 326**,** 1525-1529.

JOHNSON, D., UTEMBE, S., JENKIN, M., DERWENT, R., HAYMAN, G., ALFARRA, M., COE, H. & MCFIGGANS, G. 2006. Simulating regional scale secondary organic aerosol formation during the TORCH 2003 campaign in the southern UK. *Atmospheric Chemistry and Physics,* 6**,** 403-418.

JONES, A. M. & HARRISON, R. M. 2006. Estimation of the emission factors of particle number and mass fractions from traffic at a site where mean vehicle speeds vary over short distances. *Atmospheric Environment,* 40**,** 7125-7137.

JORDAN, C., ZIEMANN, P., GRIFFIN, R., LIM, Y., ATKINSON, R. & AREY, J. 2008. Modeling SOA formation from OH reactions with C_8–C_{17}n-alkanes. *Atmospheric Environment,* 42**,** 8015-8026.

KALLIO, M., JUSSILA, M., RISSANEN, T., ANTTILA, P., HARTONEN, K., REISSELL, A., VREULS, R., ADAHCHOUR, M. & HYÖTYLÄINEN, T. 2006. Comprehensive two-dimensional gas chromatography coupled to time-of-flight mass spectrometry in the identification of organic compounds in atmospheric aerosols from coniferous forest. *Journal of Chromatography A,* 1125**,** 234-243.

KARANASIOU, A., SITARAS, I., SISKOS, P. & ELEFTHERIADIS, K. 2007. Size distribution and sources of trace metals and n-alkanes in the Athens urban aerosol during summer. *Atmospheric Environment,* 41**,** 2368-2381.

KAUPP, H. & MCLACHLAN, M. S. 1999. Gas/particle partitioning of PCDD/Fs, PCBs, PCNs and PAHs. *Chemosphere,* 38**,** 3411-3421.

KAWASHIMA, H., MINAMI, S., HANAI, Y. & FUSHIMI, A. 2006. Volatile organic compound emission factors from roadside measurements. *Atmospheric Environment,* 40**,** 2301-2312.

KERBACHI, R., BOUGHEDAOUI, M., BOUNOUA, L. & KEDDAM, M. 2006. Ambient air pollution by aromatic hydrocarbons in Algiers. *Atmospheric Environment,* 40**,** 3995-4003.

KIRCHSTETTER, T. W., SINGER, B. C., HARLEY, R. A., KENDALL, G. R. & CHAN, W. 1996. Impact of oxygenated gasoline use on California light-duty vehicle emissions. *Environmental Science & Technology,* 30**,** 661-670.

KIRCHSTETTER, T. W., SINGER, B. C., HARLEY, R. A., KENDALL, G. R. & HESSON, J. M. 1999. Impact of California reformulated gasoline on motor vehicle emissions. 2. Volatile organic compound speciation and reactivity. *Environmental Science & Technology,* 33**,** 329-336.

KISS, G., VARGA, B., GALAMBOS, I. & GANSZKY, I. 2002. Characterization of water-soluble organic matter isolated from atmospheric fine aerosol. *Journal of Geophysical Research: Atmospheres,* 107**,** ICC 1-1-ICC 1-8.

KLEINDIENST, T., CONVER, T., MCIVER, C. & EDNEY, E. 2004. Determination of secondary organic aerosol products from the photooxidation of toluene and their implications in ambient $PM_{2.5}$. *Journal of Atmospheric Chemistry,* 47**,** 79-100.

KROLL, J. H., DONAHUE, N. M., JIMENEZ, J. L., KESSLER, S. H., CANAGARATNA, M. R., WILSON, K. R., ALTIERI, K. E., MAZZOLENI, L. R., WOZNIAK, A. S. & BLUHM, H. 2011. Carbon oxidation state as a metric for describing the chemistry of atmospheric organic aerosol. *Nature Chemistry,* 3**,** 133.

KUMAR, P., FENNELL, P. & BRITTER, R. 2008. Effect of wind direction and speed on the dispersion of nucleation and accumulation mode particles in an urban street canyon. *Science of the Total Environment,* 402**,** 82-94.

KWOK, E. S. & ATKINSON, R. 1995. Estimation of hydroxyl radical reaction rate constants for gas-phase organic compounds using a structure-reactivity relationship: an update. *Atmospheric Environment,* 29**,** 1685-1695.

LAITINEN, T., MARTIN, S. H., PARSHINTSEV, J., HYOTYLAINEN, T., HARTONEN, K., RIEKKOLA, M. L., KULMALA, M. & PAVON, J. L. 2010. Determination of organic compounds from wood combustion aerosol nanoparticles by different gas chromatographic systems and by aerosol mass spectrometry. *Journal of Chromatography A,* 1217**,** 151-9.

LAMBE, A. T., ONASCH, T. B., CROASDALE, D. R., WRIGHT, J. P., MARTIN, A. T., FRANKLIN, J. P., MASSOLI, P., KROLL, J. H., CANAGARATNA, M. R., BRUNE, W. H., WORSNOP, D. R. & DAVIDOVITS, P. 2012. Transitions from functionalization to fragmentation reactions of laboratory secondary organic aerosol (SOA) generated from the OH oxidation of alkane precursors. *Environmental Science & Technology,* 46**,** 5430-7.

LAVOIE, G. A., HEYWOOD, J. B. & KECK, J. C. 1970. Experimental and theoretical study of nitric oxide formation in internal combustion engines. *Combustion Science Technology,* 1**,** 313-326.

LEAL-GRANADILLO, I. A., ALONSO, J. I. G. & SANZ-MEDEL, A. 2000. Determination of n-alkanes and polycyclic aromatic hydrocarbons in atmospheric particulate and vapour phases in Oviedo, Spain, by GC-MS. *Journal of Environmental Monitoring,* 2**,** 218-222.

LECO. 2019. Available: https://www.leco.com/product/pegasus-bt-4d [Accessed June 2019].

LEPPARD, W. R., RAPP, L. A., BURNS, V. R., GORSE, R. A., KNEPPER, J. C. & KOEHL, W. J. 1992. Effects of gasoline composition on vehicle engine-out and tailpipe hydrocarbon emissions-The Auto/Oil Air Quality Improvement Research Program. SAE Technical Paper.

LESKINEN, A. P., JOKINIEMI, J. K. & LEHTINEN, K. E. J. 2007. Transformation of diesel engine exhaust in an environmental chamber. *Atmospheric Environment,* 41**,** 8865-8873.

LEWIS, A. C., CARSLAW, N., MARRIOTT, P. J., KINGHORN, R. M., MORRISON, P., LEE, A. L., BARTLE, K. D. & PILLING, M. J. 2000. A larger pool of ozone-forming carbon compounds in urban atmospheres. *Nature,* 405**,** 778.

LI, X., DALLMANN, T. R., MAY, A. A., TKACIK, D. S., LAMBE, A. T., JAYNE, J. T., CROTEAU, P. L. & PRESTO, A. A. 2016. Gas-particle partitioning of vehicle emitted primary organic aerosol measured in a traffic tunnel. *Environmental Science & Technology,* 50**,** 12146-12155.

LIANG, C., PANKOW, J. F., ODUM, J. R. & SEINFELD, J. H. 1997. Gas/particle partitioning of semivolatile organic compounds to model inorganic, organic, and ambient smog aerosols. *Environmental Science & Technology,* 31**,** 3086-3092.

LIANG, Z., CHEN, L., ALAM, M. S., REZAEI, S. Z., STARK, C., XU, H. & HARRISON, R. M. 2018. Comprehensive chemical characterization of lubricating oils used in modern vehicular engines utilizing GC×GC-TOFMS. *Fuel,* 220**,** 792-799.

LIM, Y. B. & ZIEMANN, P. J. 2005. Products and mechanism of secondary organic aerosol formation from reactions of n-alkanes with OH radicals in the presence of NO_x. *Environmental Science & Technology,* 39**,** 9229-9236.

LIM, Y. B. & ZIEMANN, P. J. 2009a. Chemistry of secondary organic aerosol formation from OH Radical-initiated reactions of linear, branched, and cyclic alkanes in the presence of NO$_x$. *Aerosol Science and Technology,* 43**,** 604-619.

LIM, Y. B. & ZIEMANN, P. J. 2009b. Effects of molecular structure on aerosol yields from OH radical-initiated reactions of linear, branched, and cyclic alkanes in the presence of NO$_x$. *Environmental Science & Technology,* 43**,** 2328-2334.

LIM, Y. B. & ZIEMANN, P. J. 2009c. Kinetics of the heterogeneous conversion of 1, 4-hydroxycarbonyls to cyclic hemiacetals and dihydrofurans on organic aerosol particles. *Physical Chemistry Chemical Physics,* 11**,** 8029-8039.

LIPSKY, E. M. & ROBINSON, A. L. 2006. Effects of dilution on fine particle mass and partitioning of semivolatile organics in diesel exhaust and wood smoke. *Environmental Science & Technology,* 40**,** 155-162.

LOHMANN, R., HARNER, T., THOMAS, G. O. & JONES, K. C. 2000. A comparative study of the gas-particle partitioning of PCDD/Fs, PCBs, and PAHs. *Environmental Science & Technology,* 34**,** 4943-4951.

LOZA, C. L., CRAVEN, J. S., YEE, L. D., COGGON, M. M., SCHWANTES, R. H., SHIRAIWA, M., ZHANG, X., SCHILLING, K. A., NG, N. L., CANAGARATNA, M. R., ZIEMANN, P. J., FLAGAN, R. C. & SEINFELD, J. H. 2014. Secondary organic aerosol yields of 12-carbon alkanes. *Atmospheric Chemistry and Physics,* 14**,** 1423-1439.

LYU, R., ALAM, M. S., STARK, C., XU, R., SHI, Z., FENG, Y. & HARRISON, R. M. 2019. Aliphatic carbonyl compounds (C$_8$–C$_{26}$) in wintertime atmospheric aerosol in London, UK. *Atmospheric Chemistry and Physics,* 19**,** 2233-2246.

MADER, B. T. & PANKOW, J. F. 2001. Gas/solid partitioning of semivolatile organic compounds (SOCs) to air filters. 2. Partitioning of polychlorinated dibenzodioxins, polychlorinated dibenzofurans, and polycyclic aromatic hydrocarbons to quartz fiber filters. *Atmospheric Environment,* 35**,** 1217-1223.

MANDALAKIS, M., TSAPAKIS, M., TSOGA, A. & STEPHANOU, E. G. 2002. Gas–particle concentrations and distribution of aliphatic hydrocarbons, PAHs, PCBs and PCDD/Fs in the atmosphere of Athens (Greece). *Atmospheric Environment,* 36**,** 4023-4035.

MANNING, A., NICHOLSON, K., MIDDLETON, D. & RAFFERTY, S. 2000. Field study of wind and traffic to test a street canyon pollution model. *Environmental Monitoring Assessment,* 60**,** 283-313.

MAO, D., VAN DE WEGHE, H., LOOKMAN, R., VANERMEN, G., DE BRUCKER, N. & DIELS, L. 2009. Resolving the unresolved complex mixture in motor oils using high-performance liquid chromatography followed by comprehensive two-dimensional gas chromatography. *Fuel,* 88**,** 312-318.

MASIOL, M., HOFER, A., SQUIZZATO, S., PIAZZA, R., RAMPAZZO, G. & PAVONI, B. 2012. Carcinogenic and mutagenic risk associated to airborne particle-phase polycyclic aromatic hydrocarbons: a source apportionment. *Atmospheric Environment,* 60**,** 375-382.

MAY, A. A., PRESTO, A. A., HENNIGAN, C. J., NGUYEN, N. T., GORDON, T. D. & ROBINSON, A. L. 2013. Gas-particle partitioning of primary organic aerosol emissions:(1) Gasoline vehicle exhaust. *Atmospheric Environment,* 77**,** 128-139.

MAZUREK, M. & SIMONEIT, B. 1984. Characterization of biogenic and petroleum-derived organic matter in aerosols over remote, rural and urban areas. *Identification and Analysis of Organic Pollutants in Air,* 22**,** 353.

MCCONNELL, G. 1963. Oxides of nitrogen in diesel engine exhaust gas: their formation and control. *Proceedings of the Institution of Mechanical Engineers,* 178**,** 1001-1010.

MERKER, G. P., HOHLBAUM, B. & RAUSCHER, M. 1993. Two-zone model for calculation of nitrogen-oxide formation in direct-injection diesel engines. *SAE Transactions***,** 2043-2050.

MET OFFICE, M. O. 2006. *MIDAS: UK hourly weather observation data. NCAS British Atmospheric Data Centre* [Online]. Available: http://catalogue.ceda.ac.uk/uuid/916ac4bbc46f7685ae9a5e10451bae7c [Accessed 21 March 2019].

MILLER, F. J., GARDNER, D. E., GRAHAM, J. A., LEE JR, R. E., WILSON, W. E. & BACHMANN, J. D. 1979. Size considerations for establishing a standard for inhalable particles. *Journal of the Air Pollution Control Association,* 29**,** 610-615.

MIRANTE, F., ALVES, C., PIO, C., PINDADO, O., PEREZ, R., REVUELTA, M. A. & ARTIÑANO, B. 2013. Organic composition of size segregated atmospheric particulate matter, during summer and winter sampling campaigns at representative sites in Madrid, Spain. *Atmospheric Research,* 132-133**,** 345-361.

MORRIS, R. E., KOO, B., GUENTHER, A., YARWOOD, G., MCNALLY, D., TESCHE, T., TONNESEN, G., BOYLAN, J. & BREWER, P. 2006. Model sensitivity evaluation for organic carbon using two multi-pollutant air quality models that simulate regional haze in the southeastern United States. *Atmospheric Environment,* 40**,** 4960-4972.

NAEI. 2019. *National Atmospheric Emissions Inventory* [Online]. [Accessed Accessed 21 March 2019].

NELSON, R. K., KILE, B. M., PLATA, D. L., SYLVA, S. P., XU, L., REDDY, C. M., GAINES, R. B., FRYSINGER, G. S. & REICHENBACH, S. E. 2006. Tracking the weathering of an oil spill with comprehensive two-dimensional gas chromatography. *Environmental Forensics,* 7**,** 33-44.

NEWHALL, H. K. Kinetics of engine-generated nitrogen oxides and carbon monoxide. Symposium (International) on Combustion, 1969. Elsevier, 603-613.

NG, N., KROLL, J., CHAN, A., CHHABRA, P., FLAGAN, R. & SEINFELD, J. 2007. Secondary organic aerosol formation from m-xylene, toluene, and benzene. *Atmospheric Chemistry and Physics,* 7**,** 3909-3922.

NIKOLOVA, I., MACKENZIE, A. R., CAI, X., ALAM, M. S. & HARRISON, R. M. 2016. Modelling component evaporation and composition change of traffic-induced ultrafine particles during travel from street canyon to urban background. *Faraday discussions,* 189**,** 529-546.

NTZIACHRISTOS, L., SAMARAS, Z., KOURIDIS, C., SAMARAS, C., HASSEL, D., MELLIOS, G., MCCRAE, I., HICKMAN, J., ZIEROCK, K.-H., KELLER, M., REXEIS, M., ANDRE, M., WINTHER, M., PASTRAMAS, N., GORISSEN, N., BOULTER, P., KATSIS, P., JOUMARD, R., RIJKEBOER, R., GEIVANIDIS, S. & HAUSBERGER, S. 2017. EMEP/EEA air pollutant emission inventory guidebook 2016.

O'MEARA, S., BOOTH, A. M., BARLEY, M. H., TOPPING, D. & MCFIGGANS, G. 2014. An assessment of vapour pressure estimation methods. *Physical Chemistry Chemical Physics,* 16**,** 19453-19469.

OCHIAI, N., IEDA, T., SASAMOTO, K., FUSHIMI, A., HASEGAWA, S., TANABE, K. & KOBAYASHI, S. 2007. Comprehensive two-dimensional gas chromatography coupled to high-resolution time-of-flight mass spectrometry and simultaneous nitrogen phosphorous and mass spectrometric detection for characterization of nanoparticles in roadside atmosphere. *Journal of Chromatography A,* 1150**,** 13-20.

ODUM, J. R., JUNGKAMP, T., GRIFFIN, R. J., FORSTNER, H., FLAGAN, R. C. & SEINFELD, J. H. 1997. Aromatics, reformulated gasoline, and atmospheric organic aerosol formation. *Environmental Science & Technology,* 31**,** 1890-1897.

OMAR, N. Y. M. J., ABAS, M. R. B., RAHMAN, N. A., TAHIR, N. M., RUSHDI, A. I. & SIMONEIT, B. R. T. 2007. Levels and distributions of organic source tracers in air and roadside dust particles of Kuala Lumpur, Malaysia. *Environmental Geology,* 52**,** 1485-1500.

ÖZEL, M. Z., WARD, M. W., HAMILTON, J. F., LEWIS, A. C., RAVENTÓS-DURAN, T. & HARRISON, R. M. 2010. Analysis of organic nitrogen compounds in urban aerosol samples using GCxGC-TOF/MS. *Aerosol Science and Technology,* 44**,** 109-116.

PAKKANEN, T. A., KERMINEN, V.-M., OJANEN, C. H., HILLAMO, R. E., AARNIO, P. & KOSKENTALO, T. 2000. Atmospheric black carbon in Helsinki. *Atmospheric Environment,* 34**,** 1497-1506.

PANKOW, J. F. 1994. An absorption model of gas/particle partitioning of organic compounds in the atmosphere. *Atmospheric Environment,* 28**,** 185-188.

PANKOW, J. F. & BIDLEMAN, T. F. 1992. Interdependence of the slopes and intercepts from log-log correlations of measured gas-particle paritioning and vapor pressure I. theory and analysis of available data. *Atmospheric Environment. Part A. General Topics,* 26**,** 1071-1080.

PANT, P. & HARRISON, R. M. 2013. Estimation of the contribution of road traffic emissions to particulate matter concentrations from field measurements: a review. *Atmospheric Environment,* 77**,** 78-97.

PAVAGEAU, M., RAFAILIDIS, S. & SCHATZMANN, M. 1997. A comprehensive experimental databank for the verification of urban car emission dispersion models. *International Journal of Environment Pollution,* 8**,** 738-746.

PERRONE, M. G., CARBONE, C., FAEDO, D., FERRERO, L., MAGGIONI, A., SANGIORGI, G. & BOLZACCHINI, E. 2014. Exhaust emissions of polycyclic aromatic hydrocarbons, n-alkanes and phenols from vehicles coming within different European classes. *Atmospheric Environment,* 82**,** 391-400.

PIO, C., ALVES, C. & DUARTE, A. 2001. Identification, abundance and origin of atmospheric organic particulate matter in a Portuguese rural area. *Atmospheric Environment,* 35**,** 1365-1375.

PIRJOLA, L., LÄHDE, T., NIEMI, J., KOUSA, A., RÖNKKÖ, T., KARJALAINEN, P., KESKINEN, J., FREY, A. & HILLAMO, R. 2012. Spatial and temporal characterization of traffic emissions in urban microenvironments with a mobile laboratory. *Atmospheric Environment,* 63**,** 156-167.

POLIDORI, A., TURPIN, B. J., DAVIDSON, C. I., RODENBURG, L. A. & MAIMONE, F. 2008. Organic $PM_{2.5}$: fractionation by polarity, FTIR spectroscopy, and OM/OC ratio for the Pittsburgh aerosol. *Aerosol Science and Technology,* 42**,** 233-246.

PRESTO, A. A., HENNIGAN, C. J., NGUYEN, N. T. & ROBINSON, A. L. 2012. Determination of volatility distributions of primary organic aerosol emissions from internal combustion engines using thermal desorption gas chromatography mass spectrometry. *Aerosol Science and Technology,* 46**,** 1129-1139.

PRESTO, A. A., HUFF HARTZ, K. E. & DONAHUE, N. M. 2005. Secondary organic aerosol production from terpene ozonolysis. 2. Effect of NO x concentration. *Environmental Science & Technology,* 39**,** 7046-7054.

PRESTO, A. A., MIRACOLO, M. A., DONAHUE, N. M. & ROBINSON, A. L. 2010. Secondary organic aerosol formation from high-NO_x photo-oxidation of low volatility precursors: n-alkanes. *Environmental Science & Technology,* 44**,** 2029-2034.

PRESTO, A. A., MIRACOLO, M. A., KROLL, J. H., WORSNOP, D. R., ROBINSON, A. L. & DONAHUE, N. M. 2009. Intermediate-volatility organic compounds: A potential source of ambient oxidized organic aerosol. *Environmental Science & Technology,* 43**,** 4744-4749.

PYE, H. O. & POULIOT, G. A. 2012. Modeling the role of alkanes, polycyclic aromatic hydrocarbons, and their oligomers in secondary organic aerosol formation. *Environmental Science & Technology,* 46**,** 6041-7.

PYE, H. O. & SEINFELD, J. H. 2010. A global perspective on aerosol from low-volatility organic compounds. *Atmospheric Chemistry and Physics,* 10**,** 4377-4401.

RAJKUMAR, W. S. & CHANG, A. S. 2000. Suspended particulate matter concentrations along the east–west corridor, Trinidad, West Indies. *Atmospheric Environment,* 34**,** 1181-1187.

RECHE, C., QUEROL, X., ALASTUEY, A., VIANA, M., PEY, J., MORENO, T., RODRÍGUEZ, S., GONZÁLEZ, Y., FERNÁNDEZ-CAMACHO, R. & ROSA, J. 2011. New considerations for PM, Black Carbon and particle number concentration for air quality monitoring across different European cities. *Atmospheric Chemistry and Physics,* 11**,** 6207-6227.

REFF, A., TURPIN, B. J., OFFENBERG, J. H., WEISEL, C. P., ZHANG, J., MORANDI, M., STOCK, T., COLOME, S. & WINER, A. 2007. A functional group characterization of organic $PM_{2.5}$ exposure: Results from the RIOPA study. *Atmospheric Environment,* 41**,** 4585-4598.

REICHENBACH, S. E., KOTTAPALLI, V., NI, M. & VISVANATHAN, A. 2005. Computer language for identifying chemicals with comprehensive two-dimensional gas chromatography and mass spectrometry. *Journal of Chromatography A,* 1071**,** 263-269.

RISSLER, J., SWIETLICKI, E., BENGTSSON, A., BOMAN, C., PAGELS, J., SANDSTRÖM, T., BLOMBERG, A. & LÖNDAHL, J. 2012. Experimental determination of deposition of diesel exhaust particles in the human respiratory tract. *Journal of Aerosol Science,* 48**,** 18-33.

ROBINSON, A. L., DONAHUE, N. M., SHRIVASTAVA, M. K., WEITKAMP, E. A., SAGE, A. M., GRIESHOP, A. P., LANE, T. E., PIERCE, J. R. & PANDIS, S. N. 2007. Rethinking organic aerosols: Semivolatile emissions and photochemical aging. *Science,* 315**,** 1259-1262.

ROGGE, W. F., HILDEMANN, L. M., MAZUREK, M. A., CASS, G. R. & SIMONEIT, B. R. 1993a. Sources of fine organic aerosol. 2. Noncatalyst and catalyst-equipped automobiles and heavy-duty diesel trucks. *Environmental Science & Technology,* 27**,** 636-651.

ROGGE, W. F., HILDEMANN, L. M., MAZUREK, M. A., CASS, G. R. & SIMONEIT, B. R. 1993b. Sources of fine organic aerosol. 3. Road dust, tire debris, and organometallic brake lining dust: roads as sources and sinks. *Environmental Science & Technology,* 27**,** 1892-1904.

ROGGE, W. F., MAZUREK, M. A., HILDEMANN, L. M., CASS, G. R. & SIMONEIT, B. R. 1993c. Quantification of urban organic aerosols at a molecular level: identification, abundance and seasonal variation. *Atmospheric Environment. Part A. General Topics,* 27**,** 1309-1330.

ROGGE, W. F., MAZUREK, M. A., HILDEMANN, L. M., CASS, G. R. & SIMONEIT, B. R. T. 1993d. Quantification of urban organic aerosols at a molecular level: Identification,

abundance and seasonal variation. *Atmospheric Environment. Part A. General Topics,* 27**,** 1309-1330.

ROTH, C. M., GOSS, K.-U. & SCHWARZENBACH, R. P. 2005. Sorption of a diverse set of organic vapors to diesel soot and road tunnel aerosols. *Environmental Science & Technology,* 39**,** 6632-6637.

RUSSELL, L. M., BAHADUR, R. & ZIEMANN, P. J. 2011. Identifying organic aerosol sources by comparing functional group composition in chamber and atmospheric particles. *Proceedings of the National Academy of Sciences,* 108**,** 3516-3521.

SAKURAI, H., TOBIAS, H. J., PARK, K., ZARLING, D., DOCHERTY, K. S., KITTELSON, D. B., MCMURRY, P. H. & ZIEMANN, P. J. 2003. On-line measurements of diesel nanoparticle composition and volatility. *Atmospheric Environment,* 37**,** 1199-1210.

SAMY, S. & ZIELINSKA, B. 2010. Secondary organic aerosol production from modern diesel engine emissions. *Atmospheric Chemistry and Physics,* 10**,** 609-625.

SANGIORGI, G., FERRERO, L., PERRONE, M., PAPA, E. & BOLZACCHINI, E. 2014. Semivolatile PAH and n-alkane gas/particle partitioning using the dual model: up-to-date coefficients and comparison with experimental data. *Environmental Science and Pollution Research,* 21**,** 10163-10173.

SCHAUER, J. J., KLEEMAN, M. J., CASS, G. R. & SIMONEIT, B. R. 1999. Measurement of emissions from air pollution sources. 2. C_1 through C_{30} organic compounds from medium duty diesel trucks. *Environmental Science & Technology,* 33**,** 1578-1587.

SCHAUER, J. J., KLEEMAN, M. J., CASS, G. R. & SIMONEIT, B. R. 2002. Measurement of emissions from air pollution sources. 5. C_1− C_{32} organic compounds from gasoline-powered motor vehicles. *Environmental Science & Technology,* 36**,** 1169-1180.

SCHNELLE-KREIS, J., SKLORZ, M., PETERS, A., CYRYS, J. & ZIMMERMANN, R. 2005. Analysis of particle-associated semi-volatile aromatic and aliphatic hydrocarbons in urban particulate matter on a daily basis. *Atmospheric Environment,* 39**,** 7702-7714.

SIGSBY, J. E., TEJADA, S., RAY, W., LANG, J. M. & DUNCAN, J. W. 1987. Volatile organic compound emissions from 46 in-use passenger cars. *Environmental Science & Technology,* 21**,** 466-475.

SIMONEIT, B. R. 1999. A review of biomarker compounds as source indicators and tracers for air pollution. *Environmental science and pollution research,* 6**,** 159-169.

SIMONEIT, B. R., KOBAYASHI, M., MOCHIDA, M., KAWAMURA, K., LEE, M., LIM, H. J., TURPIN, B. J. & KOMAZAKI, Y. 2004. Composition and major sources of organic compounds of aerosol particulate matter sampled during the ACE‐Asia campaign. *Journal of Geophysical Research: Atmospheres,* 109.

SMMT 2015. The society of motor manufacturers and traders – Motor industry facts

SONG, C., NA, K. & COCKER, D. R. 2005. Impact of the hydrocarbon to NO x ratio on secondary organic aerosol formation. *Environmental Science & Technology,* 39**,** 3143-3149.

SONG, C., NA, K., WARREN, B., MALLOY, Q. & COCKER, D. R. 2007. Secondary organic aerosol formation from m-xylene in the absence of NO_x. *Environmental Science & Technology,* 41**,** 7409-7416.

SPINDT, R., WOLFE, C. L. & STEVENS, D. R. 1956. Nitrogen oxides, combustion, and engine deposits. *Journal of the Air Pollution Control Association,* 6**,** 127-133.

SPRINGER, G. 2012. *Engine emissions: pollutant formation and measurement*, Springer Science & Business Media.

STAEHELIN, J., KELLER, C., STAHEL, W., SCHLÄPFER, K. & WUNDERLI, S. 1998. Emission factors from road traffic from a tunnel study (Gubrist tunnel, Switzerland).

Part III: Results of organic compounds, SO_2 and speciation of organic exhaust emission. *Atmospheric Environment, 32,* 999-1009.

TAKEGAWA, N., MIYAZAKI, Y., KONDO, Y., KOMAZAKI, Y., MIYAKAWA, T., JIMENEZ, J., JAYNE, J., WORSNOP, D., ALLAN, J. & WEBER, R. 2005. Characterization of an Aerodyne Aerosol Mass Spectrometer (AMS): Intercomparison with other aerosol instruments. *Aerosol Science and Technology, 39,* 760-770.

TERZI, E. & SAMARA, C. 2004. Gas-particle partitioning of polycyclic aromatic hydrocarbons in urban, adjacent coastal, and continental background sites of western Greece. *Environmental Science & Technology, 38,* 4973-4978.

TKACIK, D. S., PRESTO, A. A., DONAHUE, N. M. & ROBINSON, A. L. 2012. Secondary organic aerosol formation from intermediate-volatility organic compounds: cyclic, linear, and branched alkanes. *Environmental Science & Technology, 46,* 8773-8781.

TOPPING, D., BARLEY, M., BANE, M., HIGHAM, N. J., AUMONT, B., DINGLE, N. & MCFIGGANS, G. 2016. UManSysProp v1. 0: an online and open-source facility for molecular property prediction and atmospheric aerosol calculations. *Geoscientific Model Development, 9,* 899-914.

TRANCHIDA, P. Q., PURCARO, G., SCIARRONE, D., DUGO, P., DUGO, G. & MONDELLO, L. 2010. Accurate quadrupole MS peak reconstruction in optimized gas-flow comprehensive two-dimensional gas chromatography. *Journal of Separation Science, 33,* 2791-2795.

TURPIN, B. J. & LIM, H.-J. 2001. Species contributions to $PM_{2.5}$ mass concentrations: Revisiting common assumptions for estimating organic mass. *Aerosol Science and Technology, 35,* 602-610.

UMANSYSPROP. 2016. Available: http://umansysprop.seaes.manchester.ac.uk/tool/vapour_pressure [Accessed 18 Jan 2019].

UTELL, M. & SAMET, J. 1996. Airborne particles and respiratory disease: clinical and pathogenetic considerations. *Particles in Our Air (Cambridge, MA: Harvard University Press, 1996).*

VAN DEURSEN, M., BEENS, J., REIJENGA, J., LIPMAN, P., CRAMERS, C. & BLOMBERG, J. 2000. Group-type identification of oil samples using comprehensive two-dimensional gas chromatography coupled to a time-of-flight mass spectrometer (GC× GC-TOF). *Journal of High Resolution Chromatography, 23,* 507-510.

VARDOULAKIS, S., FISHER, B. E., PERICLEOUS, K. & GONZALEZ-FLESCA, N. 2003. Modelling air quality in street canyons: a review. *Atmospheric Environment, 37,* 155-182.

VENTURA, G. T., KENIG, F., REDDY, C. M., FRYSINGER, G. S., NELSON, R. K., VAN MOOY, B. & GAINES, R. B. 2008. Analysis of unresolved complex mixtures of hydrocarbons extracted from Late Archean sediments by comprehensive two-dimensional gas chromatography (GC×GC). *Organic Geochemistry, 39,* 846-867.

VUTUKURU, S., GRIFFIN, R. J. & DABDUB, D. 2006. Simulation and analysis of secondary organic aerosol dynamics in the South Coast Air Basin of California. *Journal of Geophysical Research: Atmospheres, 111.*

WANG, G., KAWAMURA, K., XIE, M., HU, S., GAO, S., CAO, J., AN, Z. & WANG, Z. 2009. Size-distributions of n-alkanes, PAHs and hopanes and their sources in the urban, mountain and marine atmospheres over East Asia. *Atmospheric Chemistry and Physics, 9,* 8869–8882.

WATSON, J. G., CHOW, J. C., LOWENTHAL, D. H., PRITCHETT, L. C., FRAZIER, C. A., NEUROTH, G. R. & ROBBINS, R. 1994. Differences in the carbon composition of source profiles for diesel-and gasoline-powered vehicles. *Atmospheric Environment,* 28**,** 2493-2505.

WEHNER, B., BIRMILI, W., GNAUK, T. & WIEDENSOHLER, A. 2002. Particle number size distributions in a street canyon and their transformation into the urban-air background: measurements and a simple model study. *Atmospheric Environment,* 36**,** 2215-2223.

WEITKAMP, E. A., SAGE, A. M., PIERCE, J. R., DONAHUE, N. M. & ROBINSON, A. L. 2007. Organic aerosol formation from photochemical oxidation of diesel exhaust in a smog chamber. *Environmental Science & Technology,* 41**,** 6969-6975.

WELTHAGEN, W., MITSCHKE, S., MÜHLBERGER, F. & ZIMMERMANN, R. 2007. One-dimensional and comprehensive two-dimensional gas chromatography coupled to soft photo ionization time-of-flight mass spectrometry: a two-and three-dimensional separation approach. *Journal of Chromatography A,* 1150**,** 54-61.

WELTHAGEN, W., SCHNELLE-KREIS, J. & ZIMMERMANN, R. 2003. Search criteria and rules for comprehensive two-dimensional gas chromatography–time-of-flight mass spectrometry analysis of airborne particulate matter. *Journal of Chromatography A,* 1019**,** 233-249.

WESTBROOK, C. K. 2000. Chemical kinetics of hydrocarbon ignition in practical combustion systems. *Proceedings of the Combustion Institute,* 28**,** 1563-1577.

WHALLEY, L., STONE, D., BANDY, B., DUNMORE, R., HAMILTON, J. F., HOPKINS, J., LEE, J. D., LEWIS, A. C. & HEARD, D. E. 2016. Atmospheric OH reactivity in central London: observations, model predictions and estimates of in situ ozone production. *Atmospheric Chemistry and Physics,* 16**,** 2109-2122.

WHITE, W. H. & ROBERTS, P. 1977. On the nature and origins of visibility-reducing aerosols in the Los Angeles air basin. *Atmospheric Environment,* 11**,** 803-812.

WILLIAMS, B., GOLDSTEIN, A., KREISBERG, N., HERING, S., WORSNOP, D., ULBRICH, I., DOCHERTY, K. & JIMENEZ, J. 2010a. Major components of atmospheric organic aerosol in southern California as determined by hourly measurements of source marker compounds. *Atmospheric Chemistry and Physics,* 10**,** 11577-11603.

WILLIAMS, B. J., GOLDSTEIN, A. H., KREISBERG, N. M. & HERING, S. V. 2010b. In situ measurements of gas/particle-phase transitions for atmospheric semivolatile organic compounds. *Proceedings of the National Academy of Sciences,* 107**,** 6676-6681.

WOLFF, E. W. & CACHIER, H. 1998. Concentrations and seasonal cycle of black carbon in aerosol at a coastal Antarctic station. *Journal of Geophysical Research: Atmospheres,* 103**,** 11033-11041.

WORTON, D. R., ISAACMAN, G., GENTNER, D. R., DALLMANN, T. R., CHAN, A. W., RUEHL, C., KIRCHSTETTER, T. W., WILSON, K. R., HARLEY, R. A. & GOLDSTEIN, A. H. 2014. Lubricating oil dominates primary organic aerosol emissions from motor vehicles. *Environmental Science & Technology,* 48**,** 3698-3706.

XU, J., GRIFFIN, R. J., LIU, Y., NAKAO, S. & COCKER III, D. R. 2015. Simulated impact of NO_x on SOA formation from oxidation of toluene and m-xylene. *Atmospheric Environment,* 101**,** 217-225.

XU, X., STEE, L., WILLIAMS, J., BEENS, J., ADAHCHOUR, M., VREULS, R., BRINKMAN, U. & LELIEVELD, J. 2003a. Comprehensive two-dimensional gas

chromatography (GC×GC) measurements of volatile organic compounds in the atmosphere. *Atmospheric Chemistry and Physics,* 3**,** 665-682.

XU, X., WILLIAMS, C., PLASS-DÜLMER, H., BERRESHEIM, H., SALISBURY, G., LANGE, L. & LELIEVELD, J. 2003b. GC×GC measurements of C_7-C_{11} aromatic and n-alkane hydrocarbons on Crete, in air from Eastern Europe during the MINOS campaign. *Atmospheric Chemistry and Physics,* 3**,** 1461-1475.

YAMASAKI, H., KUWATA, K. & MIYAMOTO, H. 1982. Effects of ambient temperature on aspects of airborne polycyclic aromatic hydrocarbons. *Environmental Science & Technology,* 16**,** 189-194.

YEE, L. D., CRAVEN, J. S., LOZA, C. L., SCHILLING, K. A., NG, N. L., CANAGARATNA, M. R., ZIEMANN, P. J., FLAGAN, R. C. & SEINFELD, J. H. 2012. Secondary organic aerosol formation from low-$NO_{(x)}$ photooxidation of dodecane: evolution of multigeneration gas-phase chemistry and aerosol composition. *The Journal of Physical Chemistry* 116**,** 6211-30.

YEE, L. D., CRAVEN, J. S., LOZA, C. L., SCHILLING, K. A., NG, N. L., CANAGARATNA, M. R., ZIEMANN, P. J., FLAGAN, R. C. & SEINFELD, J. H. 2013. Effect of chemical structure on secondary organic aerosol formation for C_{12} alkanes. *Atmospheric Chemistry and Physics,* 13**,** 11121-11140.

YIN, J., CUMBERLAND, S. A., HARRISON, R. M., ALLAN, J., YOUNG, D. E., WILLIAMS, P. I. & COE, H. 2015. Receptor modelling of fine particles in southern England using CMB including comparison with AMS-PMF factors. *Atmospheric Chemistry and Physics,* 15**,** 2139-2158.

ZHANG, Q., JIMENEZ, J. L., CANAGARATNA, M., ALLAN, J., COE, H., ULBRICH, I., ALFARRA, M., TAKAMI, A., MIDDLEBROOK, A. & SUN, Y. 2007. Ubiquity and dominance of oxygenated species in organic aerosols in anthropogenically‑influenced Northern Hemisphere midlatitudes. *Geophysical Research Letters,* 34.

ZHANG, X. & SEINFELD, J. 2013. A functional group oxidation model (FGOM) for SOA formation and aging. *Atmospheric Chemistry and Physics,* 13**,** 5907-5926.

ZHAO, L., WANG, X., HE, Q., WANG, H., SHENG, G., CHAN, L. Y., FU, J. & BLAKE, D. R. 2004. Exposure to hazardous volatile organic compounds, PM_{10} and CO while walking along streets in urban Guangzhou, China. *Atmospheric Environment,* 38**,** 6177-6184.

ZHAO, Y., HENNIGAN, C. J., MAY, A. A., TKACIK, D. S., DE GOUW, J. A., GILMAN, J. B., KUSTER, W. C., BORBON, A. & ROBINSON, A. L. 2014. Intermediate-volatility organic compounds: a large source of secondary organic aerosol. *Environmental Science & Technology,* 48**,** 13743-13750.

ZHAO, Y., KREISBERG, N. M., WORTON, D. R., ISAACMAN, G., GENTNER, D. R., CHAN, A. W., WEBER, R. J., LIU, S., DAY, D. A. & RUSSELL, L. M. 2013. Sources of organic aerosol investigated using organic compounds as tracers measured during CalNex in Bakersfield. *Journal of Geophysical Research: Atmospheres,* 118.

ZHAO, Y., NGUYEN, N. T., PRESTO, A. A., HENNIGAN, C. J., MAY, A. A. & ROBINSON, A. L. 2016. Intermediate volatility organic compound emissions from on-road gasoline vehicles and small off-road gasoline engines. *Environmental Science & Technology,* 50**,** 4554-4563.